FINITE ELEMENT MODELLING OF R C INFILLED FRAME

A Thesis submitted in the partial fulfilment of
requirement for the award of the degree of

MASTER OF ENGINEERING

IN

STRUCTURES

Submitted By
Arun Goyal
Roll No.- 801022005

Under the Supervision of

Dr. Naveen Kwatra
Associate Professor

Department of Civil Engineering
Thapar University, Patiala.

DEPARTMENT OF CIVIL ENGINEERING
THAPAR UNIVERSITY
PATIALA-147004(INDIA).

FINITE ELEMENT MODELLING OF R C INFILLED FRAME

A Thesis Report submitted in the partial fulfilment of
requirement for the award of the degree of

MASTER OF ENGINEERING
IN
STRUCTURES

Submitted By
Arun Goyal
Roll No.- 801022005

Under the Supervision of

Dr. Naveen Kwatra
Associate Professor

Department of Civil Engineering
Thapar University, Patiala.

DEPARTMENT OF CIVIL ENGINEERING
THAPAR UNIVERSITY
PATIALA-147004(INDIA).

CONTENTS

CERTIFICATE

This is to certify that the work presented in this thesis titled being submitted by **AUN GOYAL** in partial fulfilment of requirements for the award of degree of **MASTER OF ENGINEERING IN STRUCTURES**, submitted in the **CIVIL ENGINEERING DEPARTMENT, THAPAR UNIVERSITY, PATIALA** is an authentic record of the initial work carried out by her under the supervision of **Dr.NAVEEN KWATRA, Associate Professor, DEPARTMENT OF CIVIL ENGINEERING, THAPAR UNIVERSITY, PATIALA,**

The matter embodied in this report has not been submitted in part or full to any other university or institute for the award of any degree.

(Dr. Naveen Kwatra)
Associate Professor,
Deptt. Of Civil Engineering,
Thapar University, Patiala.

Counter signed by:

(Dr. Maneek Kumar)
Professor & Head,
Deptt. Of Civil Engineering,
Thapar University, Patiala.

(Dr. S.K Mohpattra)
Dean Academic Affairs
Thapar University,
Patiala.

Page | iv

ACKNOWLEDGEMENT

First of all, I thank the almighty God who always runs before my path to pave it for a comfortable stride.

I would like to express my deep and sincere gratitude to my supervisor, Dr. Naveen Kwatra, Associate Professer, for his gracious efforts and keen pursuit, which has remained as a valuable asset for the successful instrument of my thesis report. His dynamism and diligent enthusiasm has been highly helpful in keeping my spirit high. His flawless and forthright suggestion blended with an innate intelligent application has crowned my task with success.

My thanks are due to Dr. Maneek Kumar, Professor and Head, Department of Civil Engineering for their constant encouragement. I would also like to thank Dr. Pankaj Aggarwal, Assistant Professer, IIT Roorkee , for his unconditional help during my work.

I would like to give special word of thanks to my friends for their patience and constant moral support during the entire course of my work. I would also like to thank my parents for their blessings.

ARUN GOYAL
ME CIVIL (Structures)

ABSTRACT

A comprehensive study has been conducted to evaluate the safety of existing masonry infilled RC reinforced concrete structures under earthquake loadings.The construction of reinforced concrete building with unreinforced infill or reinforced masonry is common practice even in seismically active countries. All buildings prior 1998 were constructed without seismic provisions while those constructed after this period adopted seismic codes. However, the codes have limited information on the design of infilled structures besides having differences in architectural requirements which may compound the structural problems. Although the influence of infill on reinforced concrete framed structures is known, the present seismic codes do not consider it due to the lack of sufficient information. From various research paper studies, it shows that the influence of infill on the structural performance is significant. The structural responses such as Fundamental period, roof displacement, inter-storey drift ratio, stresses in infill wall and structural member forces of beams and column generally reduce, with incorporation of infill wall. The structures designed and constructed with or without seismic provision perform in a similar manner if the infills of high strength are used.

To study the means and methods of modeling masonry-infilled RC structures, a comprehensive review of previous work and an analytical investigation is conducted. This thesis summarizes the results of those studies and verify on ATTENA, which specifically addressed the performance of RC frames infilled with unreinforced concrete masonry panels and subjected to in-plane lateral loading. The objective in modeling masonry-infilled frames has always been to develop a simple model that would capture characteristics of the masonry. Achieving this objective requires understanding the behaviour in more detail. The only feasible approach for simple and accurate modeling is to identify relevant parameters and employ numerical simulation, using well-calibrated analytical and experimental models to replace most of the expensive physical modeling. The aim here is to identify such numerical finite element models, demonstrate their capabilities, and facilitate the use of those models by identifying a commercial finite element analysis program having similar capabilities. The finite element models identified are a cohesive interface model to simulate the behaviour of mortar joints between masonry units and the frame/panel interface, and a discrete element approach to model the concrete. Analytical verification studies were carried out to determine the capabilities and limitations of the models.

LIST OF FIGURES

LIST OF TABLES

INTRODUCTION CHAPTER-1

1.1 General

A large number of Reinforced concrete (RC) and steel frames buildings containing unreinforced masonry (URM) infill walls are commonly used in structural system around the world. Masonry infills are often used to fill the void between the vertical and horizontal resisting elements of the building frames with the assumption that these infills will not take part in resisting any kind of load either axial or lateral load, hence its significance in the analysis of frame is generally neglected. Many buildings of this type have performed poorly during earthquakes. Kircher et al. (2006) indicate that concrete frames, including those with and without infill, represent one of the three major sources of seismic risk in the earthquake prone zone (the other two sources being URM bearing wall buildings and soft-story wood-frame structures) because approximately 80% of the cost of damages of structures from earthquakes is due to damages of the infill walls and to consequent damages of doors, windows, electrical and hydraulic installations (Asteris, P.G et al.2011). Moreover in seismic areas, ignoring the frame-infill panel interaction is not always safe, because under lateral loads the infill walls dramatically increase the stiffness by acting as a diagonal strut, resulting in a possible change of the seismic demand because of significant reduction in the natural period of the composite structural system (El-Dakhakhni et al. 2003, 2006).Non availability of realistic and simple analytical models of infill becomes another hurdle for its consideration in analysis. In fact it has been recognised that frames with infill have more strength and rigidity in comparison to the bared frames and their ignorance has become the cause of failure of many the multi storeyed buildings. The recent example in this category given by Jaiswal et al. (2002) report that RC frames with URM infill are currently being built in India in violation of the building codes, and that they performed poorly during the **2001 January,26 Bhuj earthquake**. The main reason of the failure is the stiffening effect of infilled frame that changes the basic behaviour of buildings during earthquake and creates new failure mechanism. The **2008 earthquake** in **Wenchuan, China**, provides numerous examples of frame-wall interaction (Li et al. 2008); see Figs. 1.1.

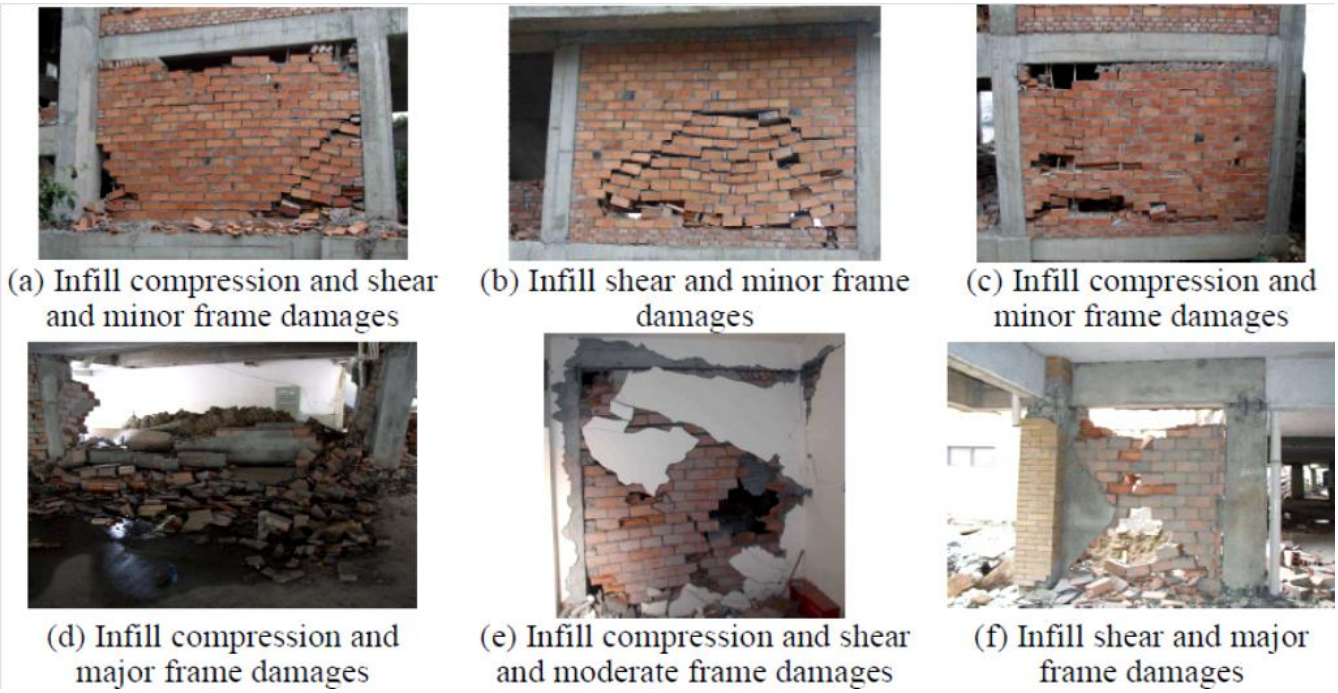

Fig-1.1 Damages of masonry infilled RC frames after the Wenchuan earthquake (Bixiong, Li et al.(2008))

The general outlines of the behavior and vulnerabilities of structures with URM infill are well known. Paulay and Priestley (1992) point out that infill walls may have beneficial or detrimental effects on the behavior of the overall structure. The beneficial effects derive from the fact that the infill walls add, at least during the initial stages of an earthquake, to the lateral force- resisting capacity and damping of the structure. However, the URM is brittle and prone to early failure due to in-plane (IP) loads, and interacts with the surrounding frame in such a way that column shear failure is made more likely. Also, the infill wall failure may lead to the formation of a soft story and consequent column failure. Failure of the URM walls in the out-of-plane (OOP) direction leads to life-safety hazard from falling debris. It is also known that there is an interaction effect between the IP strength of the wall and the OOP strength, with load in one direction reducing the strength in the other. This interaction is generally ignored in current engineering practice, such as **FEMA 356 (FEMA 2000).**

From various research paper studies, it shows that the influence of infill on the structural performance is significant. The structural responses such as Fundamental period, roof displacement, inter-storey drift ratio, stresses in infill wall and structural member forces of beams and column generally reduce, with incorporation of infill wall. The structures designed and constructed with or without seismic provision perform in a similar manner if the infills of high strength are used. A number of conceptual models have been proposed to simulate the behaviour of RC frame and infill wall structures. This diversity of models reflects an epistemic uncertainty, one that stems from the rather complex interaction between the flexure-dominated frame and the shear-dominated infill wall panel as shown in fig1.2. It is recognized that there is a need for a simple analytical model for the infill, one that can

be incorporated into a model of the overall structure, and that will produce acceptably accurate responses. Here we will try to discuss the structural action of infill panel and failure modes and modelling of infill walls with or without openings.

(a) Infill damage and minor damage to the RC frame

(b) Infill damage and minor damage to the RC frame

(c) Moderate damages to RC frame and infill wall

Fig-1.2,Effect of solid infill walls on the behavior of the bounding RC frame(Bixiong, Li et al.(2008))

Masonry walls have been used as both load-bearing structural elements and architectural non-structural elements in single- and multi-story buildings. Both reinforced and unreinforced masonry partitions have been used, sometimes filling the space within structural frames and other times not bounded by any confining structure. In load-bearing walls of the latter type, ties and columns are generally used to increase the structural integrity. In cases where the masonry infill interacts with the bounding frame, that interaction must be accounted for in design and evaluation of structures subjected to lateral loading such as an earthquake.

Although there has been much previous work to develop analytical models that realistically capture the behavior characteristics of experimentally tested masonry-infilled R/C frame prototypes, many technical difficulties in analytical modeling remain unresolved. A simplified analytical model that captures the salient characteristics of infilled masonry structures has not yet been developed. Success toward that end will require understanding masonry-infilled frame behavior in much more detail than offered by a strut or beam model. The required understanding can be accomplished only through experimental investigation followed by numerical simulation and parametric studies. The correct approach will facilitate the introduction and calibration of a simple yet accurate model for infill walls.

Recent research has shed new light on the behavior of infill frames and has produced advanced analytic tools. Classical diagonal strut models have been subjected to more thorough evaluations with new experimental data, and various limit analysis methods have been developed to account for the different load-resisting mechanisms of infilled frames. Sophisticated finite element models have been developed to analyze the nonlinear behavior of infilled frames in a detailed manner. This thesis summarizes some of those findings and developments, identifies numerical models, and demonstrates

their capabilities. Also, to facilitate the use of these models by researchers and designers, a commercial finite element program is identified with similar capabilities and is tested for its capabilities.

The behavior of infilled frames is briefly discussed to determine important aspects that need to be considered and accommodated by the FE modeling approaches. Then, a brief review of the modeling approaches and models used specifically for masonry-infilled frames is presented. From the successful experiences of other investigators, assemblies and infilled frame samples for which laboratory test and numerical results are available are selected. A summary of the results of verification studies conducted at the constitutive model level using the selected commercial software program is presented. The program was used to develop a sophisticated model and analysis of the behavior of infill frames, with two distinctive failure mechanisms, subjected to in-plane lateral loading. The numerical results are compared with available experimental and other numerical results.

1.1.1 IMPORTANCE OF FINITE ELEMENT MODELLING

To model the complex behaviour of reinforced concrete analytically in its non-linear zone is difficult. This has led engineers in the past to rely heavily on empirical formulas which were derived from numerous experiments for the design of reinforced concrete structures.

The Finite Element method makes it possible to take into account non-linear response. The FE method is an analytical tool which is able to model RCC infilled frame structure and is able to calculate the non-linear behaviour of the structural members is Finite element method. For structural design and assessment of reinforced concrete members, the non-linear finite element (FE) analysis has become an important tool. The method can be used to study the behaviour of reinforced and pre-stressed concrete structures including both force and stress redistribution.

With the advent of digital computers and powerful methods of analysis, such as the finite element method many efforts to develop analytical solutions which would obviate the need for experiments have been undertaken by investigators. The finite element method has thus become a powerful computational tool, which allows complex analyses of the nonlinear response of RC structures to be carried out in a routine fashion.

FEM is useful for obtaining the load deflection behaviour and its crack patterns in various loading conditions.

1.1.2 NEED FOR ANALYTICAL WORK

The results of any analytical model have to be verified by comparing them with experiments already conducted by pervious researchers. The development of reliable analytical models can, however, reduce the number of required test specimens for the solution of a given problem; recognizing and conducting those tests are time consuming and costly and often do not simulate exactly the loading and support conditions of the actual structure.

1.2 Importance of Study

Unreinforced masonry is widely used in seismically active regions, particularly as infill walls affecting both the structural and nonstructural performance of buildings. The loss of exterior and interior URM infill walls has serious implication not only for life safety but also the functionality of the building. Additionally, the loss of URM infill walls change the dynamic behavior of the building in terms of stiffness(as increase in stiffness is often associated with an increase of forces on the building when subjected to earthquake loading), natural frequency, damping, and overall structural behavior. Typically, URM infill walls are made of brittle material that loose capacity in rapid manner. The combined effect of brittleness and higher stiffness has a negative implication on seismic performance of the building frames. This thesis report presents a study of the behavior of RC frames with URM infill walls, carried out in recent years by the various researchers.

Polyakov (1958) suggested the possibility of considering the effect of the infilling in each panel as equivalent to diagonal bracing(macro modelling) and this suggestion was later taken up by Holmes (1961) who replaced the infill by an equivalent pin-jointed diagonal strut made of the same material and having the same thickness as the infill panel and a width equal to one third of the infill diagonal length.

Mallick and Severn (1967), and Mallick and Garg (1971) suggested first finite element approach. The infill panels were simulated by means of linear elastic rectangular finite elements approach (micro modelling) to analyze infilled frames, addressing the problem of an appropriate representation of the interface conditions between frame and infill.

Liauw and Kwan (1984) used three different types of elements; the infill-frame interface was modelled by simple bar type element; the infill panel was modelled by triangular plane stress elements, to study the behaviour of infill frames.

Dhanasekar and Page (1986) using one dimensional joint element to model the motor joint between the infill and frame.

Chrysostomou (1991) proposed to model each infill panel by six compression-only inclined struts. Three parallel struts are used in each diagonal direction ones and the off diagonal ones are positioned at critical locations.

1.3 Background of this study

When constructed in buildings with steel or RC moment frames, URM or lightly reinforced masonry infill walls are traditionally not considered as a part of the lateral load-resisting system. An argument for ignoring the effect of these infill walls is that such walls typically do not offer much displacement capacity, and in an event of significant lateral demands, the infill wall would disintegrate, whereas the original lateral load-resisting system acts as intended in the design assumptions and processes. The problem, however, is that on one hand such a simplified design approach does not predict the level at which the damage in the URM infill wall occurs—this can be significant in terms of nonstructural damage—on the other hand it does not consider the global and local effects of having these stiff and brittle elements coupled with the primary lateral load-resisting system, e.g, the shift in the natural frequency of the structure, the overall change of structural behavior, and the increases in shear demand on the columns, in diaphragm demands, and in collector element forces.

Masonry wall infilled frames have been experimentally investigated for both in-plane and out-of-plane forces by many engineers and researchers. Most of these studies are focused on the behavior of single-frame single-bay URM infilled frames under monotonic or cyclic lateral loading. Some of these investigations, past and recent, are documented. (Benjamin and Williams 1958; Holmes 1963; Stafford-Smith 1968; Moghaddam and Dowling 1987; Dawe et al. 1989; (Mander et al. 1993; Mehrabi et al. 1994); Negro and Verzeletti 1996; Durrani and Haider 1996; Pires et al. 1998; and Fardis et al. 1999b). Studies of tests on multi-story multi-bay s can be found in Liauw and Kwan 1985a; Gergely et al. 1994; Mosalam 1996a, b; Mosalam et al. 1997a, b and 1998). These studies provide evaluations of (1) the importance of infill wall confinement from bounding frames, (2) the types of failure that can be observed in the infill and/or the bounding frame members, (3) the stiffness and strength of the infilled frames, and (4) the degradation of strength upon load reversals. Since these experimental investigations are predominantly performed using static, quasi-static, or pseudo-dynamic loading, it is not clear how well these experimental data represent the dynamic performance of the framed structural system, e.g., damping characteristics, when masonry infill walls are introduced and the entire system is subjected to true earthquake loading.

Limited data exist on the dynamic properties of masonry wall infilled frames, since very few shake-table experiments are performed on masonry infilled structures. Fardis et al. (1999) report on the shake-table test performed on single-bay two-story RC frames with eccentric (asymmetric in plan) masonry infill walls subjected to bidirectional ground accelerations. Their study focused on the effects of the eccentricity on the displacement demands on the corner columns. They also report that the infill panels survived out-of-plane peak accelerations of 0.6g at the base of the test structure or 1.3–1.75g at their mid-height. Zarnic et al. (2001) report on two shake-table tests performed on ¼-scale one- and two-story RC frames with strong-block weak-mortar masonry infill walls subjected to unidirectional sinusoidal motion at the base of the test structure. Dolce et al. (2005) report shake-table tests performed on 3/1 -scale three-story twobay RC plane frames without infill walls, with masonry infill wall, and with two different types of energy-dissipating and re-centering braces. Their study compares the overall response and the dynamic properties of the tested three frames when subjected to a sequence of artificially generated accelerograms with increasing intensity.

The dynamic experiments discussed in the previous paragraph are generally performed on small-scale models limited by the size limitations of the available shake tables, and are focused on other aspects of the problem, e.g., torsional effects due to eccentric infill walls.

1.4 Review of Commercial FE Programs

The approach and constitutive models described above have thus far been implemented mostly by researchers. Those implementations have been developed using analytical software programs that are not necessarily available in the public domain and typically have limited scope and applicability. For effective modeling and simulation of infilled frames in the design and engineering community, a commercial finite element program must be employed. The advantages of commercial modeling programs include ease of model construction, large element and model libraries, user-friendly input and output formats, and integrated graphics capabilities. Four available FE programs capable of modeling concrete and interfaces were selected for review. These were ANSYS, ADINA, ABAQUS, ATTENA and DIANA. The programs were reviewed for their capabilities in modeling structural discontinuities, such as mortar joints, in otherwise heterogeneous materials such as concrete and masonry. For the type of infilled frames considered in this study, i.e., R/C frames infilled with unreinforced concrete masonry (UCM) blocks, the defining parameters are (1) separation of mortar joints and infill-to-frame interfaces, and (2) cracking and crushing of the infill material. Degradation of shear properties, especially at the interfaces and joints, was of specific interest.

Based on stated selection criteria, the ATTENA finite element program was identified as the best fit for the purpose of this study.

1.5 Aim & Objectives

The objectives of this study are:- The objective of this study is to carry out numerical simulation and parametric studies and compare them with the results of a previous experimental investigation. The investigation also attempted to determine the best suitable model to find out the interaction between the infill and the frame, which has a major impact on the structural behavior and load-resisting mechanism, and would capture characteristics of reinforced concrete infilled with masonry in much more detail than a strut or beam.

1) To study the behavior of RC Infilled or Bare frames by using computer software, which is then compared with the experimental results, to check the applicability of software.

2) To present finite element analysis of different types RC Strut model (Single or Three) under monotonic loading using finite element based software ATENA.

3) To compare the results of F.E.M. analysis of RC Strut Model with Analytical Infilled frame or experimental Infilled frame with results of already conducted experimental investigations on same detailing so as to validate the result of F.E.M. analysis & to find difference in behavior of RC Strut frame with Infilled frame.

4) To compare the strut results with model used by pervious researcher give values closer to the experimental infilled frame results.

1.6 Scope of work

In the first phase of the present study of FE modelling of the displacement control RCC bare and Infilled frame under the monotonic loads has been analyzed using ATENA software and the results so obtained have been compared with available experimental results from the test conducted by Meharbi et al (1994).

The control frame is analyzed using ATENA software up to the failure and the load deformation curves are plotted and the cracking behaviour is monitored. The control frame has been analyzed and results have been compared with the experimental results.

In the second phase of the study, FE modelling the bare frame with Single Strut of different thickness and three Strut model given by different researcher analyzed. The frame with single or three strut is modelled and analyzed. The results obtained from the analysis of FF model have been plotted in the shape of Lateral load v/s lateral deflection graphs. Comparisons are made by the load deflection curves and values. Deflection and cracking behaviour of the RCC Single or three Strut frame are also studied.

This work mainly focuses on the following parameters:

i) Nonlinear load-deflection behaviour.

ii) Study of crack patterns at different load steps.

iii) Behaviour or load carrying capacity of Infilled RC frame with Single.

1.7 Outline of thesis

The thesis is organized as par detail given below:

Chapter 1: Introduces to the topic of thesis in brief.

Chapter 2: Discusses the Structural Overview i.e. the work done related to RC Infilled frames.

Chapter 3: In this chapter, discusses the literature review of RC Infilled, Single Strut or Three Strut frame has been discussed in detail. The theory related to RCC Infilled frame and Strut models also discussed in brief.

Chapter 4: Deals with the details of the structure modelled in by past. Second part comprises of FEM modelling, theory related to the ATENA, material modelling and analytical programming procedure steps involved in modelling of the control frame. It also deals with the description of the material behaviour of concrete, reinforced steel bars

Chapter 5: The results from the analysis, comparison between the analytical and the experimental results. Comparison of results b/w Single strut models, Single and Three strut models.

Chapter 6: Finally, salient conclusions and recommendations of the present study are given in this chapter followed by the reference.

2.1 Structural and Constructional Aspects of Infill

The presence of masonry infills is the cause of

(i) Unequal distribution of lateral forces in the different frames of a building-overstressing of some frames;Fig-2.1

(ii) Vertical irregulation in the strength and stiffness-Soft storey as a result higher interstorey drifts and higher ductility demands of RC elements of the soft storey in comparison to remaining stories; as shown in Fig-2.2

(iii) Horizontal irregularities-significant amount of unexpected torsional forces since the centre of rigidity is moved towards the stiffer infilled frames of increased stiffness and as a result occurrence of very large displacement in the extreme bare frames;

(iv) Including the effect of short column or captive column in infilled frame-a captive column is full storey slender column whose clear height is reduced by its part-height contact with a relatively stiff masonry infill wall, which constraints its lateral deformation over the height of contact **(CEB,1996)** resulting in premature brittle failure of columns and as shown in Fig-2.3

(v) Failure of masonry infills-out of plane and in plane failure results which become the cause of causalities as shown in Fig-2.4

A significant amount of research work has been carried out on the consideration of stiffness effect of infill panels and its constructional details. A clear decision has to be taken by structural engineers, whether the infill walls will be made to participate in resisting the load or not. Depending upon its load resisting mechanism of infills the construction details will be followed as.

(i) Only axial load – infill walls tight to the underside of the floor system – Arching action is the dominant mechanism,

(ii) Axial and lateral load – friction or mechanical anchorage along the top to transfer lateral load to the wall – connection must be able to transfer reaction,

(iii) Only lateral load – wall built tight to the columns and a movement joint at the top of wall, and no axial and lateral movement joints along all the sides of walls and must be sufficiently thick to isolate the effects of inter storey drift, Floor deflection and differential movement – this type of wall is called PARTITION WALL.

Fig 2.1(a) Overstressing of RCC frame.

Fig-2.1(b) Beam failure due to overstressing

Fig 2.1, Overstressing of frame causing column, beam or frame failure (Bixiong, Li et al.(2008)

Fig-2.2(a) Leaned 6-story building in Dujiangyan

Fig-2.2(b) Measuring column drift

Fig-2.2(c) Typical column damage.

Fig-2.2 Formation of a soft and weak story (Bixiong, Li et al.(2008)

Fig-2.3(a)Windows in both sides

Fig-2.3(b)Infill in one side only

Fig-2.3(c)Partial infills in both sides

Fig-2.3, Short columns observed after the Wenchuan earthquake (Bixiong, Li et al.(2008)

Fig-2.4(a) Partial collapse of 3-story RC frame building with masonry infill walls in Yingxiu

Fig-2.4(b) In-plane infill failure in yinxiu

Fig-2.4(c) Out of plane failure of infill

Fig-2.4, In-plane and Out plane failure of masonry infill. (Bixiong, Li et al.(2008)

2.2 FAILURE MECHANISM OF INFILLED FRAME

The failure of the infilled frame is quite complex and depends upon a number of factors such as relative strength and stiffness properties of infill and frame, frame wall interface gaps, openings, shear connectors, and such other characteristics. Fig-2.1, shows the five most common modes of failure of masonry infilled frame under increasing intensity of lateral loads (Benson, P Shing and Armin, B Mehrbi (2002).

The experimental as well as the numerical research performed over last few decades showed different failure mechanism of an infilled frame structure. Most of them have used single storey system under in-plane loads. It has been reported that the separation takes place between the infill and the frames at the early stage of loading all around the interface excepting the two compressive ends. The angular distortion of the infill varied in its value between $\Delta/h = 0.03x10^{-3}$ to $0.7x10^{-3}$ (where Δ is the horizontal displacement and h is the height of the storey), depending on the relative stiffness of the

infill to the frame stiffness and the external load. The onset of separation may also depend on the quality of workmanship, lack of fit and material quality. However, the prediction of separation is not important as it does not considerably affect the rigidity of the infilled-frame (CEB(1996)).

Stafford Smith (1966) reported that the weak frame cannot transmit the forces to the compressive diagonal of infill and thus suffers local crushing at the ends of compressive diagonal. On the contrary, the strong frame can transmit high forces to the compressed diagonal which set infill to initiate cracking from the central region and propagates towards the compressed diagonal ends. It was also reported that when the weaker infill is use with stronger frame system, horizontal sliding failure occurs along the bed joints of the masonry. On the contrary, when the stronger infill was used with the weak frame, the frame underwent premature failure of columns before the onset of frame failure**.** It means that the infilled frame does not reach to its full capacity.

Generally mortar joints are considered to be the planes of weakness due to low shear resistance. Cracks can appear in the interface column and infill, beam and infill and between the infill elements which give negative impression on performance of the structures. The shearing failure of joint was reported in research carried out by (Abdou, 2006) and (Miranda Dias, 2007) occurred along the plane of weakness.

Merabi (2002) studied brittle shear failure of the column on windward side while investigating the infilled frame structure which had strong infill panel and weak frame. However, the increase in lateral load resistance was found even after the shear failure in column, indicating some kind of ductility due to infill. On the contrary, the formation of hinges in columns and slip in the bed joints were observed in the weak infill frame test specimen. The stronger frame with stronger infill had failed by crushing of infill as the shear failure of columns was prevented due to enough shear reinforcement and bigger column size.

In principal, failure mechanism of an infilled frame depends to a great extent on the relative strength of the frame and the infill**.**

Main five modes of failure of unreinforced masonry in Reinforce Concrete structures as shown in fig 2.52.

Mode-1

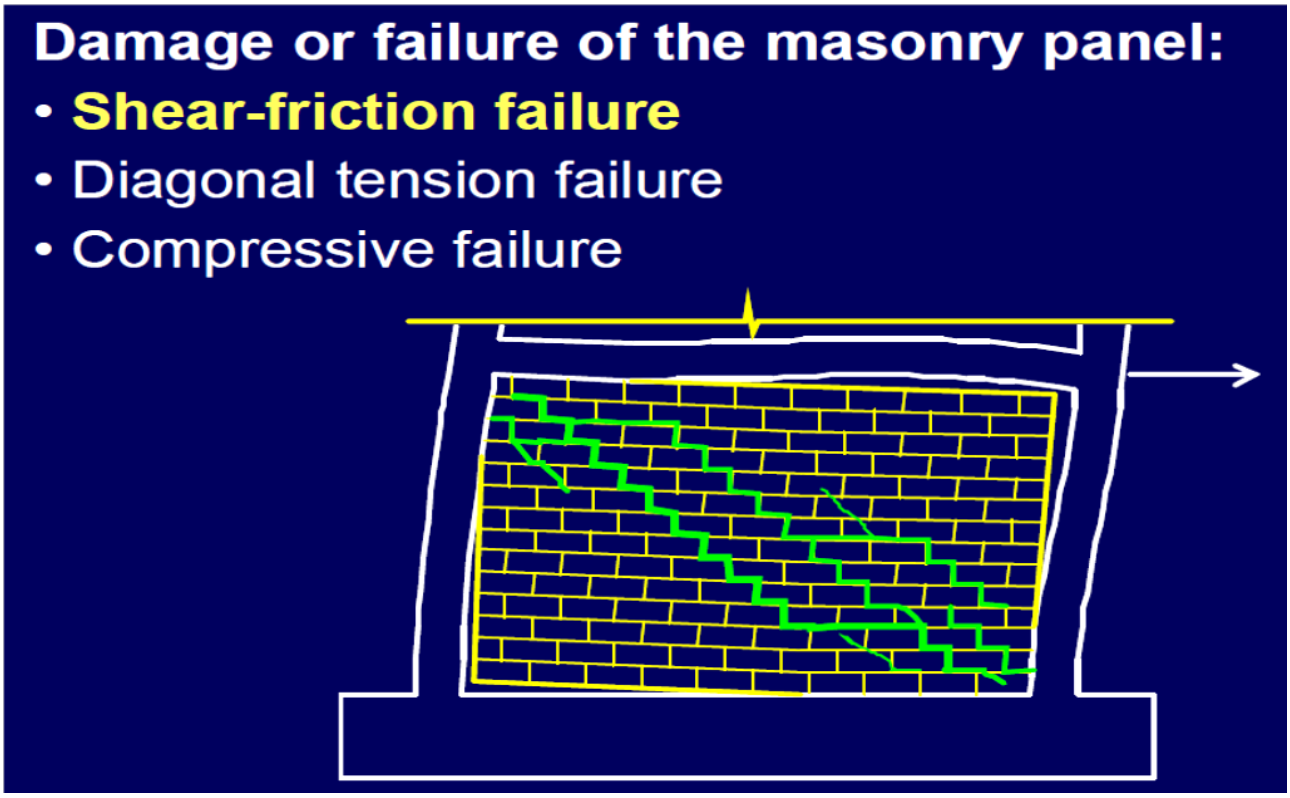
Damage or failure of the masonry panel:
• Shear-friction failure
• Diagonal tension failure
• Compressive failure

Mode-2

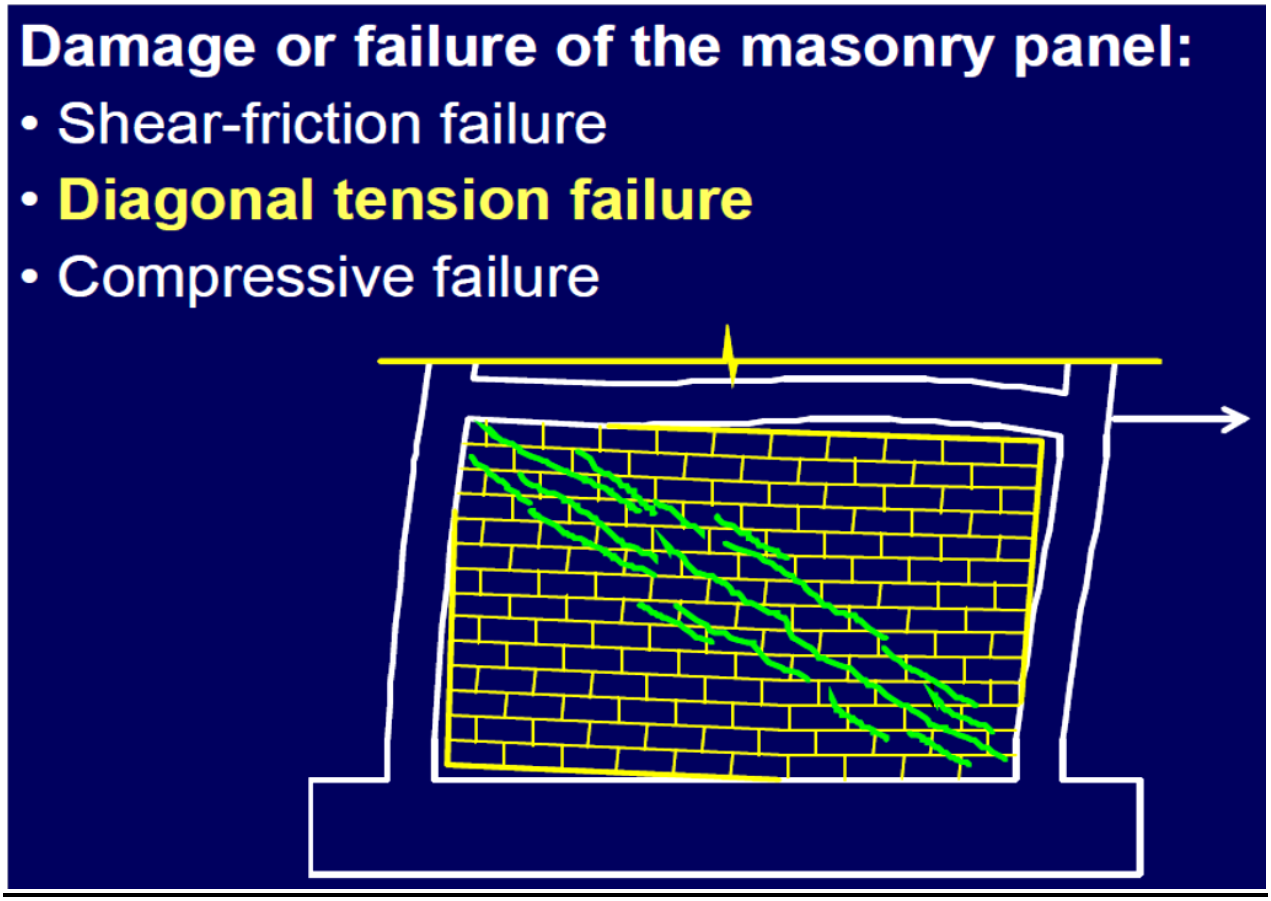
Damage or failure of the masonry panel:
• Shear-friction failure
• Diagonal tension failure
• Compressive failure

Mode-3 and 4

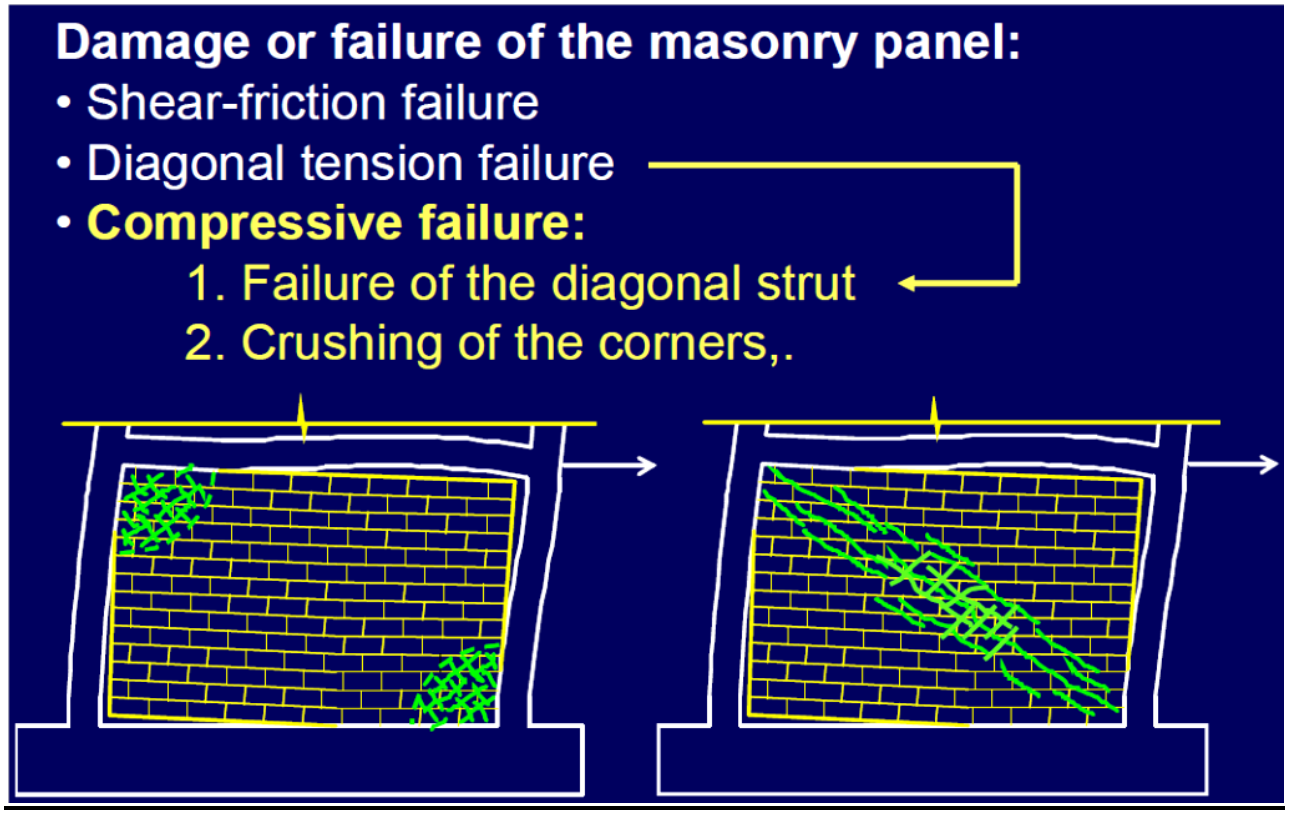

Mode-5

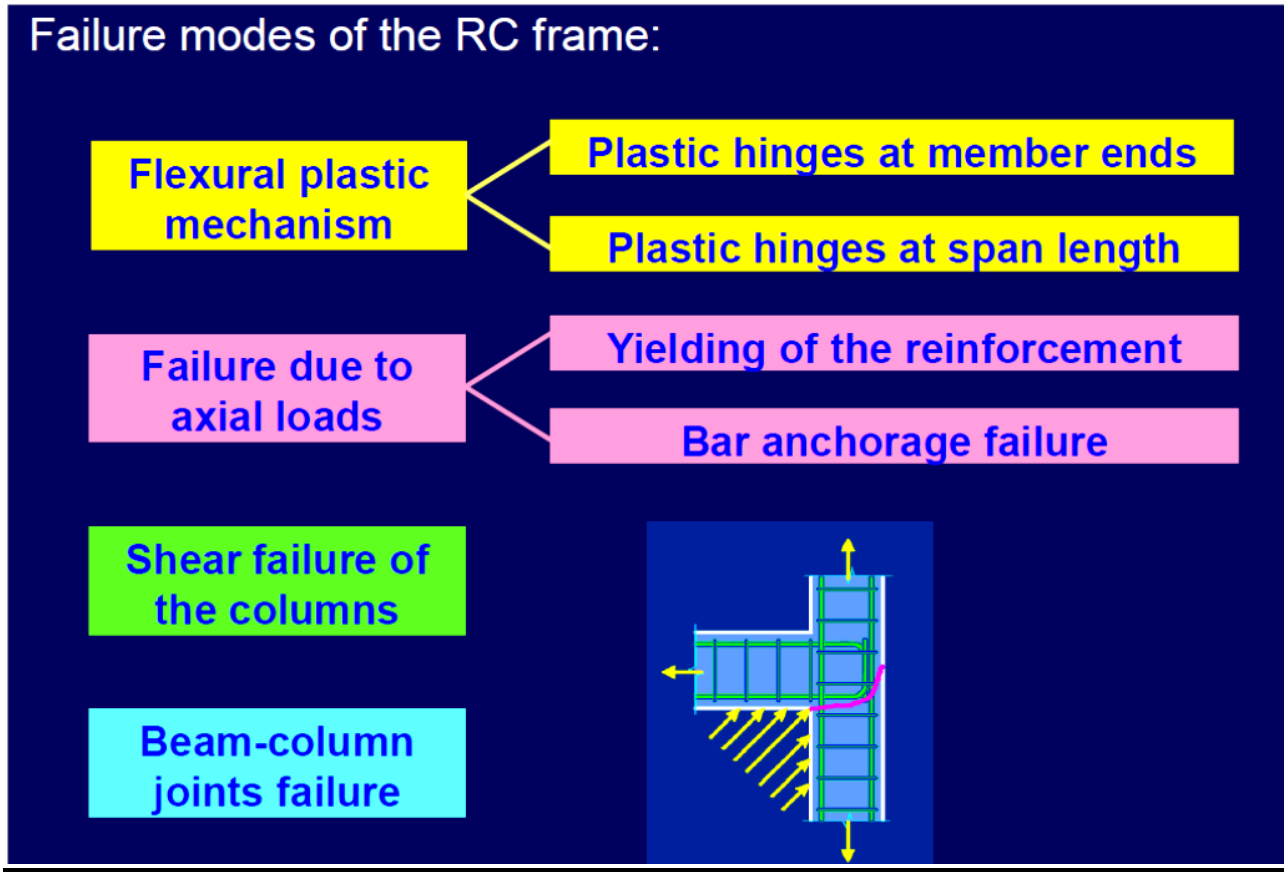

Fig.2.5; Infilled frame failure modes (Benson, P Shing and Armin, B Mehrbi (2002)

Mode 1: Sliding shear failure through bed joint of a masonry infill – associated with infill with weak joint and strong members. This formation of the shear crack separation the panel into two parts, which reduces the effective column height approximately to half. At this cracked conditions, the system will behave as a knee-braced system.

Mode 2: Shear failure at the loaded side columns or beam-column joints–associated with strong infill and a weak frame. The diagonal/Sliding cracks in the infills have been first noticed followed by shear failure of the loaded sided columns also known as diagonal tension failure.

Mode 3: Corner Crushing in the infill at least one of its loaded corners – associated with strong infill surrounded by a strong frame.

Mode 4: Diagonal shear cracking in the form of a crack connecting the two loaded corners and columns yielding in flexure – associated with strong infill surrounding by a weak frame with weak joints and strong members. Cracking of the walls occur from one corner to the diagonally opposite corner and the masonry wall fails in shear or diagonal tension.

Mode 5: Frame failure in the form of plastic hinges in the columns or the beam column connection – also associated with strong infill surrounded by a weak frame or frame with weak joints and strong members.

Most of the studies are focused on the corner crushing mode of failure i.e mode 3 in which, the diagonal compression strut mechanism is fully developed that converts the frame system into the truss (Fig 2.6), increasing the lateral stiffness of the frame manifold. In fact, one may expect an initial lateral stiffness of the infilled frame 5 to 40 times of the respective bare frame. Now a day the diagonal strut model is widely accepted as a simple and rational way to describe the influence of the frame-panel interaction.

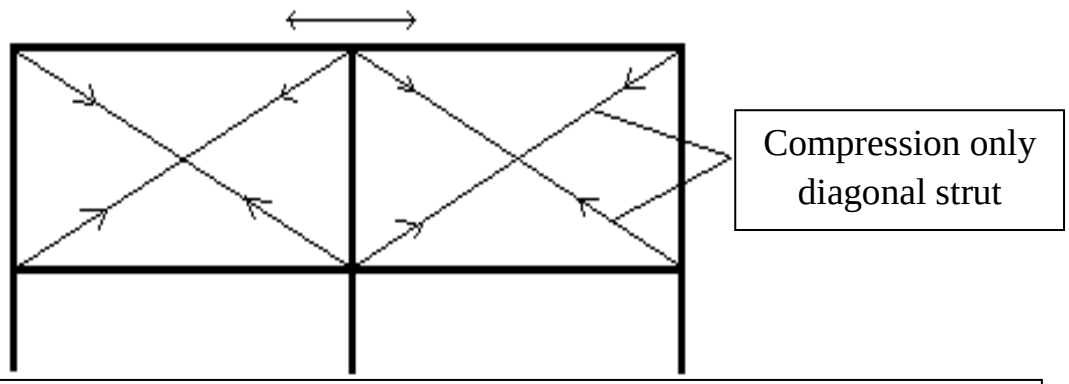

Fig.2.6 Diagonal compression strut mechanism; Benson, P Shing, Armin, B Mehrbi (2002)

2.3 Strength

Numerous experimental and numerical investigations carried out in past have proven that the presence of infill improves significantly the lateral strength of an infilled- frame system. The parameters involved in increasing the strength are strength of infill materials, strength of surrounding frame elements, relative stiffness of infill to frame ratio, presence of opening, reinforcement of infill panel, strength of mortar and masonry blocks, lack of initial fit between infill and the frame etc.

The presence of gap between the infill and the frame were studied by (Dorji, J; 2009) and studied the decrease of strength of the infilled-frame system, however the result varied from one another depending on the gap considered and the material used.

Mortar strength of 2.4 MPa was used and columns failed prior to the failure of infill. This type of failure mechanism is against the desire of current seismic codes, yet, limitation on the strength of mortar is rarely given in the Standards and further studies is required for high rise building under dynamic loading. Research also found that there is a small increase in lateral strength by providing the reinforcement in the infill's, however did not observed any increase of strength due to poor bond condition between the mortar and the reinforcement due to early cracking along bed joints.

2.4 Lateral Stiffness

It is known that the presence of infill in the frames increases the lateral stiffness of the system by four to twenty times to that of bare frame system studied by Gosh, Asok A and Amde, M Amde(2002)**.** However, it is difficult to quantify the extra stiffness contributed by the infill in terms of absolute figure due to numerous parameters involved in the system. The stiffness of the infilled-frame system depends significantly on the strength of infilling materials. However, this study was limited to Static linear procedure considering a single storey single bay model.

Numerous research were carried out by various researcher to study on the influence of the stiffness from the infill walls, by considering a gap at the interface between the frame and the infill wall. It was reported by various researcher that there is a noticeable decrease in the stiffness of the system while observed 40% decreases in stiffness. Experimental and FE investigations were carried out for an infill frame by various researchers considering various parameters, and reported significant influence on strength and stiffness of an assemblage. Lateral strength of building can be increased by introducing infill panel (Anil, 2006) if the structure has problem with drift.

The lateral stiffness of retrofitted RC frame on two test specimens. The first specimen was with reinforced concrete infill while the second specimen was with hollow concrete block with diagonally placed CFRP strip. It was reported that the stiffness of the first specimen increased by 500%, however the second specimen showed better strength degradation beyond the peak load. Form the above review, it was learnt that the infill generally increases the lateral stiffness of the structural system which could be used for resisting the lateral load from earthquakes.

Jain, S.K and Mondal, G (2008) has proposed a reduction factor for effective width of diagonal strut over that of the solid infilled frame to calculate its initial stiffness when a central window opening is present. With the present of central opening the lateral stiffness of the infill frame has changed is given in Table (2.1) by using strut and tie method or FE method with the experimental data by considering single strut or multiple struts as shown in fig (2.8). Lateral stiffness also depends upon the material used for bond in between infills and its strength.

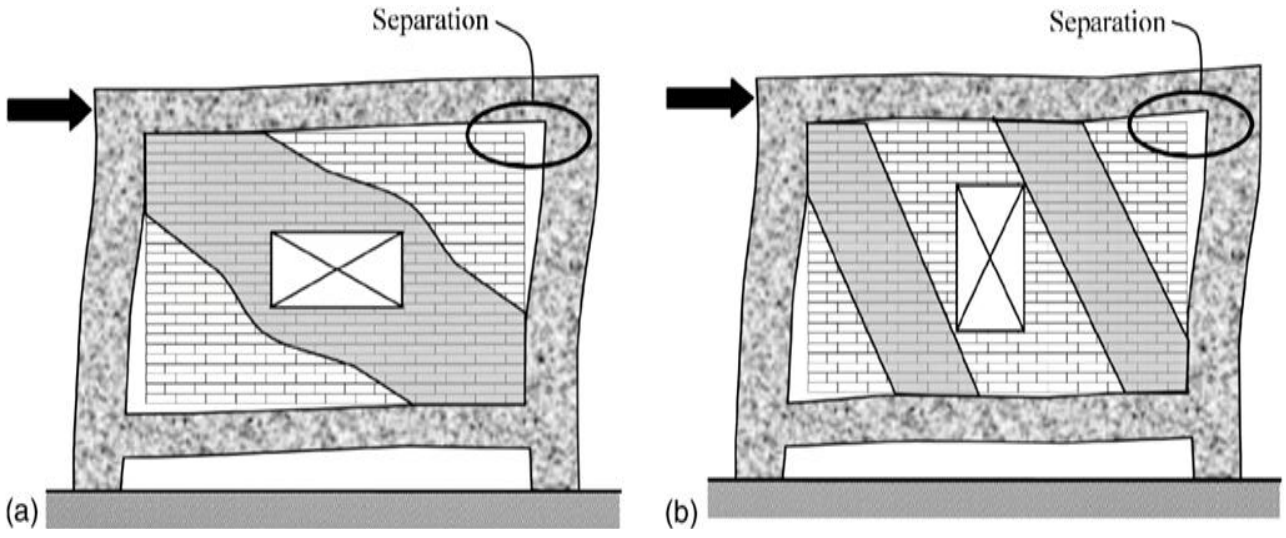

Fig 2.8 Formation of diagonal strut (a) Single diagonal strut, (b) Multi strut. Jain, S.K and Mondal, G (2008)

Width smaller than Height		Width larger than heights		
Opening Size (mm x mm)	Lateral Stiffness (kN/mm^2)	Opening Size (mm x mm)	Lateral Stiffness (kN/mm^2)	Difference (%)
Single storey				
500 × 1000	125	1000 × 500	120	-4.2
500 × 1500	114	1500 × 500	117	2.5
500 × 2000	98	2000 × 500	105	5.8
1000 × 1500	97	1500 × 1000	101	3.3
1000 × 2000	75	2000 × 1000	85	8.3
1500 × 2000	54	2000 × 1500	62	6.7
Two storey				
500 × 1000	68	1000 × 500	70	1.7
500 × 1500	62	1500 × 500	64	1.7
500 × 2000	51	2000 × 500	58	5.8
1000 × 1500	54	1500 × 1000	55	0.8
1000 × 2000	41	2000 × 1000	47	5.0
1500 × 2000	29	2000 × 1500	32	2.5
Three storey				
500 × 1000	44	1000 × 500	44	0.0
500 × 1500	40	1500 × 500	41	0.8
500 × 2000	35	2000 × 500	38	2.5
1000 × 1500	36	1500 × 1000	37	0.8
1000 × 2000	29	2000 × 1000	31	1.7
1500 × 2000	20	2000 × 1500	22	1.7

Table 2.1 Effect of dimensions of opening on initial lateral stiffness of infilled frames; Jain, S.K and Mondal, goutam (2008)

2.6 Consideration of infill in current codes

Most of the seismic codes ignore infill due to the brittle nature of failure, varying properties and low deformation capacity. However, the presence of infill changes the behaviour of structural system from frame action to truss action due to significant contribution of initial lateral stiffness. Some of the codes which consider the infill for seismic resistance are given below.

The **IS 1893 (2002)** used in india, considers the effect of infill in terms of natural period of vibration. However, there is no proper information on the basis of equation as it is empirically related to the height and width of a structure. Also, the same empirical equation is used irrespective of the extent of infill present in the structure. Moreover, there is no control over choice of infill material, giving wide options to the builders to select material whose performance during earthquakes is uncertain.

As a result, infill wall is considered as non-structural component of the buildings although literature revealed that there is a significant influence on the lateral strength and stiffness of the structures. The soft-storey problem associated with infill structures is addressed by providing a prescriptive magnification factor on structural member forces. It is not possible to compute the actual stiffness of the infilled structures due to absence of infill model generation in the code. The inter-storey drift ratio is limited to **0.004** irrespective of consideration of infill wall.

Eurocode 8 (2003) considers the effect of infill on the natural period of vibration by taking into account the correction factor (C_t) derived based on the effective cross- sectional area of infill wall in the first storey. It requires the frame members to resist 100% of the vertical loads and 50 to 60% of the total horizontal load on the structure. This code allows reasonable irregularities in plan by doubling the accidental eccentricity but recommends dynamic analysis for an unacceptable irregularity problem. It recommends that the infill wall which has only one opening, either door or window, has a significant influence on the frame. For other walls which have more than one opening, proper measures, such as reinforcing the wall and providing concrete member along the perimeter of the opening, are recommended. The code also recommends the out-of plane failure of infill wall by limiting the slenderness ration of wall to 15. It is the ratio of the length or height to thickness of the wall whichever gives more. The stiffness of infill wall is taken into consideration by recommending the use of diagonal strut. However, the thickness of strut is not specified as it varies with the opening. There is no mention about the modulus of elasticity of infill material.

Nepal code (NBC-201, 1995) considers infill by recommending the use pin-jointed diagonal struts element as an infill wall. However, the width of strut is not recommended and hence the consideration of opening is not realised. The distribution of axial forces and lateral seismic loads are specific. The code also recommends the Young's modulus of infill material to be 2500 to 3000MPa. The walls which have opening less than 10% of the wall area is treated as structural wall and if the opening exceeds 10%, the wall are provided with Reinforced concrete elements all around the opening perimeter and recommends appropriate reinforcement. The out-of plane failure is prevented by providing the concrete bands at one third and at two third of the wall height. However, there codes which recommend the isolation of infill wall from the frame (**NZS-3101, 1995).**

Ministry of Housing and Urban-Rural Development of the People's Republic of China. (1974, 1978, 1989, 2001). -Major changes were introduced into the seismic code in 1989 (GBJ11-89) and 2001 (GB50011-2001). The latest two versions of the seismic code were based on ultimate strength design of buildings (TJ11-74) became in effect since 1974 in China. A revised edition (TJ11-78) came out in 1978 after the 1976 Tangshan earthquake. Early editions (e.g. 1974 and 1978) of the code for seismic design. In the 1989 edition of the seismic design code, RC buildings should be designed to form ductile systems. The basic principles in that regard are: (a) columns should be stronger than beams, (b) shear strength of a column must exceed shear force associated with the plastic moment in the column, (c) shear resistance in beam-column joints is sufficient, and (d) beam reinforcing bars anchorage in the beam-column joint is adequate. In the 2001 edition of the code, detailing requirements are more stringent for systems with high ductility.

3.1 Modeling

Model development of any structures is critical to achieve accurate output results. However, it is difficult to model the as-built structures due to numerous constraints with as it is difficult to incorporate all physical parameters associated with the behaviour of an infilled frame structure. Even if all the physical parameters, such as contact coefficient between the frame and the infill, separation and slipping between the two components and the orthotropic of material properties are considered, there is no guarantee that the real structures behaves similar to the model as they also the structural behaviour could also depend on the quality of material and construction techniques.

It has already been discussed in the previous sections that the presence of infill affects the distribution of the lateral load in the frames of building because of the increase of stiffness of some of the frames. The distribution of lateral forces in the frames of building basically depends upon the centre of rigidity of the building and the resultant of the applied lateral load. If both nearly coincide, distribution of lateral load remains straightforward i.e in the ratio of their relative stiffness. If it is not the case, large torsional forces are introduced in the building. These types of structures can be better analysed on the basis of 3D analysis of buildings after considering the increased stiffness of the infilled frames.

The study of interaction of infill with frames has been attempted by using sophisticated analysis like Finite Element Analysis or Theory of Elasticity. But due to uncertainty in defining the interface conditions between the infilled with the frames, an approximation analysis method may be better acceptable. One of the most common approximations of infilled walls is on the basis of Equivalent Diagonal Strut i.e the system is modelled as a braced frame and infill walls as web element. The main problem in this approach is to find the effective width for the equivalent diagonal strut. Various investigations have suggested different values of width of equivalent diagonal strut.

Asteris, P.G (2008) to simulate the structural behaviour of infilled frames, two methods have been developed such as Micro Model and Macro Model. The Micro Model method is a Finite Element Method (FEM) where the frames elements, masonry work, contact surface, slipping and separation

are modelled to achieve the results. This method has seems to be generating the better results but it has not gained popularity due to its cumbersome nature of analysis and computation cost.

The Macro Models which is also called a Simplified model or Equivalent diagonal strut method was developed to study the global response of the infilled frames. This method uses one or more struts to represents the infill wall. The drawback of it is to the lack of its capability to consider the opening properly precisely as found in the infill wall.

3.2 MICRO-Model

A Finite Element (FE) method is a process of discritizing the structural components into a smaller sizes, maintaining the constitutive laws of materials, boundary conditions in order to improve the accuracy of results. However this method is mostly limited to small structures as it requires high computation equipments besides taking comparatively longer time. Relevant research on infilled frame that were done in past few decades were reviewed and presented in this section.

Jagadish et al (1985) investigated the elastic behaviour of a single storey infilled frame which had opening. The interface conditions such as slip, separation and frictional loss at the contact surface were considered using the link element. They were achieved by adjusting the axial, shear and tension force in the link element. The opening was modelled by assigning very low values of infill thickness and Young's modulus of elasticity of infill but high value of Poison's ratio. It was reported that the lateral stiffness of the structure decreases with the increases in opening size. The principal stresses were maximum at the corners of opening and the compression ends when full contact was the condition which further increased by allowing separation at the interface. However, the author stated that the equivalent diagonal strut mechanism may not be applicable for structures which have openings.

The behaviour of infilled frame under an in-plane load was studied by Dhanasekar and Page (1986). The results from biaxial tests on half scale solid brick masonry was used to develop a material model for brick and the mortar joints which were then used to construct non-linear Finite Element Model.

The results were that the Young's modulus of elasticity of the infill has a significant influence on the behaviour of the infilled frame. However, the influence of Poison's ratio was fond insignificant on the behaviour of structure. It was also reported that the infill wall failed due to shearing along the diagonal length of the wall and hence the influence of the compressive strength of infill material was

not observed. The bond strength and tensile strength of infill masonry were found to influence the behaviour and ultimate capacity of the infilled frame.

The FE model with and without a perfect contact between the infill wall and the reinforced concrete frame was studied by Combesure and Pegon et al (1995) on a single storey structure. It was reported, under unilateral contact condition (frictionless), the forces between the frame and fill panel are transferred through a compression corners at the ends of diagonal strut. However, there is no transfer of shear force from infill to frame. When a perfect contact condition was consider at the interface, shear force transfer between the two.

Haddad (1991) studied the application of a Finite Element Method to assess the effects cracking and separation between the infill of an infilled frame structure. The model considered the crack size and location, relative stiffness and contact length. It has been found that the bending and deflection decreases with the increase in infill frame relative stiffness. Bending moment further increased with the crack depth. The moment at the un-cracked section increased when the crack size on other end was increasing. The magnitude and location of principal compressive and tensile stresses were affected by crack size, contact length and infill frame relative stiffness. However, the author recommended the good use of material and construction techniques to reduce damages due to separation and cracking.

Similar research on the infilled structures, using FE technique, was carried out by (Morbiducci, 2003; Seah 1998; Louerenco, 1996; Singh, 1998). However, most of them had investigated on a single storey models under-in-plane static loads.

3.3 MACRO-MODEL (Equivalent diagonal strut)

The main disadvantage of performing Finite Element Analysis for the global structural response study is due to computation cost and the nature of complexity in model generation. Thus, to simplify the model generation, Macro-model method has been developed based on the experimental and finite element analysis results, wherein, diagonal struts are used to represent the infill.

The concept of equivalent diagonal strut method was initially introduced by Polyakov (1960) while investigating a three storey infilled structures. The cracks along the diagonal length of panel gave an insight of the strut behaviour of an infill panel. The report stated that the stress from peripheral frame members to the infill was transferred only through the compression corners of the frame-infill interface.

Benjamin and Williams (1958) investigated three different models, in which a masonry wall encased with the reinforced concrete frame and the masonry wall, masonry wall encased with the reinforced concrete frame and the masonry wall with steel frames. All these models were tested under an in-plane load. The test revealed the importance of aspect ratio which influences the ultimate capacity of the infilled frames. It was also reported that masonry has significant role in contributing lateral strength to the frame, however the size of masonry element did not affected the result. The importance of concrete cross-sections and steel reinforcement was realised. Since it was the beginning of the research in this field, dynamic loads were not considered and the thus results were conventional.

Holmes (1961) proposed the width of equivalent strut to be one third of the diagonal length from his experimental study on a single storey single bay infilled structure under an in-plane load. Smith (1962) conducted a study on infilled structure experimentally on a small scale specimen. The specimen had steel frame and concrete mortar as infill. The in-plane load was applied at the top corner of the infilled specimen and was observed a compression region within the infill panel which made the frame stiff and thus the concept of diagonal strut method was evolved. It was also reported that longer the contact length between the infill panel and the frame, wider the width of strut.

Smith (1966) proposed a formula to calculate the width of strut based on the relative stiffness of the frame and infill wall. The suggested formula was investigated by performing numerous tests on different specimens. The theoretical relation of the width of strut proposed by Staffored Smith (1966) developed the formulations for α_h and α_L on the basis of beam on an elastic foundation is shown below.

$$\alpha_h = \frac{\pi}{2}\sqrt[4]{\frac{4\,Ef\,Ic\,h}{Em\,t\,\sin 2\theta}} \qquad \alpha_L = \pi\sqrt[4]{\frac{4\,Ef\,Ib\,h}{Em\,t\,\sin 2\theta}}$$

Where;

α_L = length of contact between column and infill, mm.

H = Height of the infill wall, mm.

L = length of the infill wall, mm.

I_c = Second moment of inertia of column section, mm^4.

I_h = Second moment of inertia of beam section, mm^4.

α_h = length of contact between beam and infill, mm.

E_m = Young's modulus of elasticity of infill masonry, MPa.

E_f = Young's modulus of frame element, MPa.

Φ = Strut angle with respect to horizontal axis, degree.

t = thickness of the infill, mm.

$E_m = Ω f_m$

f_m -compressive strength of masonry.

The value of a constant Ω equals to 750 for concrete block and 500 for clay brick (Pauley, 1992).

Hendry (1998) has proposed the following equation to determine the equivalent or effective strut width w, when the strut is assumed to be subjected to uniform compressive stress.

$$W=\frac{1}{2}\sqrt{\alpha h^2 + \alpha L^2}$$

Holmes (1963) recommended a width of the diagonal strut equal to one-third of the diagonal length of the panel, where New Zealand Code (NZS 4230) specifies a width equal to one quarter of its length

Similar studies were performed by Mainstone (1971), however claimed that it is different to previous works by not considering the aspect ratio and covering the whole range of behaviours shown by infill in tall structures. The behaviour of infilled structure was distinguished into two and the first one being stressing the infill wall thoroughly assuming a perfect fit between the infill and frames. The second behaviour assumed that the infill and the frames contact only at the compressive corners, in which crushing of infill take place. It was also reported that the corner crushing and the cracking along the diagonal length of the infill would take place depending on the relative strength infill wall and the frame. Thus it was summarised that the relative stiffness of the infill and frame was the important parameter of the infilled structure. The report also includes the usefulness of the Equivalent strut method to estimate the stiffness, strength and the ultimate strength of the system.

The effects of the location of opening on the lateral stiffness of infilled frame were studied by Mallick and Garg (1971) and had recommended possible locations for door and window. The study was conducted on a model with and without shear connectors. It was reported that the structure with shear connector but having opening at either ends reduces the stiffness by 85 to 90% of the fully infilled model. On the other hand, the stiffness was reduced by 60 to 70% for the model without shear connector. Also, it was reported that the stiffness reduces by 25 to 50% when the opening is placed at the centre of the infill wall. Thus, the suggested position for the door is at the centre of the lower half of the infill wall while the window can be placed at the middle height of the infill wall at either side. However, such requirement is stringent and not practical for general residential structures and thus reinforcement of infill wall come into picture.

Since the opening of the infill cannot be considered using the above formula, there are reports in which more numbers of struts can be used to accommodate the effect of opening. Asteris (2003) developed a coefficient to reduce the width of strut element for the infill panel which has opening. Puglisi and Uzcategui (2008) proposed a plastic concentrator to be used with the diagonal strut element, which does the same function as the hinges in beam and column of the reinforced concrete frames. The advantage of using the method is to simulate the inelastic behaviour of the infilled frame, especially in terms of stiffness degradation and low cycle fatigue. Although the diagonal strut model have gained popularity in modelling and analysis of infilled structures, it is only suitable for the study of global structural responses. However, the FE technique is the most preferred method for most of the researchers as it allows understand both local and global responses.

3.4 INFILL WALL WITH OPENINGS

Infill walls in the frame are frequently contained in door and window openings at the different locations, which reduces stiffness and load carrying capacity of the diagonal strut depending upon the size of opening and its location. If openings are small and outside the one of the diagonal strut, its effect may be negligible in stiffness calculations i.e full effect of equivalent diagonal strut will be taken into considerations because the other diagonals of the panel become strut when the load is reversed. If the openings are large and centrally located, it may interfere the diagonal bracing action; thereby causing premature shear failure of the sections on the either side of the opening. Experimental and analytical studies show that centrally located openings may reduce the stiffness and strength of diagonal strut about 75% and 40% respectively.

Simple analytic method for calculating the stiffness of infill panels with openings is not easily available so far. However, Kadir (1974) has suggested an approximation method for analysing infilled panels with openings in which the panel is replaced by a diagonal member of the equivalent stiffness, and the stiffness of this diagonal can be calculated by considering the infill as a frame action from the relationship.

$$K_w = \frac{48\,Ew}{hw\,(hw + hf)} \left(\frac{J1\,Jh}{J1hw + Jh\,lw} \right)$$

Where J_1 and J_h are the moments of inertia of the vertical and horizontal section of the infill frame as shown in fig

Liaus and Lee (1977) have also put forward a method of the calculation of the stiffness and strength of infilled frames with openings using a strain energy method to establish the area of the equivalent diagonal strut. Rigid arms which store no strain energy are introduced to account for the finite width of walls and finite depth of the beam. The effective length of the beam and the height of the walls are given respectively by.

$$L_1 = B + C_1 \qquad L_2 = H + C_2 \leq L'_2$$

Where L'_2 is the distance from the bottom of the wall to the centroid axis of the beam. It is recommended that the value of C_1 should be half the depth of the beam.

3.5 Paper Review

Puglisi, M et al. (2008) proposed a model of the behaviour of the masonry in infilled frames which is based on the theory of plasticity and the concept of an equivalent strut. The conventional strut model is then modified by the inclusion of a new concept:- The plastic concentrator. The idea is that plastic concentrators can be compared with the plastic hinges in the theory of frames. The plastic concentrator links the two bars of the strut model and allows for a transfer of effects between the bars shows in (fig 3.1)

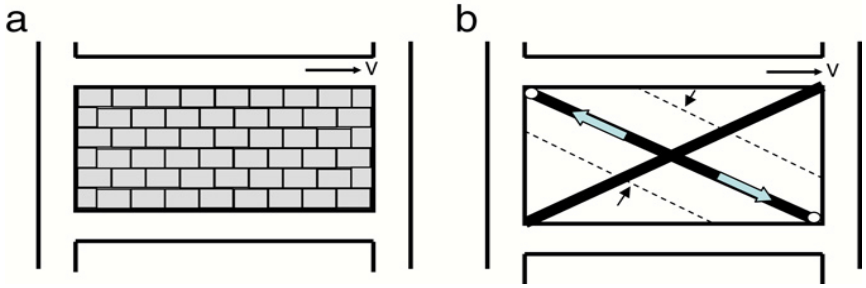

Fig.3.1 (a) Infilled frame (b) Diagonal Strut Model, Puglisi, M et al. (2008)

They modelled structure using two different kinds of elements, beam–columns and infill panels, connected together at the nodes of the frame as shown in (fig 3.2)

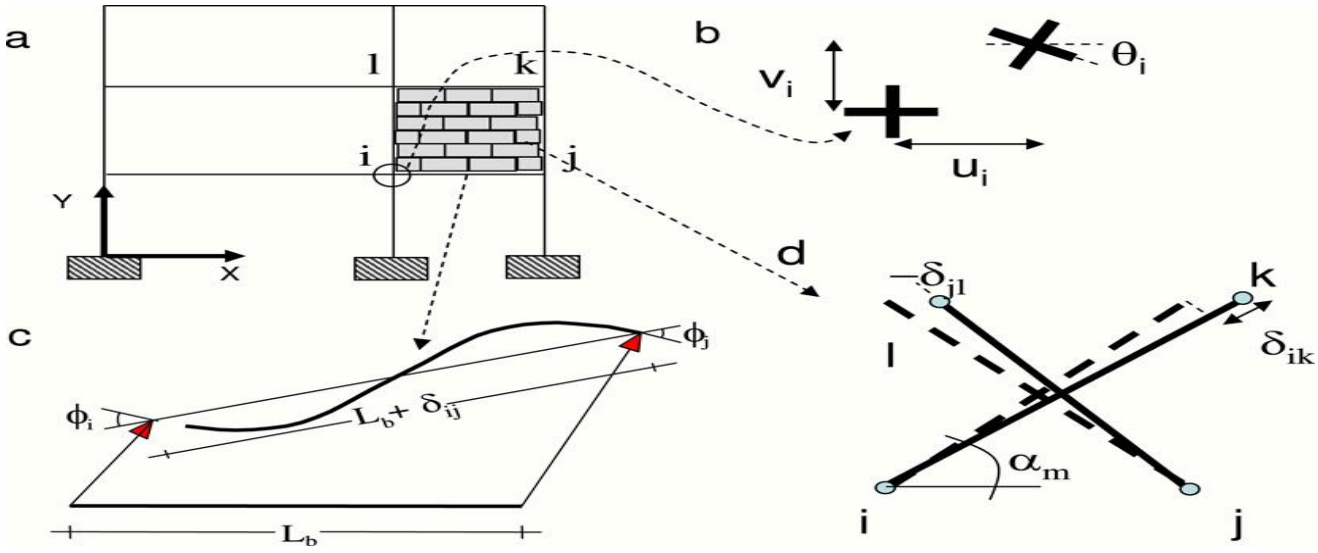

Fig 3.2 (a) Infilled frame (b) Generalized displacements of a node. (c) Generalized strains of a beam–column. (d) Generalized strains of the equivalent infill panel, Puglisi, M et al. (2008)

Perfectly elasto-plasticity without plastic concentrator-

The behavior of the infill panels is usually described by the introduction of a constitutive model for the diagonal bars. For instance, the stress–strain relationships are shown in fig 3.4, In those graphs, tension forces are positive.

In this paper perfect elastic–plastic model for strut behavior has been considered (see in fig 3.4d). It can be noticed that this behavior corresponds to a simplification of the more complex (and more realistic) behavior described in fig 3.4 a,b,c

Author suppose that, an isolated infill element subjected to horizontal displacements as shown in fig 3.5, loading the bar jl generates compressive force, When the force on the bar reaches the value of the yield force, plastic strains start to appear on the bar.

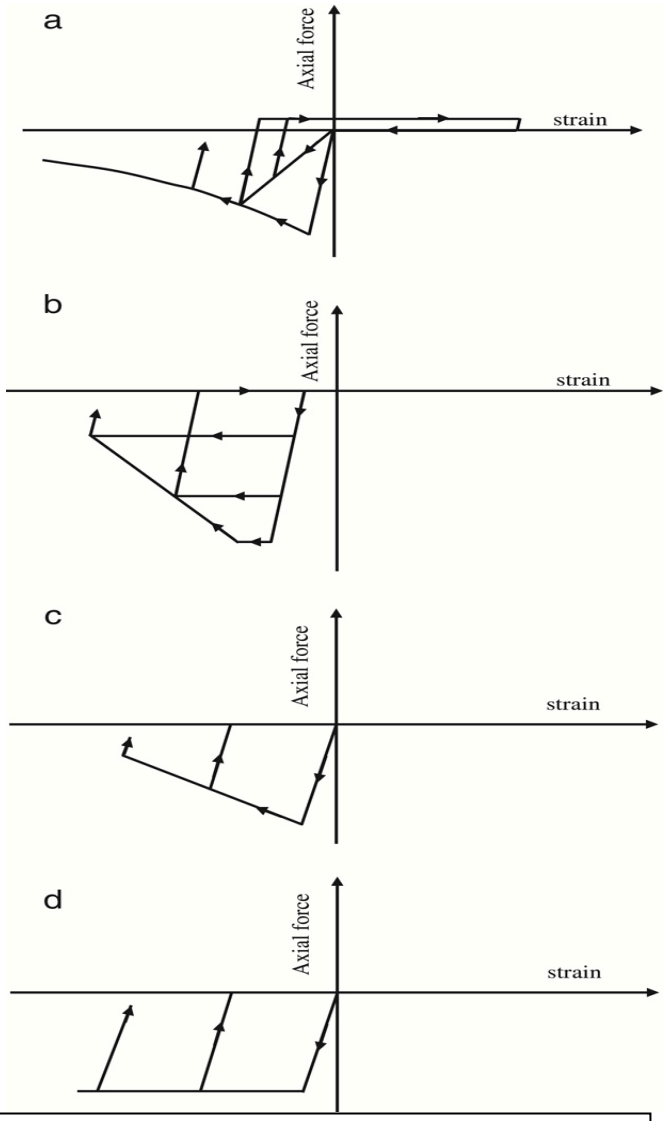

Fig 3.4 (a) Stress-strain relation proposed,
(b) Stress-strain relation proposed in,
(c) Stress-strain relation proposed in,
(d) Perfect elastoplasticity, Puglisi, M et al. (2008)

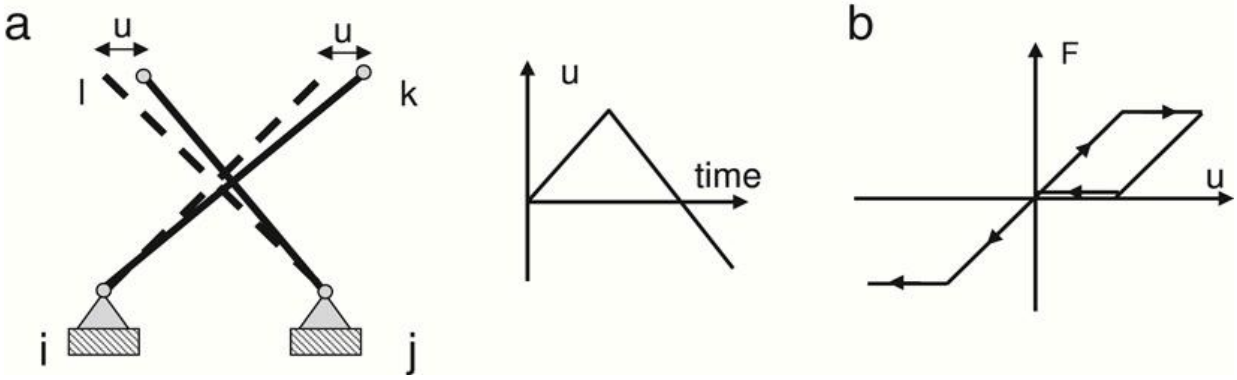

Fig 3.5(a) infill element subjected to horizontal displacements (b) Force v/s displacement, Puglisi,M et al. (2008)

The forces and strains in the ik bar remain nil. Then, there is an elastic unloading. During this process, the compression force decreases with constant plastic strains. The opposite bar remains unloaded. The compression on the bar jl finally reaches the value of zero, but the other diagonal remains unloaded due to the plastic strains in the first bar. The horizontal displacement has to reach the negative values that compensate the plastic strain in the jl bar in order to generate compressions on the bar ik. Therefore, this kind of model generates pinched curves in the load–displacement graphs during the simulation of the behavior of infilled frames. It can be noticed that the same kind of behavior is obtained independently of the envelope used to describe the behavior of the diagonal if both bars are uncoupled.

Experimental analysis of infilled frames- They have considered three types of spcimen as shown in fig 3.6,

Fig 3.6(a) 0-bar specimen (b) 1-bar specimen (c) 2-bar specimen, Puglisi, M et al. (2008)

The second one was called ‘‘1-bar’’ and is represented in in fg3.6 b, It can be noticed that only half of the masonry infill was included. The purpose of this specimen is to observe the behavior of a structure that corresponds closely to the model of uncoupled bars described in the previous section. The external features of the RC frame are: One spam and one level specimen of 1.60 m. The beam and columns’ cross sections are 0.13 x 0.16 m longitudinal reinforcement of 4 bars the 3/8’’ and bars of 0.01 m for the transversal reinforcement. In confined zones the distance between bars is 0.07 m and 0.10 m in the no confined zone. Concrete resistance (f_c) is 4.5E+ 6 kg/m^2. The columns are embedded in across section base beam of 0.25 x 0.35 m and 2.5m of length. Hollow clay bricks were used for the infill. Brick dimensions are 0.05 x 0.10 x 0.20 m. The mixtures for the mortar were done in a 3:1 proportion.

Several specimens were subjected in the laboratory to monosign and cyclic loading shown in fig 3.7. These loadings consisted of displacement controlled horizontal displacements imposed on the top of the frame. The history loading presented in the figure on the right has been called ‘‘monosign loading’’

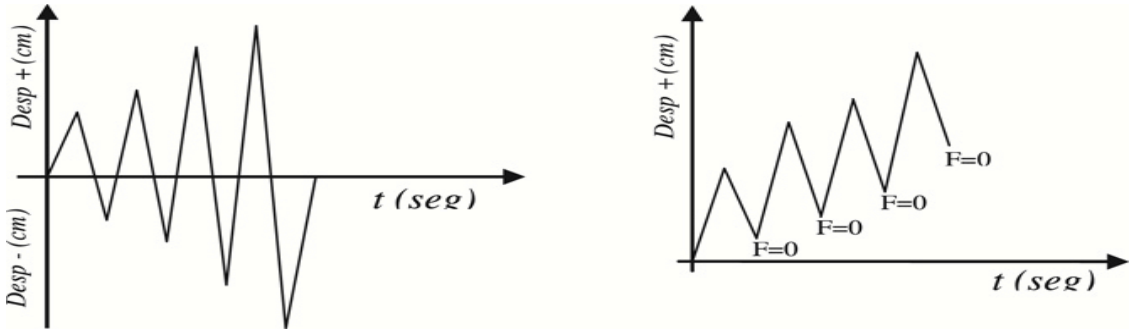

Fig 3.7 (a) Cyclic loading (b) Monosing loadings, Puglisi, M et al. (2008)

In fig 3.8, the results of a cyclic test for three specimens are presented in the form of a displacement–force graph.

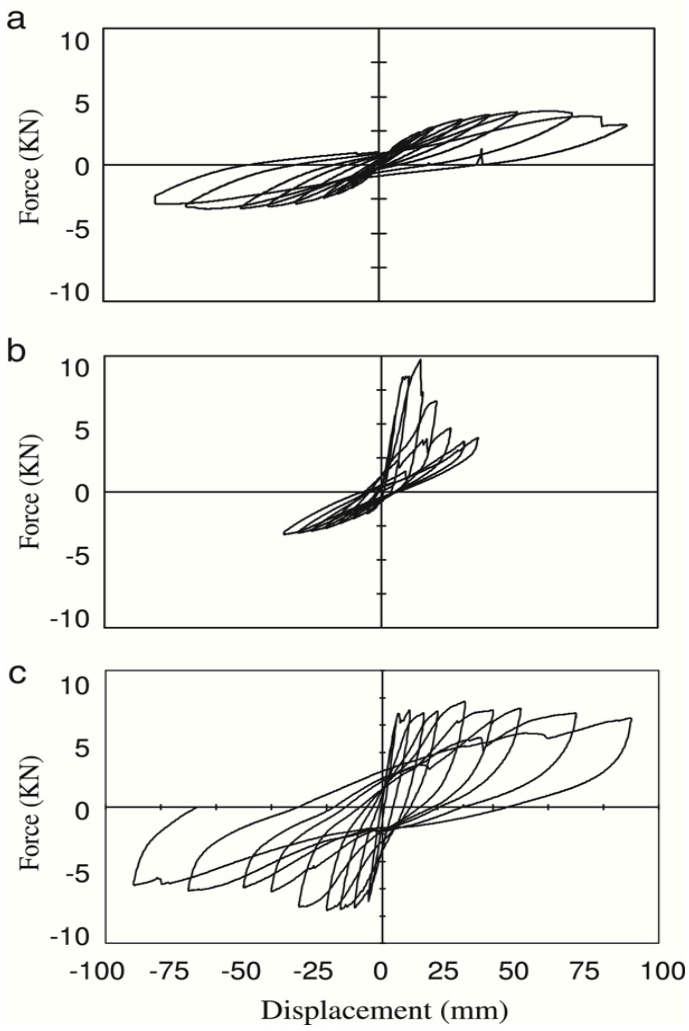

Fig 3.8 Displacement vs. Force (a)0 bar specimen (b) 1 bar specimen (c) 2-bar specimen, Puglisi, M et al. (2008)

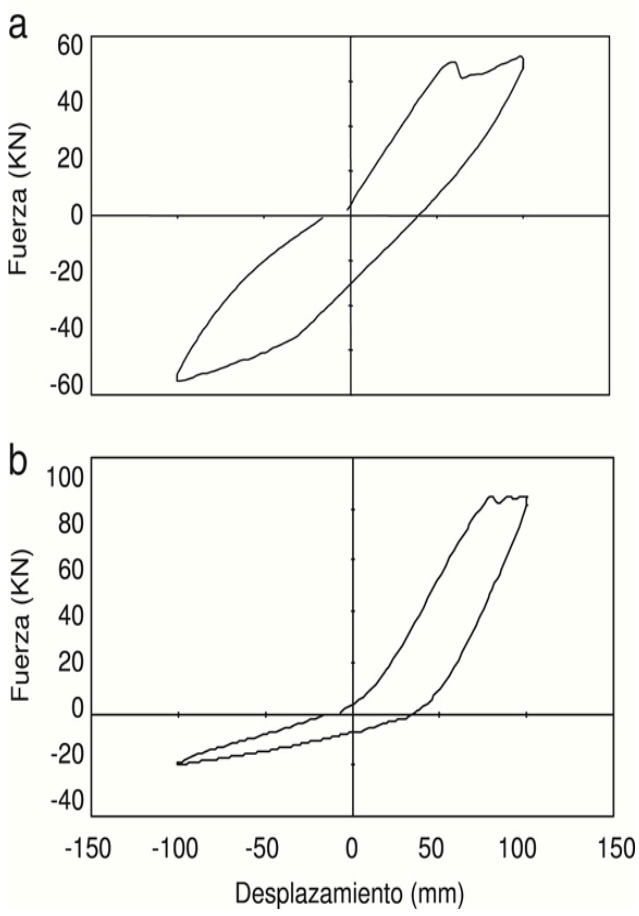

Fig 3.9 (a) Hysteretic loop in the 2 - bar specimens
(b) Hysteretic loop in the 1 – bar, Puglisi, M et al. (2008)

The test on the 0-bar specimen permits us to ensure that no pinching due to slip of the reinforcement is observed (see fig 3.9a) The maximum strength of the 1-bar specimens (see fig 3.9b) is very high, even higher than the 2-bar specimens, but it is less ductile than the 2-bar specimens, and their behavior during the elastic unloading phases is very different. The beginning of the pinching predicted by the

uncoupled bars model can even be appreciated in the hysteretic loops of 1-bar specimens as shown in fig 3.9b. As aforementioned, the 1-bar test could be represented by only one diagonal bar.

Perfect elastoplasticity with plastic concentrator-They consider slight modification of the equivalent strut model is proposed where the two bars are linked by a plastic or inelastic concentrator as shown in fig 3.10 which can be compared by plastic hinge concept for beam-column element, in the sense that plastic strains and other inelastic phenomena will be assumed to be lumped at the concentrator. The concentrator works as some kind of "bidirectional spring'' that has no influence on the elastic behaviour of the infill also noticed that inelastic concentrator does not introduce additional variables or degrees of freedom. In the theory of plasticity of a continuum, very often the assumption of plastic incompressibility is accepted. This hypothesis states that plastic strains induced changes of shape but not changes of volume.

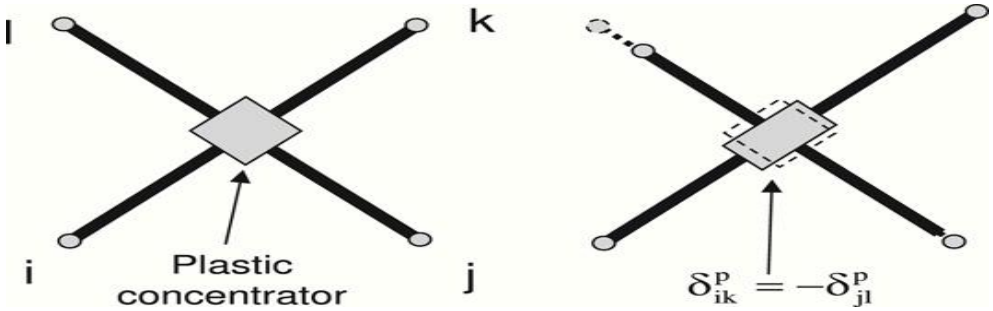

Fig 3.10 Infill panel with plastic concentrator, Puglisi, M et al. (2008)

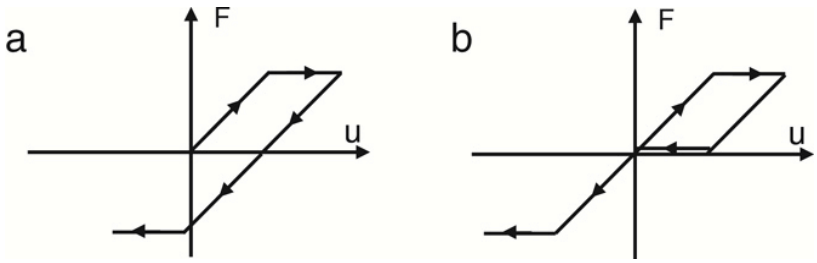

Fig 3.11 Force vs displacement (a) With plastic concentrator (b) Without plastic concentrator, Puglisi, M et al. (2008)

During monotonic loadings the envelope of the force vs. displacement curve is identical for both models (with and without the concentrator). However, in the model with the concentrator, positive plastic strains in the direction of the jl bar appear even if the axial force on this bar is zero. When the force changes sign, compression forces immediately appear on the diagonal ik because of the plastic strains that were generated during the first phase of the loading. Figure 3.5 shows the curve of displacement vs. Force in both cases, with and without plastic concentrator.

A finite element based on the equations described in the second section of the paper and the model of perfect plasticity with the concentrator was developed and included in a commercial finite element program .No additional degrees of freedom related to the plastic concentrator, are needed in the element. In this sense, the new element is as simple as the conventional one With this new element and conventional beam–column elements with perfectly plastic hinges, the tests described in reproduced. The results of this analysis are shown in fig 3.12.

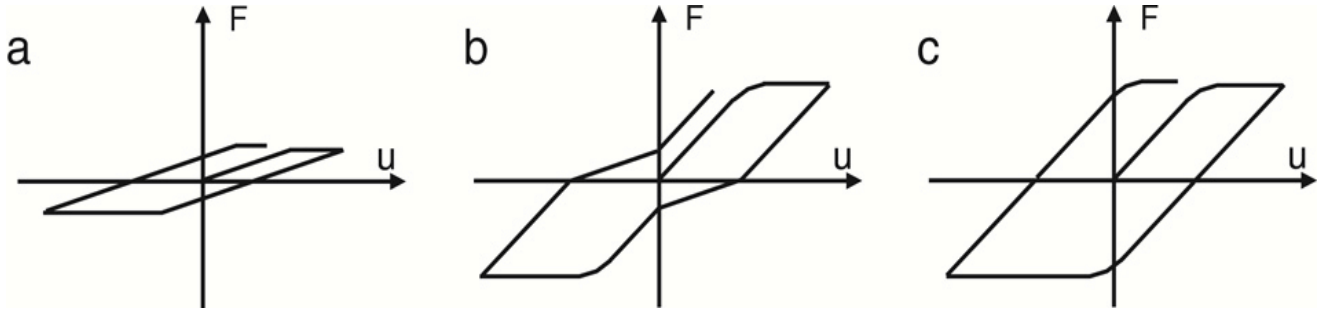

(Fig 3.12) Planar frame with perfect elasto-plasticity (a) Without infill (b) with infill and without plastic concentrator (c) with infill and plastic concentrator, Puglisi, M et al. (2008)

It can be noticed that the model with concentrator leads to the robust hysteretic loops of fig 3.9 a while the uncoupled model results do resemble the part of positive forces of the hysteretic loops in fig 3.9 It must be emphasized that in the experimental results with the entire infill, no pinching is observed. Therefore, the conventional models do not represent correctly the experiments in this important case. Of course, in the latter, the pinched curve is not completely formed It is due to the lack of a second diagonal strut.

Author Conclude that - The model of uncoupled diagonal bars is based on an unrealistic hypothesis since the real infill is a unique element. Thus, the conventional models need to be improved by the inclusion of some coupling between the bars. A coupling strategy has been proposed. The diagonal strut model is modified through the plastic concentrator concept that is similar in many aspects to the plastic hinge notion. The result is a model as simple as the original one but that represents in a more realistic way the observed behavior. Most of the models already available in the literature can be modified by the inclusion of plastic concentrators. It is important to emphasize that the proposed model is still a very simple one and the real behavior is much more complex.

Asteris, P.G (2008) proposed a realistic criterion to describe the frame-infill separation, in order to better simulate the complicated behavior of infilled frames under lateral loads. The behavior of the composite frame not only depends on the relative stiffness of the frame and the infill and the frame geometry, but is also critically influenced by the strength properties of the masonry also increase of dissipated energy. Computational complexity: The particulate in fill material and the ever changing contact conditions along its interface to concrete constitute additional sources of analytical burden. The real composite behavior of an infilled frame is a complex statically indeterminate problem. Structural uncertainties: The mechanical properties of masonry, as well as its wedging conditions against the internal surface of the frame, depend strongly on local construction conditions. He has done review on numerical models of infilled frames, A basic characteristic of a macro- (or simplified) model is that they try to encompass the overall (global) behavior of a structural element without modeling all the possible modes of local failure. Micro- (or fundamental) models, on the other hand, model the behavior of a structural element with great detail trying to encompass all the possible modes of failure.

Macro-Models- Author studied suggested by Polyakov (1960) the possibility about considering the effect of the infilling in each panel as equivalent to diagonal bracing and this suggestion was later taken up by Holmes (Holmes 1961) who replaced the infill by an equivalent pin-jointed diagonal strut made of the same material and having the same thickness as the infill panel and a width equal to one third of the infill diagonal length shown in Fig 4.11. Some researcher related the width the equivalent diagonal strut to the infill/frame contact lengths using an analytical equation which has been adapted from the equation of the length of contact of a free beam on an elastic foundation subjected to a concentrated load.

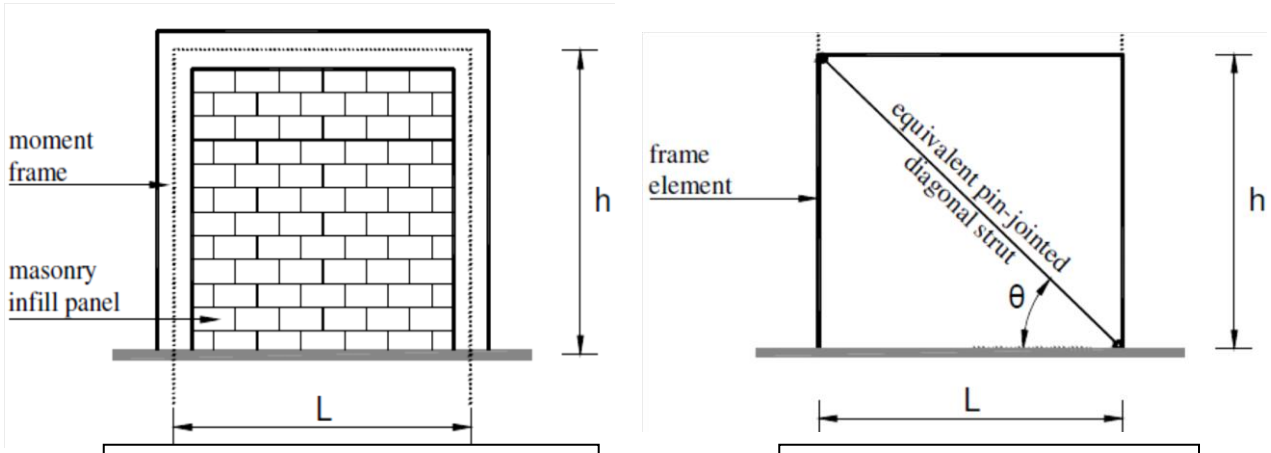

(a) Infilled frame Structures; (b) Infilled frame model

Fig 3.13 Equivalent strut model for masonry infill panel in frame, structures: Asteris, P.G (2008)

In the last two decades it became clear that one single strut element is unable to model the complex behavior of the infilled frames. As reported by many researchers the bending moments and shearing forces in the frame members cannot be replicated using a single diagonal strut connecting the two loaded corners. More complex macro-models were then proposed, but they were still usually based on a number of diagonal struts. Some researcher proposed a model each infill panel by six compression-only inclined struts (Fig. 3.14). Three parallel struts are used in each diagonal direction and the off- diagonal ones are positioned at critical locations along the frame members.

At any point during the analysis of the non-linear response only three of the six struts are active, and the struts are switched to the opposite direction whenever their compressive force reduces to zero. The advantage of this strut configuration over the single diagonal strut is that it allows the modeling of the interaction between the infill and the surrounding frame.

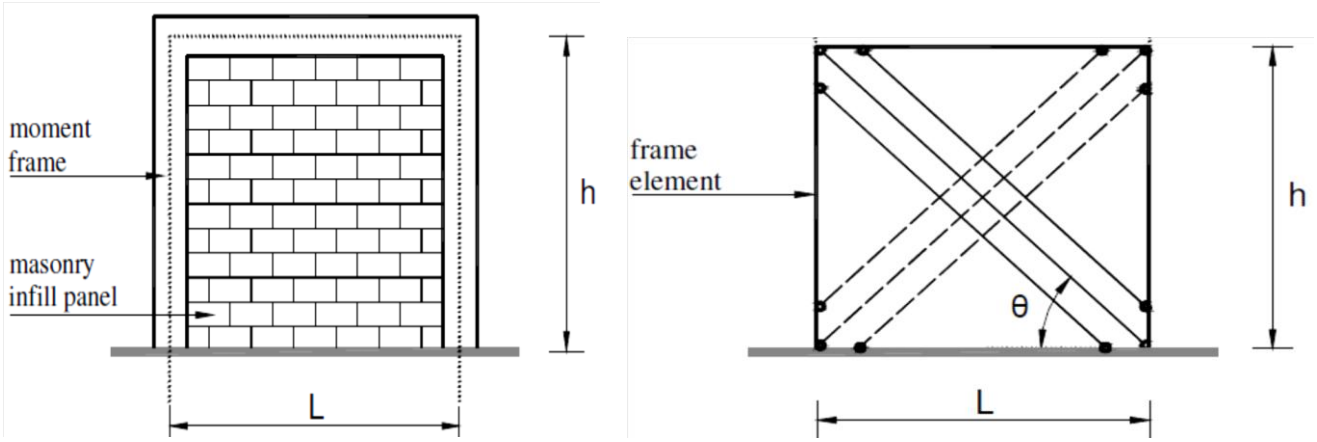

(a)Infilled frame Structures;

(b) Infill frame model

Fig.3.14 Six-strut model for masonry infill panel in frame structures: Asteris, P.G(2008)

Micro-Models

All models described in this section are based on the Finite Element Method, using three different kinds of elements the infill by plane elements, and the interface behavior by interface elements or by one dimensional joint elements..

Mallick and Severn (1967), and Mallick and Garg (1971) suggested first finite element approach. The infill panels were simulated by means of linear elastic rectangular finite elements, with two degrees of freedom at each four nodes, and the frame was simulated by beam element ignoring axial deformation. Several single story rectangular infilled frames under static loading were analyzed and the results were in a good agreement with experimental results if the height to span ratio was not greater than two.

They have studied three different types of elements to study the behavior of infilled frames subjected to monotonic loading. The infill-frame interface was modeled by simple bar type elements capable of simulating both separation and slip. The infill panel was modeled by triangular plane stress elements. In tension, the material was idealized as a linear elastic brittle material. Before cracking, the material was assumed to be isotropic and after cracking was assumed to become anisotropic due to the presence of the crack. It was assumed that for an open crack the Young's modulus perpendicular to the crack and the shear modulus parallel to the crack were zero. When the crack was closed, the Young's modulus was restored, and the shear force is assumed to be taken over by friction. In compression, the panel was assumed to exhibit extensive nonlinearity in the stress-strain relationship. Although the material was subjected to bi-axial stress, it was assumed that the panel was under uniaxial stress based on experimental results, which show that one of the principal stresses is much smaller than the other. Using an iterative procedure with incremental displacement, several four-story one-bay model frames infilled with micro-concrete were analyzed. Close agreement between experimental and analytical results has been observed.

They have studied some researcher used one-dimensional joint elements to model the mortar joint between the infill and the frame, have shown that the behavior of the composite frame not only depends on the relative stiffness of the frame and the infill and the frame geometry, but is also critically influenced by the strength properties of the masonry (in particular, the magnitude of the shear and tensile bond strengths relative to the compressive strength).

A simpler and much quicker finite element technique consists in reducing by condensation, the stiffness of the infill to the boundary degrees of freedom. It is assumed that the frame constrains the form (but not the degree) of de formation on the infill. Separate stiffness's are formed. A constraint relation is assumed between the 12 frame degrees of freedom (DOF) and the boundary degrees of freedom. Thus a congruent transformation of the separate systems to a composite approximate frame-infill system (with only 12 DOF) is possible.

They have proposed a new finite element technique for the modeling of infilled frames. The basic characteristic of the analysis is that the infill/frame contact lengths and the contact stresses are estimated as an integral part of the solution. Especially, the current study aims to calculate the infill/frame contact lengths for the case of unidirectional lateral loading and elastic response of the infill.

The elastic response of composite structure, which is considered to be critical for a thorough understanding of its response under reversed cyclic loading. In order to implement the method, the following are required;

- A criterion for the separation of masonry panel from the surrounding frame.
- A finite element to model the in-plane anisotropic behavior of masonry infill panel.
- A finite element computer program to implement this procedure.

Criterion for the Frame-Infill Separation- In order to model the complicated behaviour of the infilled plane frames under lateral load, a realistic criterion, in terms of physical meaning, is used to describe the frame-infill separation. The objective of the present study is to find a valid geometrical equilibrium condition for the composite structure of the in filled frame under certain loading conditions, given that the real overall behaviour of an infilled frame is a complex, statically indeterminate problem.

The analysis has been performed on a step-by-step basis based on the following:

- The major "physical" boundary condition between the infill and the frame is that the infill panel cannot get into the surrounding frame; the only accepted "natural" conditions between the infill and the frame are either the contact or the separation condition.

The frame, while directly carrying some of the lateral loads, serves primarily to transfer and distribute the bulk of the loads to the infill. The stiffness response of the infill is influenced, to a considerable extent, by the way in which the frame distributes the load to it. Simultaneously, the frame's contribution to the overall stiffness is affected by the change in its mode of distortion, as a result of the reaction of the infill.

The proposed finite element procedure can be summarized as follows:

Step1. Initially, the finite elements of the infill are considered to be linked to the elements of the surrounding frame, at two corner points (only), at the ends of the compressed diagonal of the infill. (When the load is applied, the infill and the frame are getting separated over a large part of the length of each side, and contact remains only adjacent to the corners at the ends of the compression diagonal).

Step 2. Compute the nodal forces, displacements, and the stresses at the Gauss points of the elements.

Step 3. Check whether the infill model points overlap the surrounding frame finite elements. If the answer is negative, step 5 of the procedure is followed.

Step 4. If the infill model points overlap the rounding frame elements, the neighbouring to the previous linked points are linked, and the procedure is repeated from step 2.

Step 5. This final step is a further check on the acceptability of the derived deformed mesh. This check will determine if at any point of the derived contact area, tension is occurred. In particular, what is checked is whether normal stresses along to the x-axis (for the linked points on the vertical part of the interface), and along to the y-axis (for the linked points on the horizontal part of the interface), are tensile. If the answer is negative, the procedure is stopped. If the answer is positive the linked points are considered to be unlinked and the procedure is repeated from step 2.

The Finite Element Model-for the analysis, a four-node isoparametric rectangular finite element model with 8 degrees of freedom (DOF) has been used (Figure 3.15). The major assumption of modeling the masonry behavior under plane stress is that the material is homogeneous and anisotropic. Especially, the material shows a different modulus of elasticity (E_x) in the x direction (direction parallel to the bed joints of brick masonry) and a different modulus of elasticity (E_y) in the y direction (perpendicular to the bed joints). Detail of FE model is given in Asteris,P.G(2008)

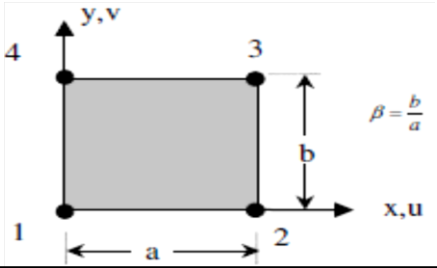

Fig-3.15, Finite element dimensions, Asteris,P.G(2008)

Author Conclude that - A simple analytical method of micro-modeling the complicated behavior of infilled frames under lateral loads. Using this technique, the behavior of single-story single-bay masonry infilled frames under lateral loads has been investigated. Based on the present study, the following conclusions can be inferred: The proposed analytical method calculates the infill/frame contact lengths as an integral part of the solution and not assumed in an ad-hoc way. Especially this technique calculates the infill/frame contact lengths for the case of unidirectional lateral loading and elastic response of the infill. Authors argue that the knowledge of the elastic response of composite structure will be very critical for a thorough understanding of its response under reversed cyclic loading. For that reason, the research focus of our paper concentrates on the elastic domain of the analysis. The proposed technique is easier and more practical to apply, and requires much less computational time than micro-modeling techniques based on discritizing the infill panel as a series of plane stress elements interconnected by a series of springs or contact elements.

Jain, S K et al.(2008) has studied that a masonry infills, which generally have high stiffness and strength, play a crucial role in lateral load response of RC frame buildings. Geographically, there is a large variation in material properties of masonry. Moreover, masonry behaves in a highly nonlinear manner. Therefore, a generalized yet rational model is required for masonry infills that can efficiently incorporate its linear and nonlinear material properties and common failure modes in RC members and masonry infills under the action of lateral forces. Several analytical models for masonry infills are available in literature, for example, equivalent diagonal strut models, finite element models, etc. Therefore, a comparative study was carried out considering different analytical models for masonry infills using experimental results for nonlinear material properties of masonry infills. Analytical models considered in the present study include single-strut model, 3-strut model, and finite element models. By linear and non-linear analyses, it was observed that the 3-strut model can estimate force resultants in RC members with sufficient accuracy, in addition to modeling the local failures in infills and in beams and columns due to interaction between masonry infills and RC frame. It was also observed that the single-strut model can be effectively used in cases where masonry infill walls are discontinued in the first storey to generate parking space.

LINEAR STATIC ANALYSES-A suitability of a model depends upon several upon namely, time required and effort involved in modeling, ability to model lateral stiffness and strength of infilled frame, and ability to model failure modes in not only infills but also in RC members of the frame. A single-bay, single-storey frame of a multi-storey RC building was considered in the comparative study (Fig. 3.16) modeling techniques and assumptions considered in the present study are discussed in the following.

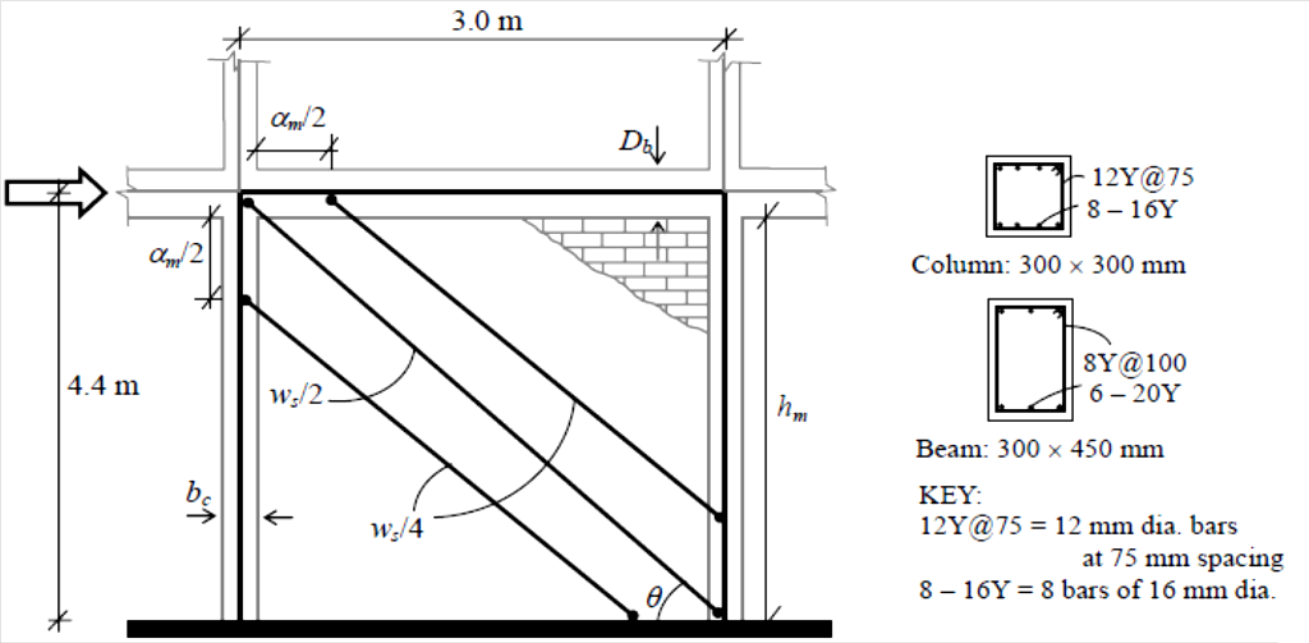

Fig 3.16 Example frame considered in the comparative study and details of 3-strut model for masonry infills, Jain, S.K et al(2008)

Analytical Modeling-The frame was assumed to be fixed at the bottom, and columns and beams of the frame were modeled using two-noded frame or beam elements. M20 Grades of concrete and Fe 415 steel were considered. Masonry infill walls were modeled as (1) equivalent diagonal struts (1-strut and 3-strut) using two-noded beam elements, (2) finite elements using 3-noded and 4-noded shell elements. Transfer of bending moments from RC frame to masonry was prevented by specifying moment releases at both ends of the struts. In case of finite element modelling (using shell elements), only membrane action in shell elements was considered, and bending action ignored. Modulus of elasticity of masonry E_m was taken as 550 f'_m in MPa, where f'_m is the compressive prism strength of masonry in MPa.

Width of equivalent diagonal struts (w_s) one-third to one-fifth has been used by author. It has also been shown that width equal to one-third of the diagonal length represents the upper bound value. An average value of one-fourth of the diagonal length of infill (d_w) was used in the present study. In case of the model with 3 struts, width of central diagonal strut was taken as one-eighth of the diagonal length of wall, and width of off-diagonal struts as half the width of the diagonal strut. In this way, total width of all equivalent struts considered was one-fourth of the diagonal length of wall. In 3-strut model, location of equivalent struts is an important parameter. Out of the three struts, the off-diagonal struts were connected to the columns at the centre of the distance α_m known as the vertical length of contact between infill and column (Fig.3.16):

$$\alpha_L = \frac{\pi}{2} \sqrt[4]{\frac{4 E_f I_b h}{E_m t \sin 2\theta}} \text{ mm}$$

where E_c and E_m are modulus of elasticity of column and masonry material in MPa, respectively, I_c is moment of inertia of column section in mm^4, h_m and t are height and thickness of masonry infill wall in mm, respectively, and θ is angle in degrees of inclination of the equivalent diagonal strut with the horizontal. It was observed in the present study that varying the length of contact between infill and beam does not change the analyses results considerably. Therefore, the horizontal length of contact between infill and beam was considered same as the vertical contact length between infill and column.

Linear analyses of the frame were carried out using SAP2000 considering six different models including the bare frame model. Under the effect of increasing lateral forces, contact area between masonry infill wall and RC frame reduces. To study the effect of reduction in contact area between

RC members and masonry infills, three finite element models were analyzed by considering different contact areas between RC frame and infill are shown in Fig. 3.17. Self weight of full masonry wall was considered in all the models. The left and right columns of the frame are referred as "L" and "R", respectively.

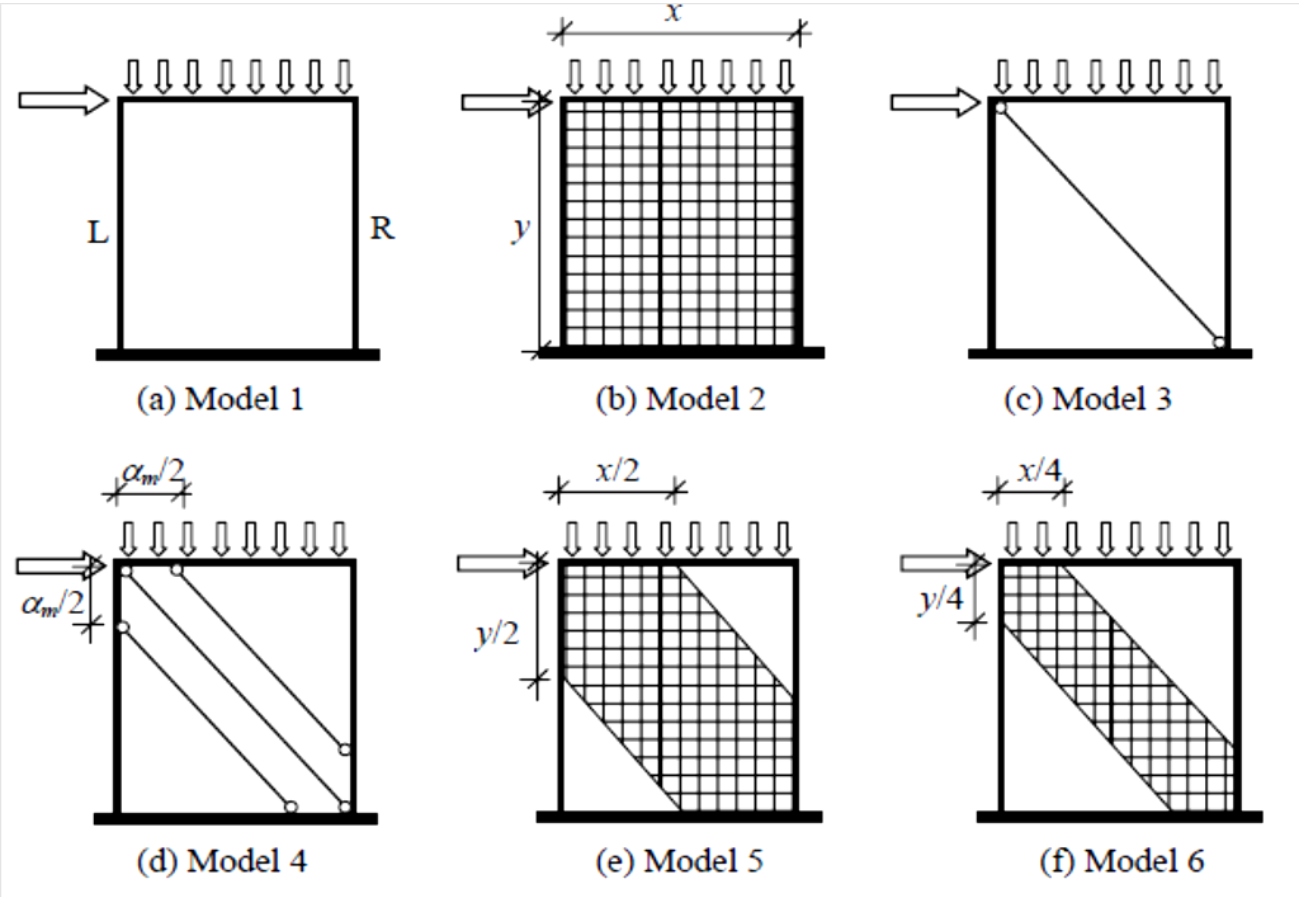

Fig 3.17 Different analytical models studied:(a) Model 1- bare frame, (b) Model 2-full infill wall modelled using finite element model,(c) Model 3-infill wall modeled using a single diagonal strut,(d) Model 4–infill wall modeled using three diagonal struts,(e) Model 5-partial infill wall modeled using finite elements such that only half of length of beam and column was in contact with the wall, and (f) Model 6-partial infill wall modeled using finite elements such that only quarter of length of beam and column was in contact with the wall, Jain, S.K et al (2008)

Results of linear static analysis-Linear static analyses of the 6 models were carried out under the action of vertical dead loads (DL) and lateral earthquake loads (EQ), and corresponding maximum force resultants in columns and beam of the frame obtained for the load case 1.5(DL+EQ) are compared in this section. It was observed that force resultants, most noticeably the bending moment, reduce considerably when stiffness of infill was considered in the analytical model, because most of the lateral forces were then transferred to the infill wall as axial forces. With increase in lateral forces on the frame, area of wall in contact with RC frame reduces because of separation of wall from RC frame near the tension-diagonal joints. In other words, effective lateral stiffness of wall, and therefore the effective width of equivalent diagonal strut reduce with increase in the lateral forces. Effect of this on RC columns may be considered similar to creation of short columns because of varying

unsupported length of columns under increasing lateral forces15. Therefore, Model 2 (full shell) and Model 3 (1-strut) may not adequately capture the actual behaviour of the masonry-infilled RC frame because these models consider full stiffness of infill wall irrespective of the extent of lateral forces.

In reality, under increasing lateral loads Model 2 (full infill) should first transform into Model 5, and then into Model 6. Interestingly, a consistent increase in force resultants was observed in columns when 3-strut model was used as compared to the 1-strut model (Fig. 3.18). This increase in force resultants of columns in 3-strut model was primarily due to partial contact between the ductile RC frame and relatively stiffer masonry infills. Force resultants in columns obtained using 3-strut model were found to be matching more closely with that obtained using partial shell models (Models 5 and 6). Therefore, the 3-strut model appears to be more accurately representing the behaviour of masonry infills under lateral forces. Similar increase in axial forces was also observed in the beam in case of 3-strut model as compared to the 1-strut model (Fig.3.19). On the other hand, a slight reduction was observed in shear forces and bending moments in beam when 3-strut model was used as compared to the 1-strut model (Fig.3.19). However, the force resultants in beam obtained using 3-strut model were also found to be more closely matching with that obtained using the partial shell models. This further supports the case of using a 3-strut model for masonry infills.

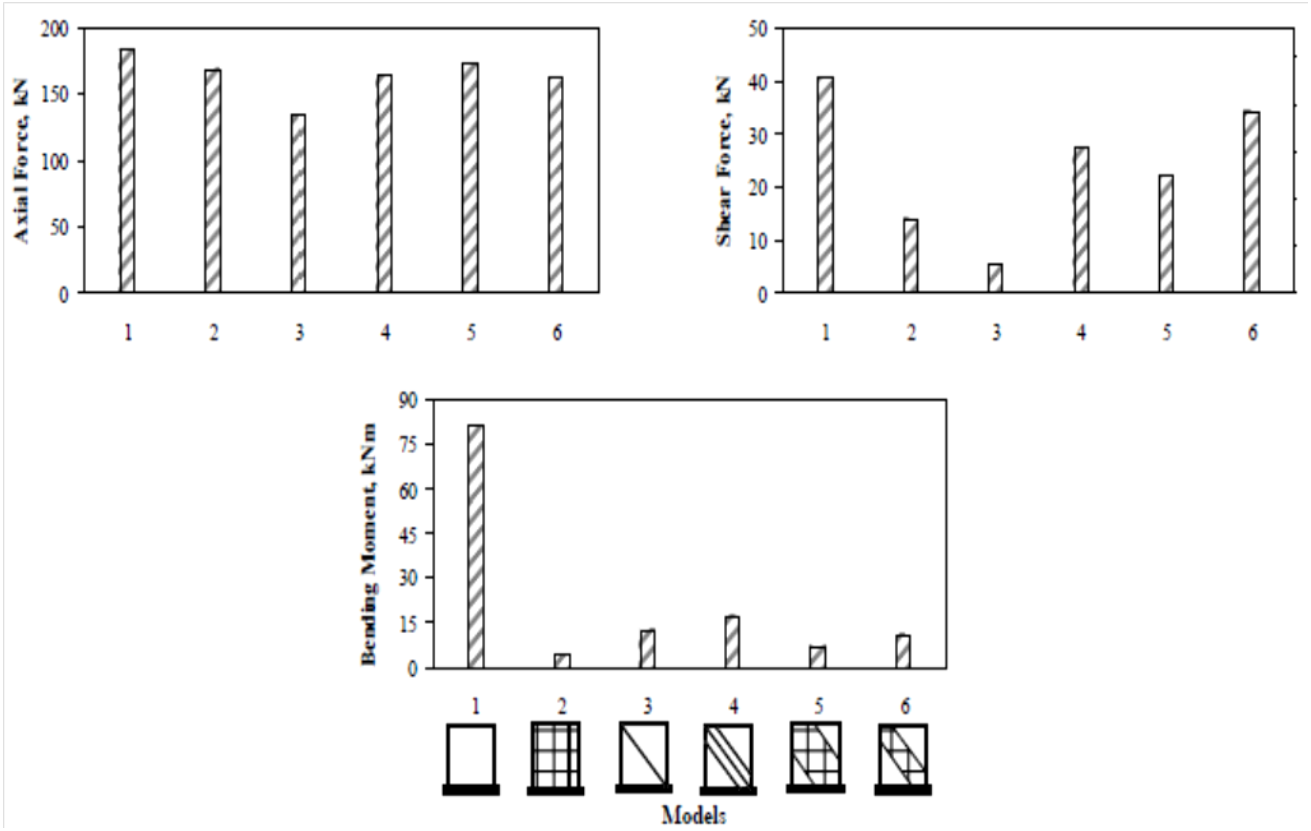

Fig 3.18, Comparison of maximum force resultants in columns for load case 1.5(DL+EQ) obtained using the six modeling schemes. Jain, S.k at el. (2008)

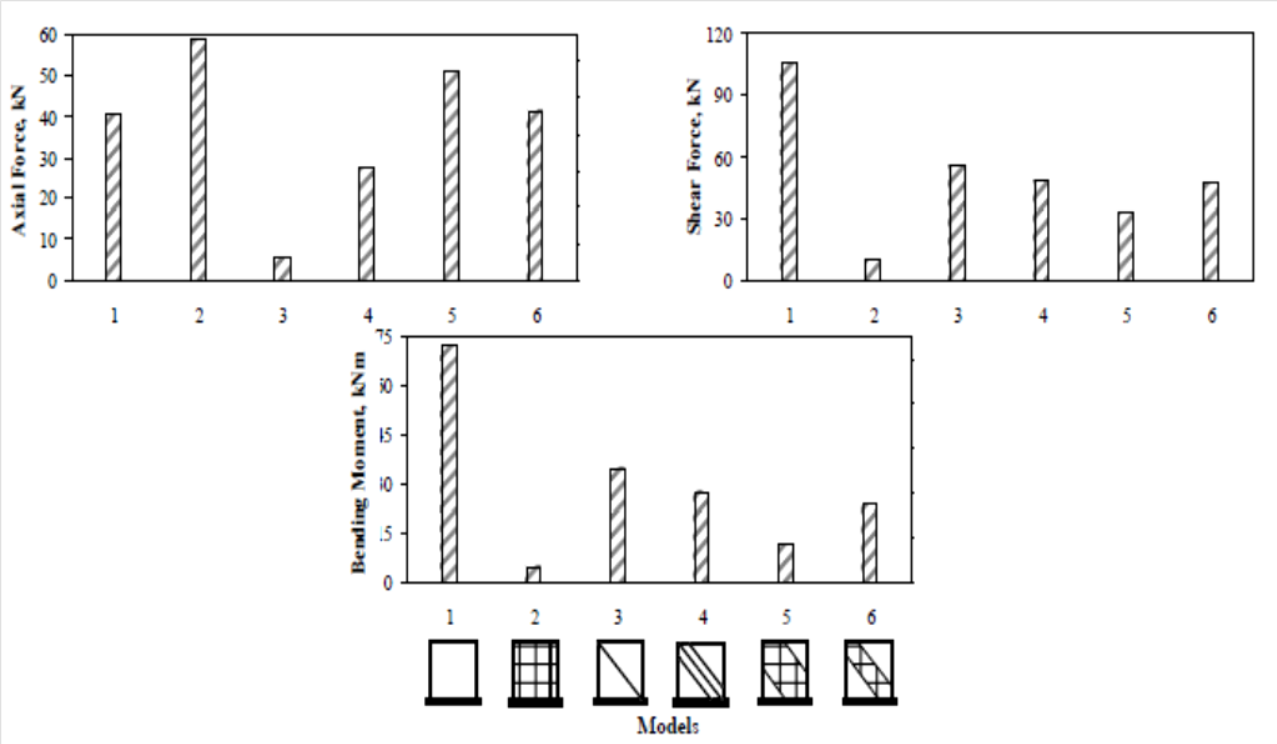

Fig 3.19, Comparison of maximum force resultants in beam for load case 1.5(DL+EQ) obtained using the six modeling schemes. Jain, S.K et al.(2008)

Results of linear static analyses indicated that the RC frame members may be subjected to significant increase in force resultants due to presence of partial masonry infills; this is in contrast to the behaviour of fully-infilled frame. Force resultants in RC columns obtained using the 1-strut models were found to be less than those obtained using 3-strut models and partial shell models. Therefore, the 1-strut model underestimated the design lateral forces for masonry-infilled RC frames. Also, force resultants in RC beam and columns in case of 3-strut model were observed to be matching more closely with those obtained using the partial shell models, which more accurately represent the lateral load behaviour of masonry infills. As a result, the 3-strut model appears to be a better choice than the other models because of its simplicity over the finite element models, and its effectiveness in predicting the realistic force resultants in RC frame elements. In order to substantiate these results further, non-linear static pushover analyses were carried out for: 1-strut model and 3-strut model.

NONLINEAR STATIC PUSHOVER ANALYSIS-Non-linear static pushover analysis involves pushing structures laterally until a pre-specified lateral force or displacement is reached. In the present study, SAP2000 was used for displacement-controlled pushover analyses of Model 1 – bare frame, Model 3 – 1-strut model, and Model 4 – 3-strut model to understand difference in their behaviour in non-linear range. Non-linear material properties for different structural members are required to be specified in pushover analysis in addition to the elastic material properties discussed in linear analysis. In SAP2000, non-linearity is not distributed along length of members; instead,

lumped plasticity is modeled at desired locations on members. Modeling of non-linear material properties in RC and masonry members of the frame is discussed in the following.

Modeling of RC members-Plasticity in RC members was assumed to be lumped at probable locations. Plastic hinges were assumed to form at a distance equal to half the average plastic hinge length l_p from the member ends; l_p was calculated using the following expression:

$$l_p = 0.08L + 0.022db\ f_y\ (m)$$

where L is length of member in m, d_b is diameter of longitudinal steel in m, and f_y is yield strength of longitudinal steel in MPa. Plastic hinges that generally develop in RC members are those corresponding to flexure and shear. Flexural hinge properties involve axial force – bending moment interaction (P-M) as failure envelope and bending moment – rotation (M-θ) as corresponding load deformation relation. On the other hand, shear hinge properties involve shear force – shear deformation relation (V-Δ). P-M interaction properties for RC columns were developed using the work of various researchers who used the stress-strain model for confined concrete developed by Razvi and Saatcioglu, and the stress-strain curves for reinforcement bars were obtained experimentally (ultimate strain ≈ 14.5%, ultimate stress ≈ 1.25fy). Strength and deformation properties for M-θ model were calculated using a simplified method in which bending moment diagram of a member under lateral forces are assumed to vary linearly. And if the point of contra-flexure is in the mid-span, a member fixed at both ends can be replaced by an equivalent cantilever of half span with a concentrated load at its tip. The *M-θ* relationship for the linear distribution of moments was obtained using the moment-curvature relationship of the section. The ultimate rotation values given in FEMA12 were simplified and taken as 1.5 times to 2.0 times the rotation corresponding to the maximum moment capacity for the section. Strength characteristics of the shear hinge (*V-Δ*) model for RC members were calculated using the relevant Indian Standards. Shear failure of RC members was considered to take place when shear strength of section was reached, and the failure was assumed to be force-controlled because of the associated brittleness. Typical hinge properties for RC members are shown in Fig. 3.20.

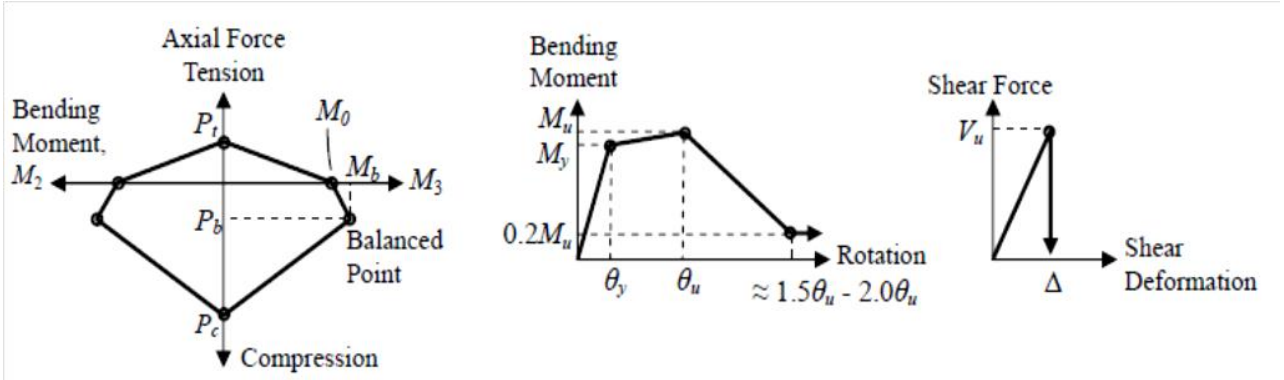

Fig 3.20 Typical hinge properties assigned to RC members of the frame. Jain, S.K et al (2008)

Modeling of masonry infills-In the model used in non-linear pushover analyses, masonry infills were modeled using compressive diagonal struts along the loaded diagonals. Stress-strain curves for masonry under compression were assigned as axial hinge properties to the struts. The non-linear stress-strain curves were obtained in an experimental study in which four different bricks and three different mortar grades were used to construct masonry prisms (5 bricks high). Average compressive strength of the burnt clay bricks used in the study was 21 MPa with coefficient of variation (COV) of about 30%. On the other hand, average compressive strength of the three grades of mortar cubes of 50 mm size was 3 MPa with about 20% COV , 20 MPa with about 8% COV, and 15 MPa with about 6% COV.The tests were carried out as per the relevant ASTM Standards.

Stress-strain curves for masonry prisms were obtained by averaging the test data from seven specimens of each combination of bricks and mortar (total 84 specimens). In order to capture non-linear characteristics of the stress-strain curves, displacement controlled servo-hydraulic actuators were used to apply compressive forces on masonry prisms and corresponding compressive deformations were recorded using Epsilon extensometers. The average stress-strain curves for masonry prisms obtained for the three grades of mortar are shown in Fig. 3.21

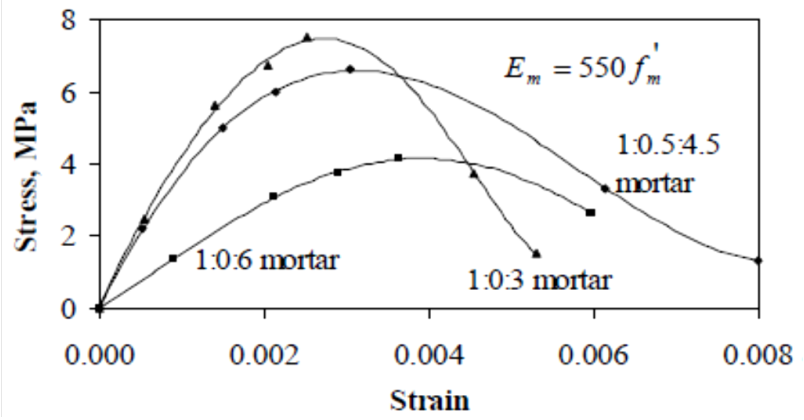

Fig 3.21 Non-linear stress-strain curves for masonry prisms under compression. Jain, S.K et al(2008)

The average compressive strength of masonry prisms obtained in the study for the three grades of mortar was 4.1 MPa with COV of about 25% , 7.5 MPa with COV of about 20% (1:0:3 mortar grade), and 6.6 MPa with COV of about 20% . In the present comparative study, stress-strain curve corresponding to the mortar grade 1:0:3 was used to model non-linear material properties of the struts.

Results of Non-Linear Static Pushover Analyses-Pushover curves obtained by non-linear static analyses of the three models are shown in Fig. 3.22. For better comparison between different models, base shear and lateral displacement obtained by pushover analyses of the three models are normalized with respect to those obtained for the 1-strut model. As expected, initial stiffness of masonry-infilled frame was found to be significantly large as compared to the bare frame, and initial stiffness exhibited

by Models 3 and 4 matched quite well. Most of the initial base shear was resisted by masonry infills because of their large initial stiffness; therefore, lateral strength of models with infills was found to be much higher than that of the bare frame.

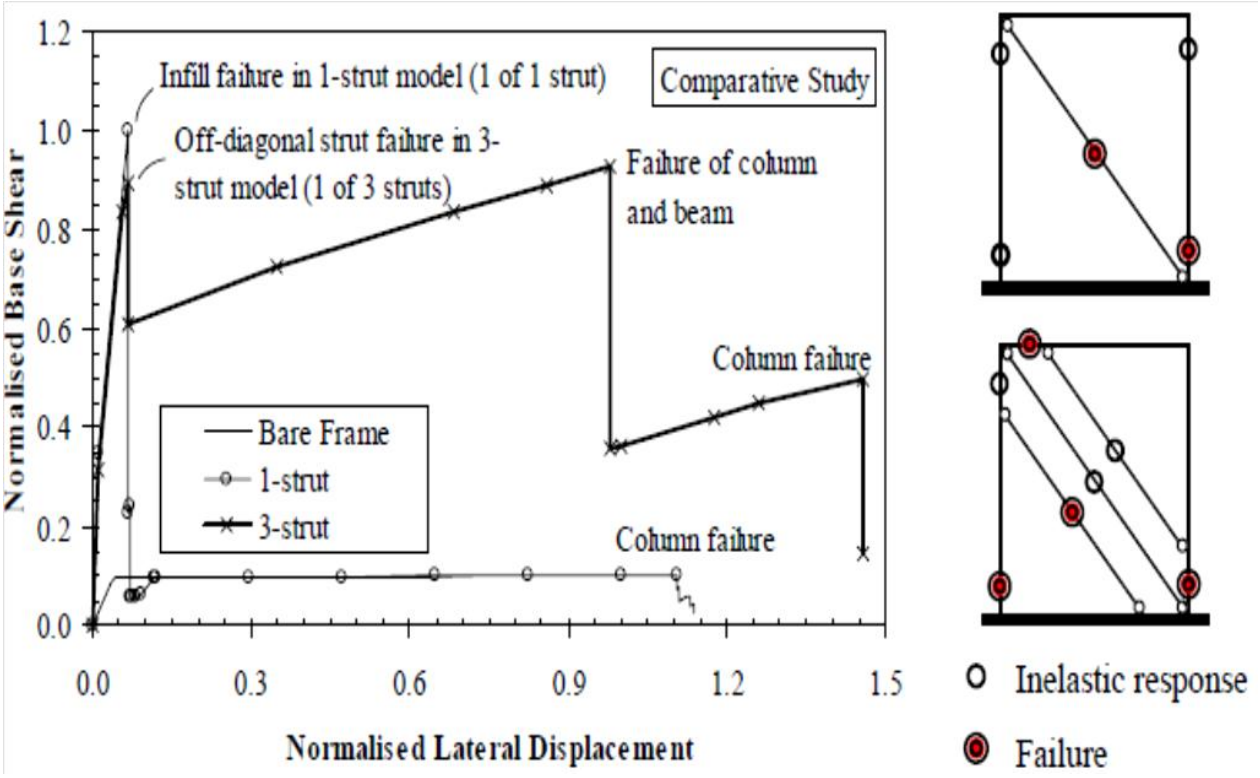

Fig 3.22, Pushover curves and plastic hinge formation in Models 1, 3, and 4. Jain, S.K et al(2008)

In Model 3, the single strut carried large amount of axial force, and therefore abrupt reduction in lateral strength of the frame was observed after failure of infill wall (modeled using a single strut). After failure of the strut, behaviour of Model 3 became similar to the bare frame model. This characteristic behaviour of 1-strut model is far from realistic performance of masonry-infilled frames in which infill walls do not fail abruptly. In comparison, lateral strength of Model 4 (3-strut model) was found to be only about 10% less than that of 1-strut model. In 3-strut model, presence of off-diagonal struts was responsible for development of large shear forces in columns of the frame. Moreover, lateral strength of the frame did not reduce drastically because of progressive (one-by-one) failure of the three struts. Flexural and shear failure of beam and columns resulted into failure of the RC frame.

Clearly, use of 3-strut model appears to be a more realistic and rational choice because of presence of off-diagonal struts, which distribute the stiffness of infills to a larger area, and therefore enforce gradual failure of infills. Moreover, unlike the 1-strut model, the 3-strut model was also found to model the local failures in RC beams and columns.

Author Conclude that-In a comparative analytical study involving various analytical models for masonry infills in a single-storey, single bay RC frame, the 1-strut model was found to be predicting the global behaviour (initial stiffness and ultimate failure load) of the system with reasonable accuracy. On the other hand, 3-strut model was found to be estimating the force resultants in the frame members more accurately as compared to that of a 1-strut model. Moreover, the 3-strut model was found to model local failures in the frame members in addition to the compressive failure of struts.

Under lateral forces when strut action develops, a finite area of infill is physically connected to the beams and columns of the frame. This finite area, which can be effectively modeled using a 3-strut model, is responsible for distribution of large stiffness of infill walls to a larger area on beams and columns; this prevents abrupt failure of masonry infills under increasing lateral forces. The finite area is also responsible for local shear failure in beams and columns, and in a 3-strut model, this failure mode can be represented in a more appropriate manner. Moreover, design force resultants in RC beams and columns can be obtained more accurately when 3-strut models are used. Therefore, the 3-strut model appears to be physically more appropriate than the 1-strut model for masonry-infilled RC frames.

Gosh, A.K and Amde M. A (2001) using reinforced concrete frames, the improvement in strength ranges from twice to over quadruple the strength of a frame with no fill. Stiffness improvement is still more substantial, with increase up-to 60 times over that of a bare frame (Mehrabi 1994). The stiffness of steel frames infilled with masonry, especially where the connections between the beams and the columns resist shear only, can be a few hundred times that of the frames without any infill. In last three decades and particularly as a result of damage from major earthquakes, the use of masonry infill has become increasingly recognized. Similarly, older buildings may be rehabilitated with infills that are compatible with the original framework. Achieving these objectives requires not only a theoretical understanding of infilled frames, but also the development of simplified, and therefore practical, design methods. At moderate load the infill of an infilled frame separates from the surrounding frame and the infill behaves as a diagonal strut. As the racking load is increased, failure occurs eventually in either the frame or the infill. In most common situations, the in-plane lateral load applied at one of the top corner is resisted by a truss formed by the loaded column and the infill along the diagonal connecting loaded corner and the opposite bottom corner. The state of stress in the infill gives rise to a principal compressive stress along the diagonal and a principal tensile stress in the perpendicular direction. If the infill is made up of concrete, successive failure, initially by cracking along the compression diagonal and then by crushing near one of the loaded corner or by crushing

alone, will lead to collapse; if the infill is made of brick masonry, an alternatively possibility of shearing failure along the motor planes may arise.

The following infilled frames tested by previous researchers have been chosen by Author.
Riddington (1984) Frames, Pook and Dawe (1986) Frame

Two square infilled frames were tested; one is stiffer compared to the other. The stiffer frame was made of 406×406×39 mm wide flange section with 2485×2485 mm block masonry. The flexible frame was made of 152×152×30 mm wide flange section with a 2,170×2,170 mm infill. Due to loading system failure during the first test at 33 days, the stiff frame was tested again at 47 days. The infills were formed from 440×215×100 mm dense aggregate blocks of 7N/mm^2 compressive strength together with the masonry cement and sand mortar. The Young's modulus and the Poisson's ratio of the block masonry infill were found to be 15.4kN/mm^2 and 0.15, respectively. The shear bond strength and the coefficient of friction of the interface between the infill and the frame were experimentally found to be 0.7 N/mm^2 and 0.64, respectively.

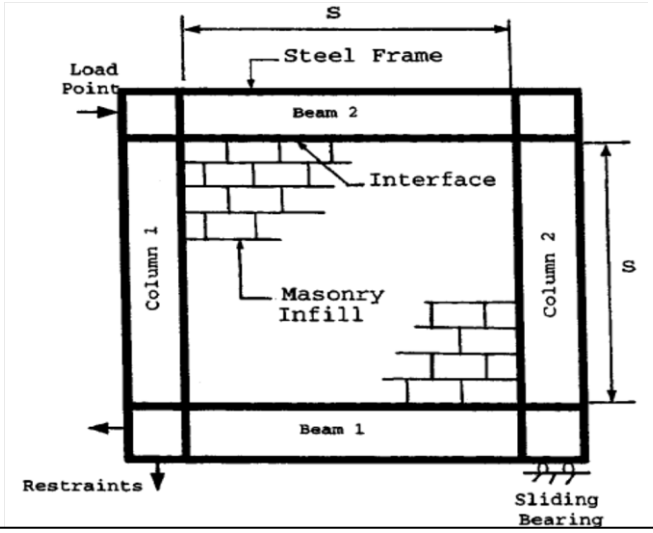

Fig 3.33 Infilled Frame tested by Riddington (1984) Gosh, A.K and Amde M. A (2001),

The test Specimen is a shear panel, consisting of standard 400×200×200 mm cellular concrete block units and type S motor joints with standard truss reinforced in alternate bed joints, enclosed in a steel frame. The steel frame, consisting of W250×46 beam rigidly connected, measured 3600mm long and 2800mm high. Material properties given are compression strength of block motor couplet= 33Mpa; motor strength =20 Mpa.

Interface Element Formulation-The mortar joint inside the infill and that between the infill and the frame are modeled by the interface element;
In pure tension, the ultimate tensile strength of the mortar joint, f_t, is its elastic limit. Similarly, in the absence of normal loading, the elastic limit in shear is the cohesive strength c. In the presence of a

compressive normal load, shear strength is the summation of the cohesive strength and the mobilized friction, c-$\mu\sigma$. When combined, these three fundamental criteria of strength lead to the yield or fracture criterion. The Mohr-Coulomb yield criterion, which predicts lower frictional coefficients at higher normal loading, has perhaps been the most commonly used criterion for modeling rock joints, mortar joints, and other similar interfaces (Plesha et al. 1989). However, experimental shear tests on mortar joints, in the presence of various normal loadings, performed by Nuss et al. (1978) and Amadei and Atkinson (1989) show very small or no variation of the frictional coefficient with variation of the normal load. A simplified yield criterion is proposed here which has two segments with a smooth transition between them. In the compressive normal loading region the yield criterion in terms of the stresses and the strength parameters is given by,

$$F(\sigma, k) = |\tau| - c + \mu\sigma = 0$$

In the above equation, k=amount of fracture energy released. For example, the current amount of energy released in pure tension is given by

$$\kappa = \int_0^{\epsilon^p} f_t d\epsilon^p = G_f^1 \left\{1 - \frac{f_t}{f_{t0}}\right\}$$

in which ϵ^p plastic strain; $G^I f$ =fracture energy release rate in pure tension; f_t and f_{t0} = current and initial tensile strengths, respectively. The current amount of energy released is also related to the initial and current cohesive strengths, and the fracture energy release rate in pure shear, $G^{II} f$, in a similar manner. The cohesive strength is normally higher than the strength in pure tension. To obtain the yield curve in the tensile normal load region, a polynomial of arbitrary order *n*, in the form $A\tau^n + B\sigma + C = 0$, is fitted to the tensile fracture strength and the cohesive strength. Also, to avoid any kink in the yield curve, the tangent to the parabola at s50 is matched with the yield line for the compressive normal load region. The yield criterion, in the tensile normal loading region, thus obtained is given by

$$F(\sigma, k) = |\tau|^n - \frac{C_0^n}{f_{to}} + (f_t - \sigma) = 0$$

in which the subscript 0 refers to the initial values of the strength parameters c and f_t and $n = \frac{C_o}{\mu f_{to}}$ is the degree of the curve, which is assumed to remain constant during the plastic deformation. At any time step during the plastic deformation, c changes as a function of the tensile normal strength $f\,t$ and the new value of c is inserted in $F(\sigma, k)$.

Experimental results on dilatant interfaces (Amadei and Atkinson 1989) indicate that the higher the compressive stress, the lower is the dilatancy. To predict this behavior, the potential function is assumed to be elliptical and is given by

$$Q(\sigma, \kappa) = \eta a^2(\sigma + p_a)^2 + b^2\tau^2 - 1 = 0$$

in which a and b are, respectively, the reciprocals of the major and minor axes, a=1/(pa+$f\,t$) and b=1/(c+$p_a\mu$). The normal stress pa is the stress at which dilatancy due to shear loading is zero and is

the center of the ellipse, and h is the dilatancy control parameter. Also, dilatancy is reduced with increase of the cumulative relative tangential displacement (Amadei and Atkinson 1989; Pande et al. 1990). Accordingly, h is assumed to decrease exponentially from an initial value of h0 with plastic shear deformation γ^pas

$$\eta = \eta_{oe^{-\theta}\gamma^p}$$

Material Properties-The material properties for the infill are determined using the formulas (1) modulus of elasticity=650*f'm* (2) elastic limit of masonry strength=1 /3 *f'm* ; (3) plastic strain at masonry compression failure ranges between 0.0008 and 0.0013; (4) tensile strength of masonry=0.05*f'm* .

The modulus of elasticity of the structural steel is the same as those listed by Riddington (1984). The elastoplastic behavior of the structural steel is given by the following: the elastic limit strength of the material is 248 MPa; then strain hardening starts and continues up to 372 MPa at plastic strain of 0.0095.

The material properties for the mortar joints between the infill and the frame, modeled as interface elements, are given in Table 4.1. In this table, *E* and *G* denote the Young's modulus and the shear modulus, respectively; f_{t0} and c_0 are the initial values of the ultimate tensile strength and the cohesive strength, respectively; m is the coefficient of friction; *pa* ,η , and θ are described in the ''Interface Element Formulation'' section. The values of these properties have either been estimated from the experimental results of Amadei and Atkinson (1989) or obtained in the process of calibration of the model using the same experimental results. The parameters h and u are unitless. The parameters $G^I f$ and $G^{II} f$ are the fracture energy release rates in pure tension and in pure shear, respectively. The shear modulus is half of the Young's modulus because the Poisson's ratio of the mortar joints is assumed to be zero.

Table 3.1 Material Parameters for Mortar Joints Modeled as Interface Elements

E(Mpa)	G(Mpa)	f_{to}(Mpa)	c_o(Mpa)	μ	p_a(Mpa)	G_f^I(Mpa)	G_f^{II}(Mpa)	η	θ
241.4	120.7	0.35	0.78	0.75	4.34	0.0016	0.016	0.03	0.35

Finite Element Modeling of Infilled Frames-The interaction between the frame and the infill due to applied load plays the most important role in the behavior of the infilled frames. The interaction between the frame and the infill through this mortar joint is modeled by an interface element capable of transferring normal and shear forces in the elastic and inelastic ranges of loading. Interface elements have been used in the past to model joints and discontinuities. An interface element has been formulated based on the results of the experiments on mortar joints performed by some researchers.

Tests by some researchers on infilled frames revealed that the cracking of the mortar joints in the infill does not influence the stiffness and strength of the infilled frame to any considerable degree.

Results obtained by author done FEM analysis on various researchers models.

The load displacement plot obtained by the finite element analyses is shown in Fig. 3.34.

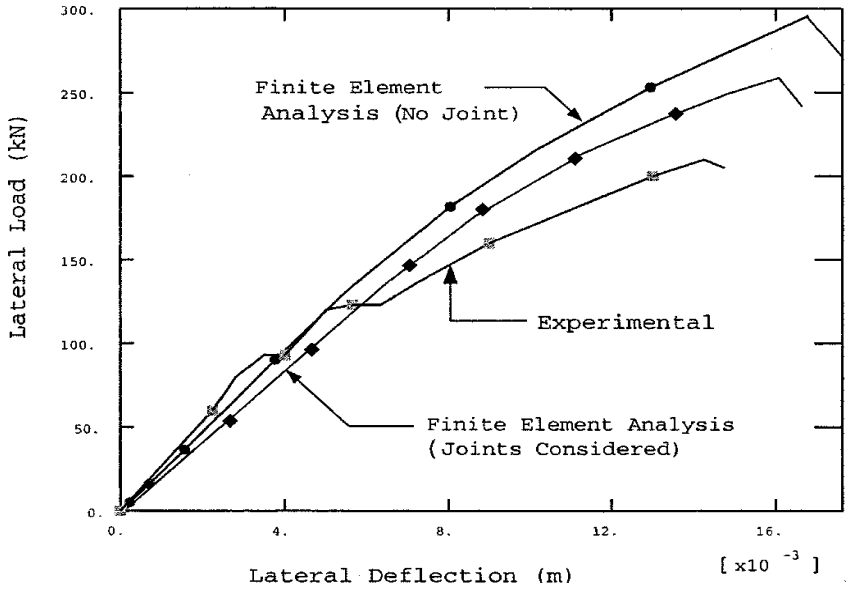

Fig 3.34 Riddington 1984 flexible frame: load displacement plot, Gosh, A.K and Amde M. Amde (2001),

The load displacement plot of the finite element analysis with mortar joints modeled separately shows better agreement with the experimental results because the finite element model simulates the experimental model more closely. The final deformed shape showing stair-step type failure in the mortar joints along the diagonal of the infill shown in Fig 4.3 is similar to that found in Riddington's 1984 stiff frame experimental results. The lesser stiffness of the infill frame seen in the plot of the finite element analysis with mortar joints modelled separately is due to the deformations seen in the mortar joints. The infill crushes at the corner, which is also seen in the nature of the load displacement plot. The mode of failure is CC. It can be seen from the stress distributions that the infill at the top right and at the bottom left corner is not stressed at all, which suggests that the infill is acting as a strut between the top left and the bottom right corners. The contact length is about 3/8 of the total length or height of the infill.

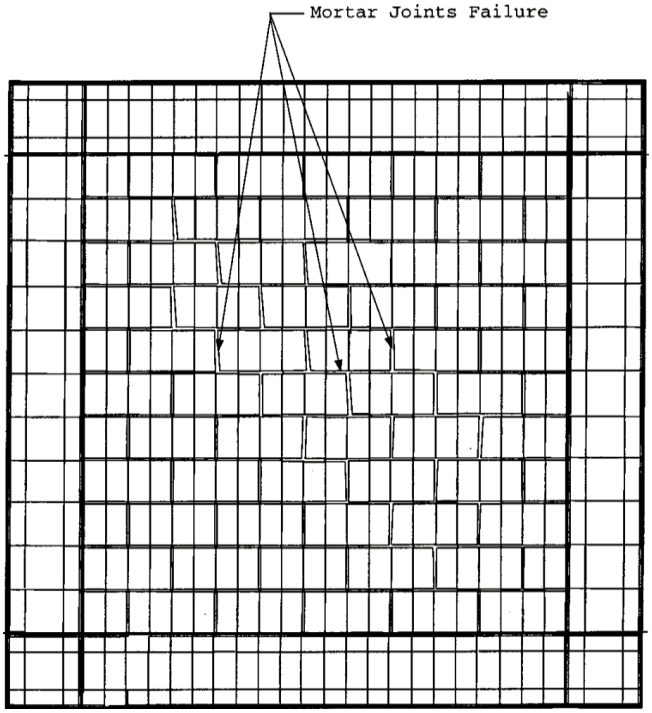

Fig-3.35 Riddington (1984) stiff frame: final deformed shape of infilled frame, Gosh, A.K and Amde M. Amde (2001)

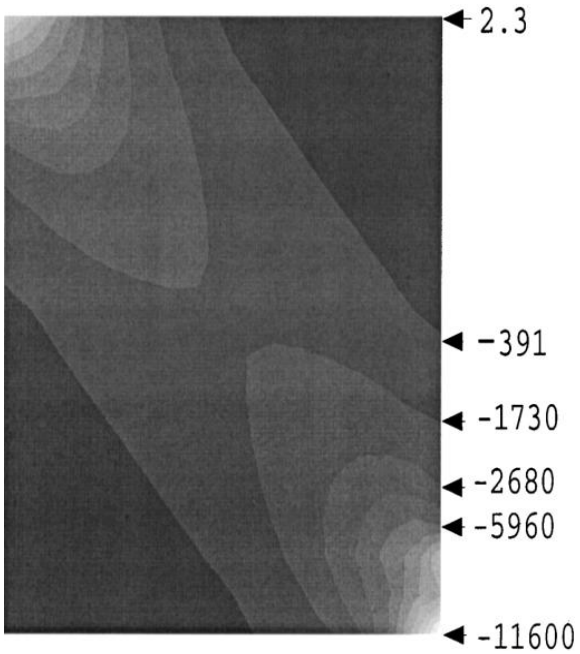

Fig-3.36 Riddington (1984) stiff frame: minimum principal stress plot at lateral ,load 216 KN. Gosh, A.K and Amde M. Amde (2001)

Riddington (1984) Stiff Frame-The load displacement plots are shown in Fig.3.37

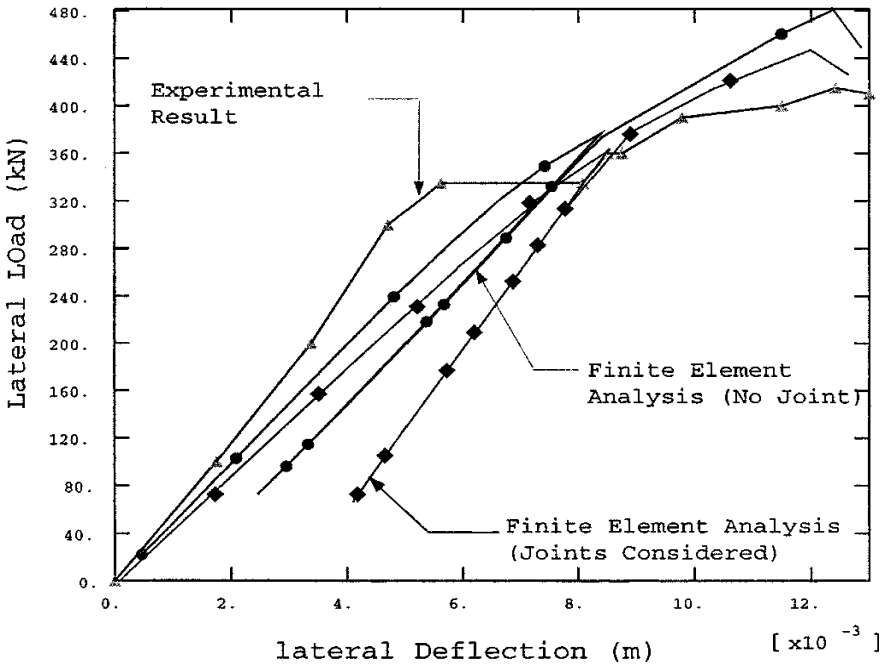

Fig 3.37 Riddington 1984 stiff frame: load displacement plot, Gosh, A.K and Amde M. Amde (2001)

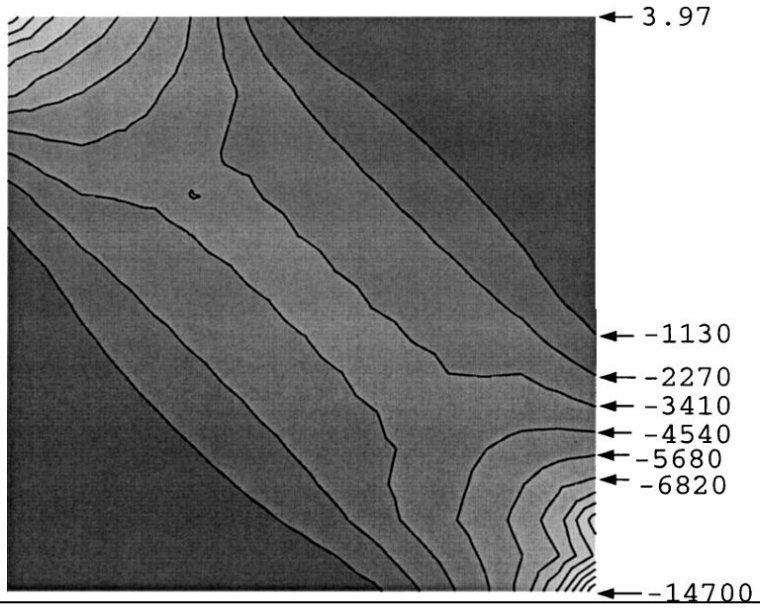

Fig-3.38, Riddington (1984) stiff frame: minimum principal stress plot at lateral load 460 KN, Gosh, A.K and Amde M. Amde (2001)

The experimental load displacement plot shows considerably higher stiffness of the infilled frame beyond 100 kN load. The plots of the finite element analyses deviate from the experimental load displacement plot incrementally. The infill starts cracking in the direction normal to the diagonal strut at about 280 kN load. At a load of 376 kN, infill cracking failure occurs. The slow load drop obtained by the finite element analyses is due to the arc length procedure employed for the analyses. This procedure can withdraw load at the limit load for equilibrium to be satisfied for the structure stiffness, which becomes negative definite after the limit load. This type of load release cannot be achieved in an experimental setup. The diagonal strut, after regaining support provided by the two opposite corners of the frame, starts resisting lateral load again. The diagonal bands are subjected to compressive stress and at high applied load start crushing, which leads to failure. The mode of failure is diagonal compression type.

Poke and Dawe (1986) Frame-The behavior of this frame is similar to that of the flexible frame of Riddington 1984, except that the contact lengths are different for the beams and the columns, because of the unequal lengths of the beams and the columns. The mode of failure is CC.

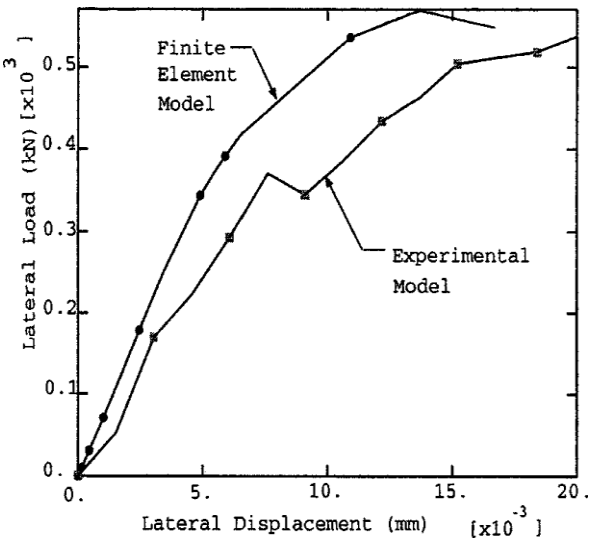

Fig-3.39, Pook and Dawe (1986) frame: load displacement plot, Gosh, A.K and Amde M. Amde (2001)

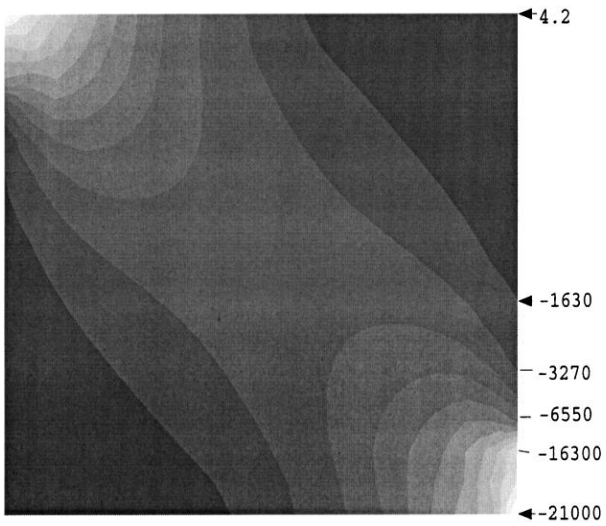

Fig-3.40,Pook and Dawe (1986) frame: minimum principal stress plot at lateral load 420 kN, Gosh, A.K and Amde M. Amde (2001)

Frames 4 and 5-Frame 4 was created by reducing the length of the stiff frame of Riddington 1984 and Frame 5 was created by increasing the length of the frame of Pook and Dawe 1986. These frames were created to see if the SR mode of failure may develop in infilled frames. The stress distributions as shown in Figs. 4.9 and 4.10 do not clearly show the SR mode of failure in either frame. However, the load displacement plot of Frame 5 shows some ductile type failure.

Fig-3.41, Frame 4: minimum principal stress distribution in infill, Gosh, A.K and Amde M. Amde (2001)

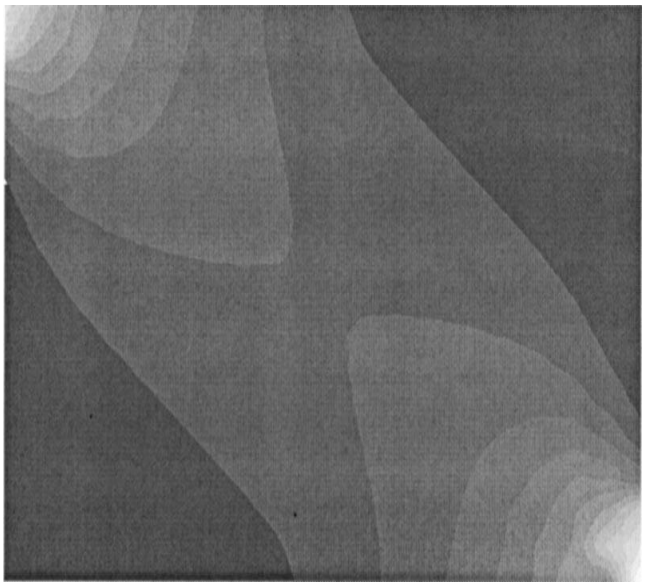

Fig-3.42,Frame 5: minimum principal stress distribution in infill, Gosh, A.K and Amde M. Amde (2001)

El-Dakhakhni, Wael W et al. (2003) Masonry infill panels in framed structures have been long known to affect strength, stiffness, and ductility of the composite structure. In seismic areas, ignoring the composite action is not always on the safe side, since the interaction between the panel and the frame under lateral loads dramatically changes the stiffness and the dynamic characteristics of the composite structure, and hence, its response to seismic loads. This paper presents a simple method of estimating the stiffness and the lateral load capacity of concrete masonry-infilled steel frames (CMISFs) failing in corner crushing mode, as well as the internal forces in the steel frame members. In this method, each masonry panel is replaced by three struts with force-deformation characteristics based on the orthotropic behavior of the masonry infill. A simplified steel frame model is also presented based on the documented modes of failure of the CMISF. The method can be easily computerized and included in nonlinear analysis and design of three-dimensional CMISF structures.

Development of Concrete Masonry(Infilled Steel Frame Model)- Subjecting a bare masonry panel to a diagonal loading usually results in a sudden failure initiated by a stepped crack and divide into two parts immediately due to un-confinement. This behavior was investigated by author using the ANSYS 5.3 FE program. The ASTM E-519 (ASTM 1996b) standard diagonal tension test specimen, representing this loading case and the FE model used to duplicate the experimental failure mechanism are both shown in Fig-3.43. Unlike the unconfined panel, as soon as a diagonal crack develops within an infilled panel (usually at a much lower load and deflection levels than ultimate), the panel finds itself confined within the surrounding frame and bearing against it over contact lengths, as shown in Fig-3.43. The contact lengths provide enough confinement to prevent failure and allowing the panel to carry more loads until the existing diagonal crack continues to widen and new cracks appear leading, eventually, to ultimate failure. This behavior was reported in the literature by many researchers. To model this behavior it is rational to consider the panel to be composed of two diagonal regions, as shown in Fig-3.43. One region connects the top beam to the leeward column and the other connects the windward column to the lower beam. The bending moments and shearing forces in the frame members cannot be replicated using a single diagonal strut although have been used frequently connecting the two loaded corners.

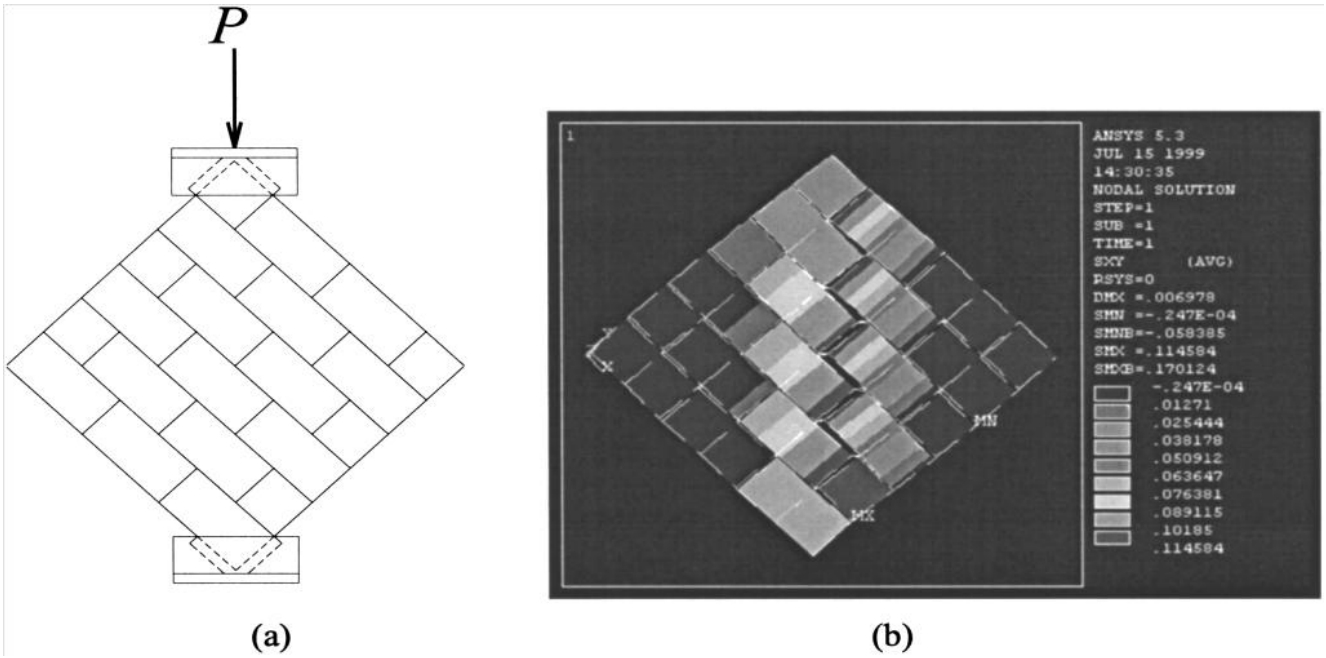

Fig-3.43, Diagonal tension specimen: (a) ASTM E-519 test setup (ASTM 1996b); (b) shear stress contours and failure mode obtained using the ANSYS 5.3 FE model, El-Dakhakhni, Wael W at el.(2003)

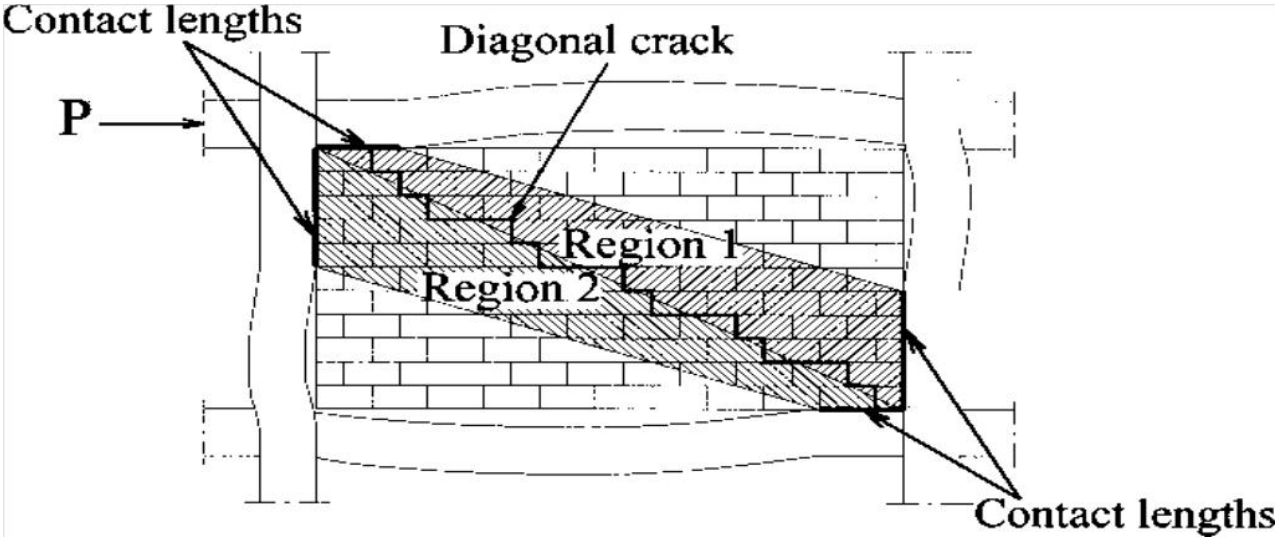

Fig-3.44, Infill panel separation into two diagonal regions, El-Dakhakhni, Wael W at el.(2003)

At least two additional off-diagonal struts located at the points of maximum field moments in the beams and the columns are required to reproduce these moments, as shown in Fig.3.45. Furthermore, since the load transfer from the frame members to the infill depends on the contact length, which in turn is affected by the stiffness and the deflected shape of the frame members, the use of a multistrut model will allow for the interaction between different panels in multistory buildings. This is due to the fact that some beams and/or columns will be loaded from the upper and lower panels or left and right panels! at different locations within the span ~or height!, which will affect their deflected shape, and hence, the panel's strains, and consequently, changing the failure load. Author modeled a single

panel infilled frame using PLANE42 plane stress elements connected to the frame member with CONTACT12 contact elements. The stressed part of the panel, as shown in Fig.4.15, is in the form of a diagonal area. The use of a multistrut model rather than a single strut will better represent the actual stressed area within the infill, and will also facilitate the modeling of the progressive failure occurring at the corner contact region, not just at the corner points. The development of the infilled frame analytical model is divided into two parts. The first part deals with the development of a model for the geometrical representation of the structural sys system's components, namely, the steel frame and the infill panel. In this geometrical model, a closer insight into previous analytical and experimental work revealed that although the frame as a whole behaves nonlinearly up to failure, yet, the source of nonlinearity is concentrated in the beam–column connection rather than being within the spans of the members. Therefore, only at the positions where the nonlinearity is expected, nonlinear elements are used. The concept of the diagonal strut region suggested that the panel behaves as a diagonal strut connecting the two loaded corners. This strut is not simply a line connecting these corners instead, it is a stressed region of the panel connecting parts of the frame in the vicinity of the two loaded corners. The panel was modeled using three struts possessing certain properties and located at certain points within the frame.

The second part deals with the material model suggested for steel and masonry. Simplified stress–strain and load–deformation relations were used for the steel and the masonry materials. The complexity of the masonry panel being anisotropic was overcome by first approximating it to be orthotropic; and then using the constitutive relations and the axis transformation matrices to obtain the panel properties in the loading direction.

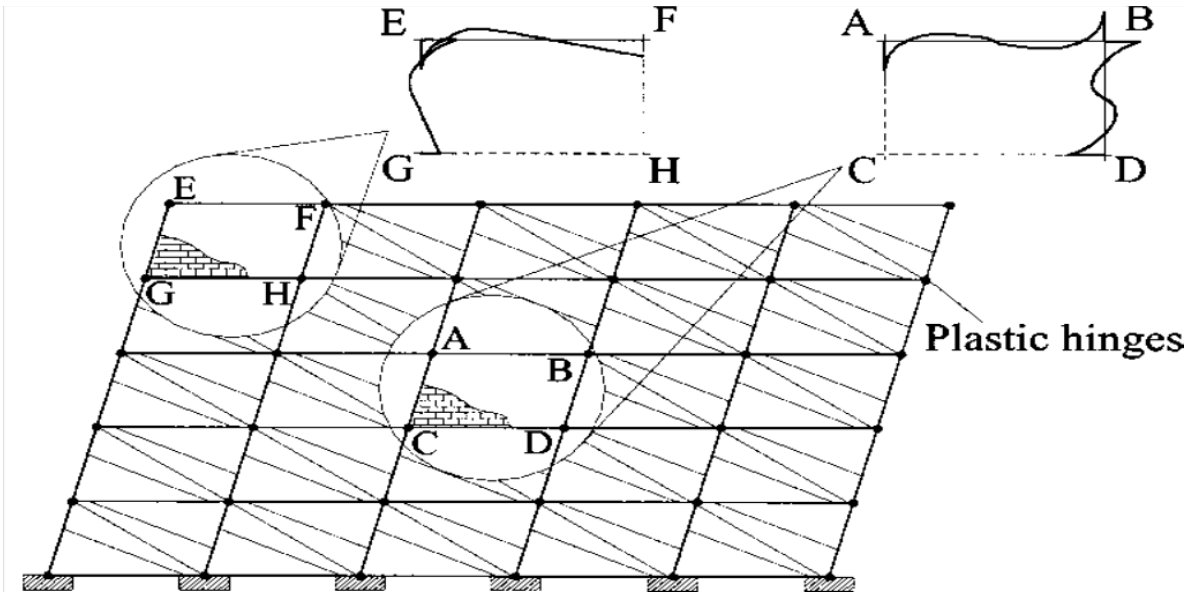

Fig-3.44, Bending moment diagrams for different bays in a multi-story infilled frame building, El-Dakhakhni, Wael W at el.(2003)

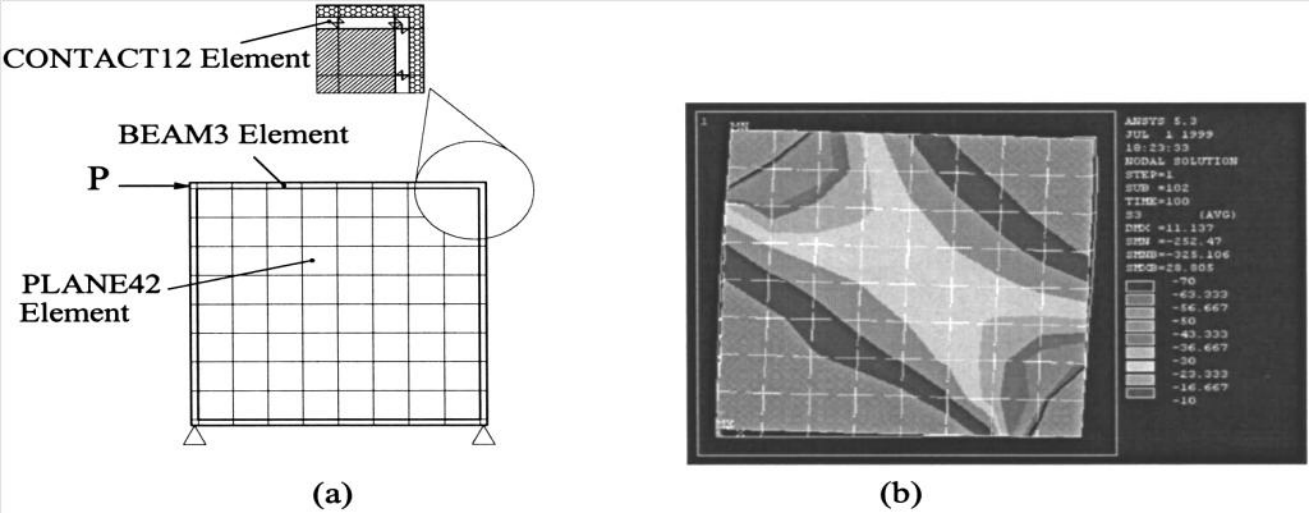

Fig-3.45, ANSYS5.3 FE model of a single panel infilled frame: (a) schematic diagram; (b) Principal stress contours, El-Dakhakhni, Wael W at el.(2003)

Steel Frame Geometrical Model- The steel frame members were modeled with *ANSYS 5.3* FE program using *BEAM3*, elastic beam elements connected by nonlinear rotational spring elements, *COMBIN39*, at the beam–column joints. The concentration of nonlinearity in the frame joints only is based on the fact that due to the limited infill ductility, and thus limited frame deformation at the peak load except at the loaded corners, the maximum field moments as well as the bending moments at the unloaded joints are lower than that at the loaded joints and has been found to be, at most, 20% of the plastic moment capacity of the section Saneinejad and Hobbs (1995). Unlike the model suggested by Seah (1998), which allows for the interaction between the axial and shear forces and the bending moment at the connection using three springs, no translational springs were used at the joint of the suggested model, instead, the degrees of freedom (DOF) coupling option provided in *ANSYS 5.3* was used to couple both the beam and the column nodes at the beam–column connection in the two planar translational DOF, forcing them to undergo the same displacement.

Infill Panel Geometrical Model- Saneinejad and Hobbs (1995) showed that for steel frame members infilled with plane concrete panel, the points of maximum field moment developed within the frame members lie approximately at the end of the contact lengths, and are located at distances from the beam–column connection given by

$$\alpha_c h = \sqrt{\frac{2\left(M_{pj} + \beta_C M_{pC}\right)}{\sigma_C t}} \leq 0.4h$$

$$\alpha_b h = \sqrt{\frac{2\left(M_{pj} + \beta_b M_{pb}\right)}{\sigma_b t}} \leq 0.4l$$

Where; α_c = ratio of the column contact length to the height of the column

α_b = ratio of the beam contact length to the span of the beam;

h=column height, l=beam span.

M_{pj} =minimum of the column's, the beam's or the connection's plastic moment capacity, referred to as the plastic moment capacity of the joint;

M_{pc} and M_{pb} = column and the beam plastic moment capacities, respectively

σc and σ_b = normal contact stresses on the face of the column and the beam, respectively

β_c and β_b = ratios between the maximum elastic field moment developed within the height of the column to;

M_{pc} and that developed within the span of the beam to M_{pb} , respectively

t=thickness of the panel.

It is worth mentioning that these contact lengths are not constant and they vary throughout the loading history. Saneinejad and Hobbs (1995) suggested that, near failure, either σ_c and β_c or σ_bb and β_b will reach their respective upper-bound values of $\sigma_{co}$and β_0 or σ_{b0} and β_0, depending on whether the infill failure is initiated on the column's or the beam's face, respectively. They suggested a method to determine σ_c and σ_b, and demonstrated, based on FEM analysis, that β_0 =0.2. For simplicity, and assuming full plastification of the infill in the loaded corners region near failure, it is suggested that β_c , β_b , σ_c and σ_b have reached their respective upper-bound values. The upper-bound values of σ_c and σ_b , namely, σ_{c0} and σ_{b0} , suggested by Saneinejad and Hobbs (1995) are given by;

$$\sigma_{co}= \frac{f_c'}{\sqrt{1+3\mu^2 r^4}}$$

$$\sigma_{bo}= \frac{f_c'}{\sqrt{1+3\mu^2}}$$

f_c'=compressive strength of the plane concrete panel; μ =coefficient of friction between the steel frame and the concrete panel; and *r*=panel's aspect ratio defined as *r*=*h*/*l*<1.

In order to modify eqs.σ_{co} & σ_{bo} to suit the concrete masonry, f'_c should be replaced by $f'_{m\text{-}0}$ and $f'_{m\text{-}90}$ in eqs.σ_{co} and σ_{bo}respectively, where $f'_{m\text{-}0}$ and $f'_{m\text{-}90}$ are the compressive strength of the masonry panel parallel and normal to the bed joint, respectively; since, unlike the isotropic plane concrete, concrete masonry is anisotropic or, at best, orthotropic. Furthermore, since m between steel and masonry is small usually, about 0.3, and the shrinkage of the concrete infill may result in a separation between the frame and the panel; a rational assumption will be to neglect the friction between the steel frame and the masonry. A similar assumption was also suggested by Liauw and

Kwan (1982) Assuming friction to be a strength reserve. It is also worth mentioning that a recent study conducted by Flanagan et al. (1999) Concluded that the method suggested by Saneinejad and Hobbs (1995) estimated twice the capacity obtained from experimental work that the best results were obtained with $\mu = 0$. Also, since r<1, then r^4 is very small and can be neglected.

Summarizing the above assumptions and simplifications, it is suggested that the distances from the beam–column connection to the points of maximum field moments in the frame columns and beams (which are also approximately the contact lengths) are to be given as;

$$\alpha_c h = \sqrt{\frac{2\left(M_{pj} + 0.2M_{pC}\right)}{\sigma_C f'_{m-o}}} \leq 0.4h$$

$$\alpha_b l = \sqrt{\frac{2\left(M_{pj} + 0.2M_{pC}\right)}{\sigma_C f'_{m-9o}}} \leq 0.4l$$

Referring to Fig-3.45, it is more practical to use struts instead of plate elements to represent the two regions of the panel. Assuming the equivalent uniformly loaded diagonal region of the panel to be of area equal to *A*, where *A* is to be determined later, each region of the panel shown in Fig-3.45, will be of area =*A*/2. Furthermore, assuming uniform contact stress distribution along the contact areas, each region will be replaced by two struts, each of area A_1=1/2(*A*/2) =*A*/4, located at the beginning and the end of the contact length. Combining the two struts connecting the loaded corners, from the two regions, into one strut of area A_2=2A_1 =*A*/2 results in representing the whole panel by three struts, an upper strut connecting the upper beam with the leeward column with area A_1=*A*/4, a middle strut connecting the two loaded corners with area A_2=*A*/2, and finally, a lower strut of area A_1 =*A*/4 connecting the windward column with the lower beam, where *A*=2A_1+A_2 . The proposed geometrical model for a typical CMISF is shown in Fig.4.16. Saneinejad and Hobbs (1995) replaced the panel by a single strut with an area *Ad* given by

$$A_d = \frac{(1-\alpha_c)\alpha_c ht \frac{\sigma'_c}{f_c} + \alpha_b lt \frac{\tau_b}{f_c}}{\cos\theta}$$

Where f_c=*reduced* strength for the concrete to account for the ultimate design limit state; $\theta = \tan^{-1}\theta = (h/l)$ and τ_b=equivalent uniform shear stress developed on the beam–infill interface and is defined as $\tau_b = \mu\sigma_b$.

Based on the above, it is suggested that the total diagonal struts area, *A*, is to be calculated by

$$A = \frac{(1-\alpha_c)\alpha_c h t}{\cos\theta}$$

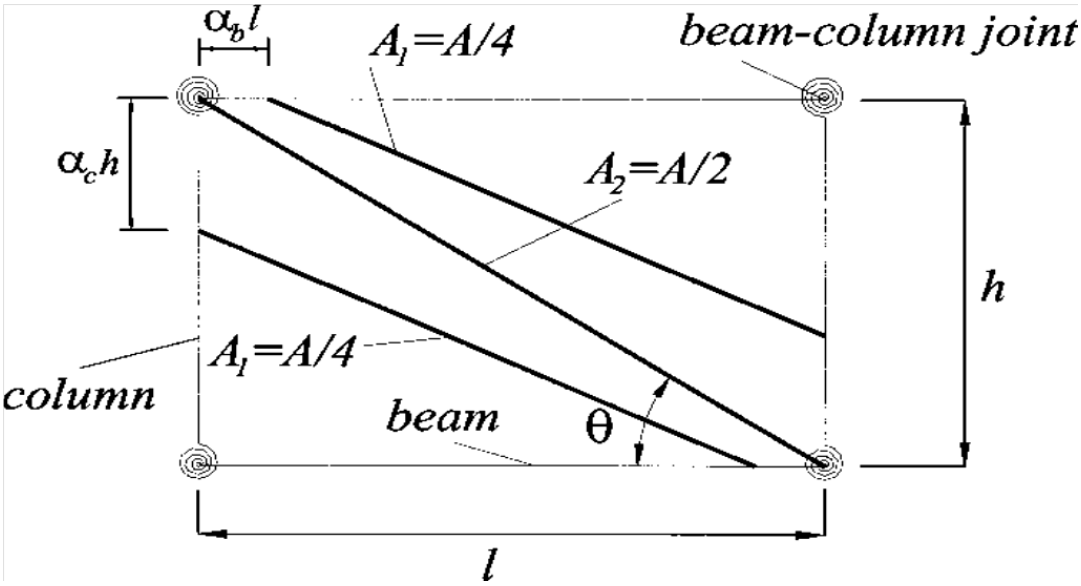

Fig-3.46, Proposed concrete masonry-infilled steel frame model, El-Dakhakhni, Wael W at el.(2003)

Steel Frame Material Model-Using elastic frame elements requires the area and the moment of inertia of the member section as well as Young's modulus of the steel to be the only required input properties for the frame sections to form the stiffness matrix; this eliminates the need to modify the stiffness matrix as well as the iteration process to account for the nonlinear behavior of the steel frame. The use of elastic elements is justified based on the earlier discussion on the steel frame geometrical model. The ultimate moment capacity of the nonlinear rotational spring, representing the beam–column joint, is defined as the minimum of the column's, the beam's, or the connection's ultimate capacity, *Mpj* , which will be referred to as the plastic moment capacity of the joint, as defined earlier in Eqs. $\alpha_c h$ and $\alpha_b l$.The rotational stiffness of the spring can be calibrated so that the lateral stiffness of the frame model matches that of the actual bare frame, which can be obtained experimentally or using simple elastic analysis or, in case of semirigidly connected members, using available data on modeling semirigid connections (Chen and Lui 1991). The joint behavior is shown in Fig. 4.17, where $\phi_{el}$is the maximum elastic rotation that the joint can undergo without yielding; fpl is the maximum plastic rotation before the joint undergoes moment reduction below *Mpj* ; and ϕ_{ult} is the maximum plastic rotation beyond which the joint cannot sustain any moment.

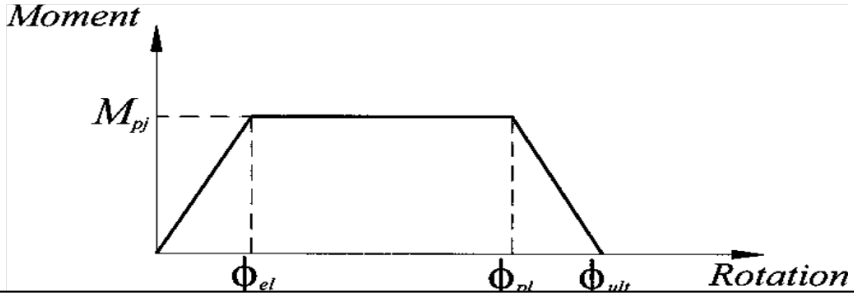

Fig-3.45 Beam–column connection material model behavior, El-Dakhakhni, Wael W at el (2003)

The bare frame ultimate capacity, *Hu* , can be checked very accurately using plastic analysis simply by applying the following:

$$H_{uj} = \frac{\sum_{n=1}^{4} M_{pj}}{h}$$

where the summation is taken for all the four joints of the frame.

Infill Panel Material Model-Based on the available literature, it is evident that the stressed part of the panel is a diagonal region connecting the two loaded corners. It is, therefore, justifiable to assume that the panel properties in the diagonal direction are the properties governing the behavior of the infill panel. Masonry panels have been known to be anisotropic (Hamid and Drysdale 1980; Khattab and Drysdale 1992; Mosalam et al. 1997c; Seah 1998). A close approximation is to consider the anisotropic masonry panel to be orthotropic. Due to the fact that the panel behaves as if it was diagonally loaded, constitutive relations, of orthotropic plates (Shames and Cozzarelli 1992) and axes transformation matrix, are used to obtain the Young's modulus, E_u, of the panel in the diagonal direction using the following equation:

$$E_\theta = \frac{1}{\frac{1}{E_o}\cos^4\theta + \left[-\frac{2\nu_{o-90}}{E_o} + \frac{1}{G}\right]\cos^2\theta \sin^2\theta + \frac{1}{E_{90}}\sin^4\theta}$$

where *E*0 and *E*90=Young's moduli in the directions parallel and normal to the bed joints, respectively; ν_{0-90}=Poisson's ratio defined as the ratio of the strain in the direction normal to the bed joints due to the strain in the direction parallel to the bed joints; and *G*=shear modulus. Although it is the common practice to use running bond in masonry infills, the use of the suggested technique also applies to walls with stacked bonds. The use of the above equation for unreinforced concrete masonry walls reduces Young's modulus in the inclined direction to about 80% of that in the direction perpendicular to the bed joints.

It is common to relate the initial Young's modulus of quasi-brittle materials such as concrete and masonry to their ultimate compressive strength. Therefore, it seems rational to assume that not only Young's modulus will change, but also the ultimate strength of the masonry panel in the u direction, $f'_{m\text{-u}}$. A simple way to account for this direction variation is to relate Eu to $f'_{m\text{-u}}$ using the same factor relating E_{90} to $f'_{m\text{-u}}$ and neglect the shear stress effect, since the infill is failing in a CC mode, as well as the effect of the biaxial state of stress in the infill corners vicinity. The reason for choosing E_{90} and $f'_{m\text{-u}}$ is that it is a common practice as well as a standard test (ASTM E-447 (ASTM 1996a)), to obtain the strength of masonry prisms in a direction perpendicular to bed joints, i.e., the vertical direction, which is usually the loading direction in load-bearing walls. The assumption that the masonry compressive strength varies according to the angle of loading was investigated by Hamid and Drysdale (1980) and a value of $f'_{m\text{-u}} = 0.7\, f'_{m\text{-}90}$ was suggested by Seah ~1998!. Fig. 4.18 shows the orthotropic model for the masonry panel.

Based on nonlinear FE analyses, Saneinejad and Hobbs (1995) suggested that the secant stiffness of the infilled frames at the peak load to be half the initial stiffness. This might be directly interpreted into the stress–strain relation for the masonry panel by assuming that the secant Young's modulus at peak load E_p is equal to half the initial Young's modulus, E_θ ,i.e $E_p = 0.5\, E_\theta$ This assumption is justified since the stiffness of the infilled frame is affected primarily by the stiffness of the infill (Dhanasekar and Page 1986).

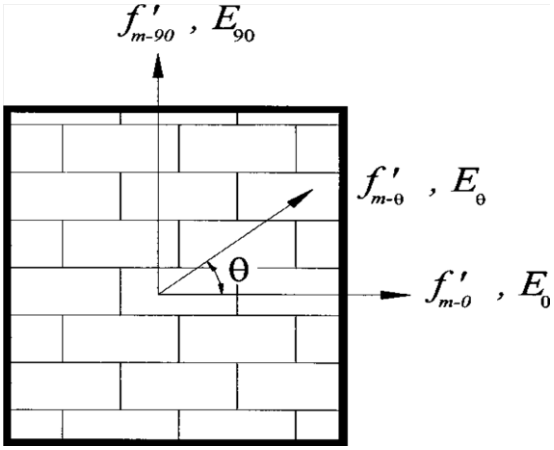

Fig-3.46, Orthotropic model of concrete masonry, El-Dakhakhni, Wael W at el (2003)

As shown in (Fig-3.47), knowing E_p and $f'_{m\text{-}\theta}$, it is now an easy task to determine the strain corresponding to the peak load ε_p. Instead of using the parabolic stress–strain relation shown in (Fig.4.19a), it is suggested to approximate it into a trilinear relation, which is simpler and more practical for analysis, as shown by the thick lines in (Fig-3.47a). Unless more accurate data are available, the parameters in (Fig.4.19a) will be assumed according to the following:

$$\varepsilon_1 = \varepsilon_p - 0.001$$

$$\varepsilon_2 = \varepsilon_p + 0.001$$

Knowing the stress–strain relation along with the area (from eq A) and the length of each of the three struts (which can be easily calculated knowing the panel dimensions and the contact lengths given by Eqs and) makes it possible to obtain a force deformation relation for each strut. As shown in (Fig. 4.19b) by simply multiplying the strains ε_1, ε_2, and $\varepsilon_u$by the length of each strut results in obtaining δ_1 , δ_2 , and δ_u respectively. Also, multiplying the stress, $f'_{m\text{-}\theta}$, by the area of each strut results in obtaining F_u for each strut. In fact, assuming that E_u and $f'_{m\text{-}\theta}$ are the same for all struts and neglecting the minor difference in the inclination angle between the middle strut and both the upper and the lower strut, will result in finding only two distinct force– deformation relations, one for the upper and lower struts and another for the middle strut. It is worth mentioning that the use of a macromodel, which is neither a single strut nor a plate to represent the panel, was previously suggested by some researchers. Chrysostomou (1991) And Mander and Nair (1994) suggested multiple strut models. Mosalam et al. (1997) used a truss with contact elements. Due to the complexity of the problem, most of the properties of these macromodels suggested by different researchers were not justified based on the material level, unlike the suggested model. In fact, the areas and the stiffnesses of the members representing the panel were generally selected to *match* either some experimental findings like the stiffness and/or the ultimate load or the natural frequency under seismic loading. In other cases the properties of the macromodel were selected merely to match some properties of a more sophisticated micromodel.

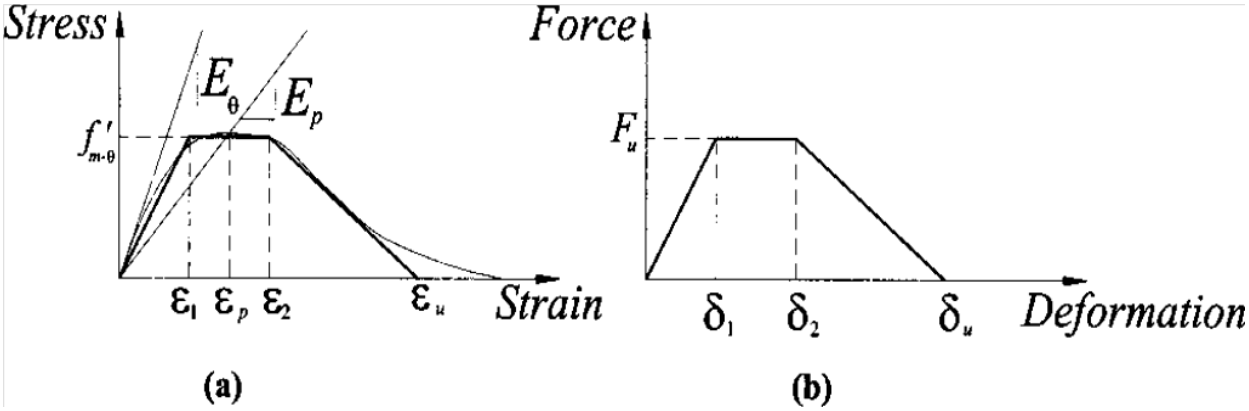

Fig-3.47, Simplified trilinear relations: (a) stress–strain relation of concrete masonry; (b) typical force–deformation relation for struts, El-Dakhakhni, Wael W at el (2003)

Modeling of Test Specimens Using Proposed Method -The suggested method was used to model five CMISF specimens. Four of the specimens were tested at the University of New Brunswick under monotonic racking load by Yong (1984), McBride (1984), and Richardson (1986). The fifth specimen was tested at Cornell University by Mosalam et al. (1997a) Under quasistatic displacement-controlled loading. The first four specimens are identical single panel CMISFs with different masonry strength. The reasons for choosing these specimens are primarily for the experimental results consistency of the test program as well as to verify the effect of changing the masonry strength on the CMISF model behavior, and because these experimental results were duplicated by Seah (1998) using a very

sophisticated *micro*-FE model consisting of a series of plane stress elements connected by ten springs at each node. The fifth specimen is a one-fourth scale, two-bay–single-story CMISF with semirigid connection, this specimen was chosen to demonstrate the effectiveness of the method to model semirigid connections as well as the effect of using three struts on changing the bending moment diagram of the CMISF, and the capability of the model to approximate the envelope of the cyclic load–deflection loops ~the capacity curve!. The details of the calculations involved in the FE modeling of these specimens can be found elsewhere (ElDakhakhni 2000).

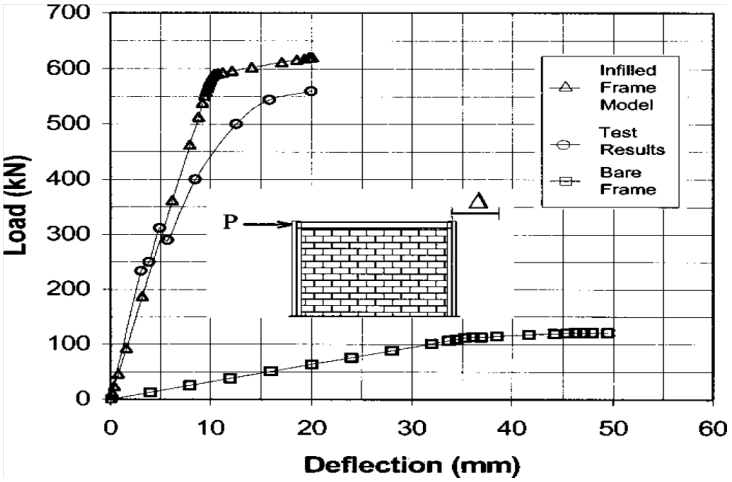

Fig-3.48, Load–deflection relations for specimen WB2 (Yong 1984), El-Dakhakhni, Wael W at el (2003)

The *ANSYS 5.3* FE program was used to generate the load– deflection relation of specimen WB2 tested by Yong (1984), utilizing the proposed technique. The load–deflection relations for the bare and the infilled frame model are shown in Fig. 4.20 along with test results for comparison. The specimen was loaded until the lateral displacement reached approximately 20 mm, at which it was assumed that the specimen failed. A sudden drop of the load–deflection curve occurred at approximately 312.0 kN due to the development of the diagonal crack discussed earlier. The developing of the diagonal crack affects neither the stiffness nor the ultimate load capacity of the infilled frame and will result only in a sudden drift, affecting the overall ductility of the system, which is outside the scope of this study. Fig3.49 shows the capabilities of the proposed method to predict both the stiffness and ultimate load capacity up to failure. The model appears to overestimate the ultimate capacity by about 9% and acceptably estimates the average stiffness up to failure.

The load–deflection relations for specimen WA3 (McBride 1984), and specimen WC7 (Amos 1986) are shown in Figs. 4.21 and 4.22, respectively. In which the model closely approximates the stiffness of the CMISF up to failure, overestimates the strength of specimen WA3 by 14%, and underestimates that of specimen WC7 by 3%. The loading of the first three specimens was stopped as soon as failure was established, usually under a displacement in the range of 20 mm. The forth specimen WD7,

tested by Richardson (1986), was loaded up to 60 mm. The specimen was modelled using the same technique utilizing the *ANSYS 5.3* FE program, and the load–deflection relations for the bare and the infilled frame model are shown in Fig. 4.23 along with test results for comparison. Again, the proposed model is efficient in duplicating the test results up to failure. The model underestimated the failure load by 10% and the experimental test data show that the infilled frame gradually degrades and eventually at some point it will reach the ultimate capacity of the bare frame. It is worth mentioning that the proposed model can predict the stiffness and strength efficiently up to failure, yet the postpeak behavior and the ductility of CMISF systems are highly uncertain and will require further research.

Specimen Q21SSB, tested by Mosalam et al. (1997a) was modeled using the same technique; Fig. 4.24 shows the load– deflection relation of the bare frame model and the infilled frame model along with the envelope of the cycling loading test after correcting it to exclude the effect of the lack of fit between the frame and the infill. The model accurately represents the infilled frame up to a deflection of 6 mm, at which the model underestimated the specimen capacity by less than 2%. After this displacement, failure occurred in the specimen yet the model continued to carry more load, but with a very low stiffness, then it gradually lost its strength and failed. Fig. 4.25 shows the bending moments in the model members at a load of 41.5 kN, before failure. These moments have the same trend as those obtained by Mosalam et al. (1997b) and suggested by Reflak and Fajfar (1991), Saneinejad and Hobbs (1995), and Buonopane and White (1999).

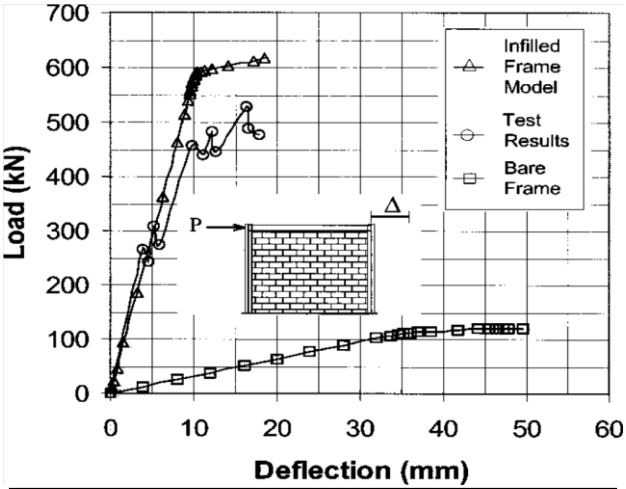

Fig-3.49, Load–deflection relations for specimen WA3 (McBride1984), El-Dakhakhni, Wael W at el (2003)

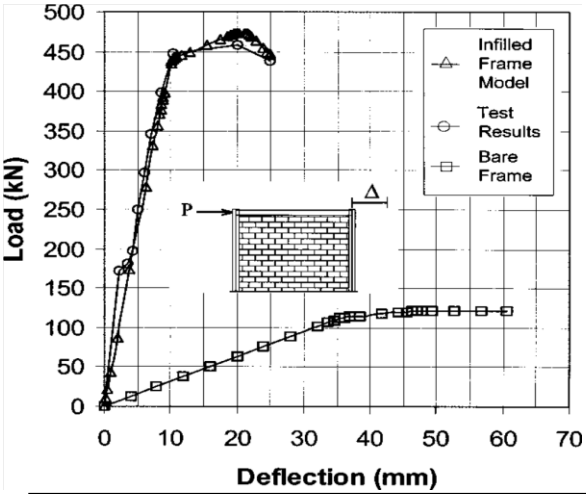

Fig-3.50 Load–deflection relations for specimen WC7 (Amos 1986), El-Dakhakhni, Wael W at el (2003)

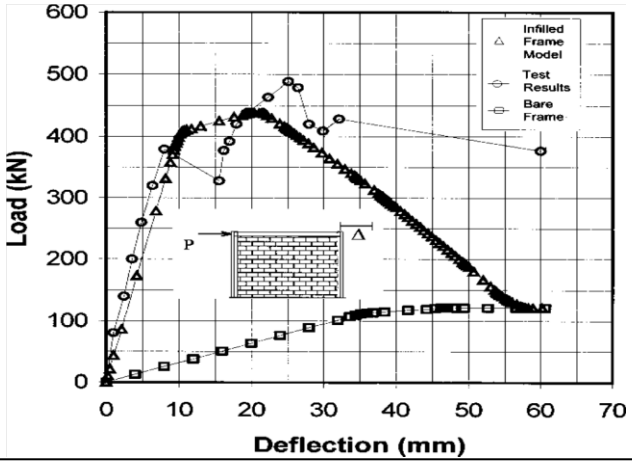

Fig-3.51, Load–deflection relations for specimen WD7 (Richardson 1986), El-Dakhakhni, Wael W at el (2003)

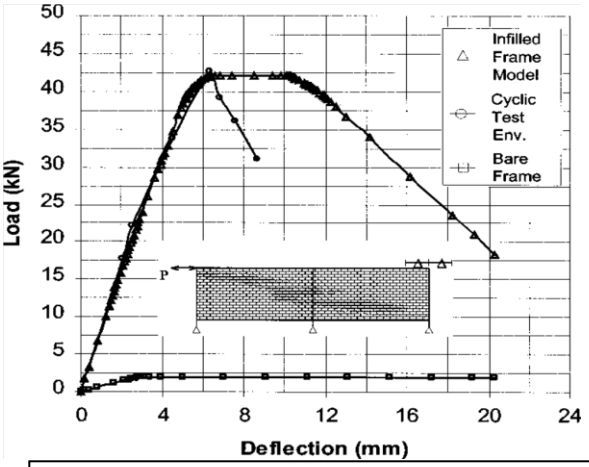

Fig-3.52, Load–deflection relations for specimen Q21SSB (Mosalam et al. 1997a), El-Dakhakhni, Wael W at el (2003)

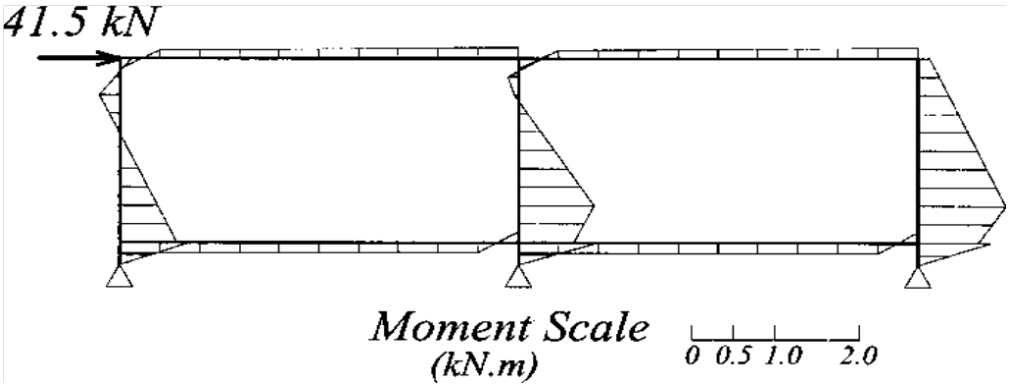

Fig-3.53, Bending moment diagram obtained using *ANSYS 5.3* model for specimen Q21SSB (Mosalam et al. 1997a) drawn on tension side, El-Dakhakhni, Wael W at el (2003)

Aateris, P.G et al.(2011) "Mathematical Macromodeling of Infilled Frames: State of the Art", primary objective of this paper is to present a general review of the different macromodels used for the analysis of infilled frames. A number of distinct approaches in the field of analysis of infilled frames have yielded several analytical models. These studies stressed that the numerical simulation of infilled frames is difficult and generally unreliable because of the very large number of parameters to be taken into account and the magnitude of the uncertainties associated with most of them. In this paper, the advantages and disadvantages of each macromodel are pointed out, and practical recommendations for the implementation of the different models are indicated

Micro Models-

Researcher Name	Year	Formula	Remarks
Mainstone	1971	$\frac{w}{d} = 0.16\lambda_h^{-0.3}$	
Mainstone & Weeks	1974	$\frac{w}{d} = 0.175\lambda_h^{-0.4}$	Formula also included in FEMA-274 (FEMA 1997) & in FEMA-306 (FEMA-1998), this equation was accepted by majority of researchers.
Bazan & Meli	1980	$\frac{w}{d} \cong 0.20 \sin 2\theta \sqrt{\frac{E_c A_c}{G_w A_w}}$ if $1 < \frac{E_c A_c}{G_w A_w} < 5$	Finite element studies for one-bay, one-storey, infilled frames for the case of failure on the diagonal.
Liauw & Kwan	1984	$\frac{w}{d} = \frac{0.95 \sin 2\theta}{2\sqrt{\lambda_h}}$ $\theta = 25^0$ & 50^0	
Decanini & Fantin	1987	Uncracked panel; $\frac{w}{d} = \begin{cases} 0.085 + \frac{0.748}{\lambda_h} & \text{if } \lambda_h \le 7.85 \\ 0.130 + \frac{0.393}{\lambda_h} & \text{if } \lambda_h > 7.85 \end{cases}$ Cracked panel; $\frac{w}{d} = \begin{cases} 0.010 + \frac{0.707}{\lambda_h} & \text{if } \lambda_h \le 7.85 \\ 0.130 + \frac{0.470}{\lambda_h} & \text{if } \lambda_h > 7.85 \end{cases}$	
Paulay & Pristley	1992	$\frac{w}{d} = \frac{1}{4}$	
Durrani & Luo	1994	$\frac{w}{d} = \gamma \sin 2\theta$; $\gamma = 0.32\sqrt{\sin 2\theta}\left(\frac{h^4 E_w t_w}{m\, E_c I_c h_w}\right)^{-0.1}$ $m = 6\left(1 + \frac{6\, E_b I_b\, h}{\pi E_c I_c L}\right)$	E_c & E_b = elastic moduli of the frame column and beam material, I_c & I_b = moment of inertia of the frame column & beam
Flangan & Bennet	1999, 2001	$A = \frac{\pi t_w}{C\lambda \cos\theta}$	C = empirical constant varying with the in-planedrift displacement

Table-3.2, Effective width of diagonal struts

Multiple-Strut Models-In the preceding two decades, it has become clear that one single strut element is unable to model the complex behavior of the infilled frames as reported by many researchers, the bending moments and shearing forces in the frame members cannot be adequately represented by using a single diagonal strut connecting the two loaded corners. More complex macromodels were proposed, still typically based on a number of diagonal struts.

Thiruvengadam (1985) proposed the use of a large number of pin-jointed diagonal and vertical multiple-strut model with moment-resisting frame. Initially, a perfect frame-infill bond condition is assumed, and the lateral stiffness of the infill by its shear deformation is modeled by a set of pin-ended diagonal struts running in both directions. These diagonals represent the shear and axial stiffness of the masonry infill. Similarly, the vertical stiffness contribution is accounted for by providing vertical struts. Because of the great number of struts, this model has been adopted by many researchers to investigate the effect of infill on the behavior of infilled frames as a method for modeling the special case of infilled frames with openings, and was also included in FEMA-356 (FEMA 2000).

Chrysostomou (1991) and Chrysostomou et al. (2002) proposed to model each infill panel by six compression only inclined struts (Fig. 4). Three parallel struts were used in each diagonal direction, and the off-diagonal ones were positioned at critical locations along the frame members. These locations are specified by parameter α, which represents a fraction of the length or height of a panel and is associated with the position of the formation of a plastic hinge in a beam or a column. during the analysis of the nonlinear response, only three of the six struts are active, and the struts are switched to the opposite direction whenever their compressive force reduced to zero.

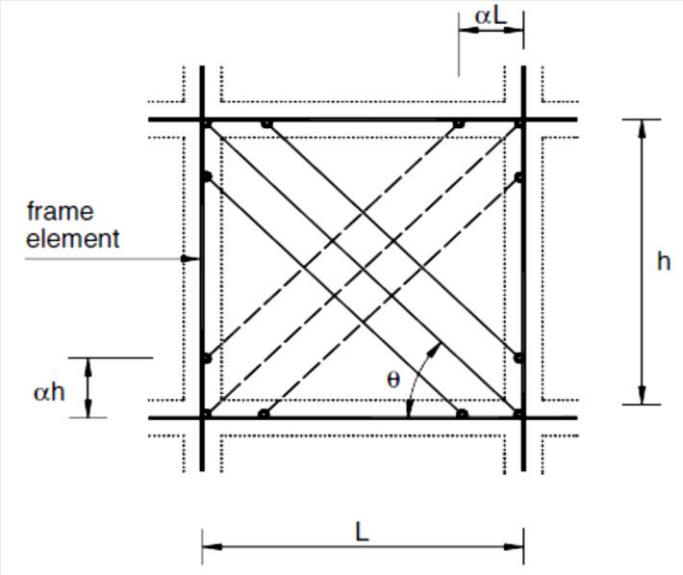

Fig-3.56,Six-strut model for masonry-infill panel in frame structures, Asteris, P.G et al(2011)

Saneinejad and Hobbs (1995) proposed analytical model assumes that the contribution of the infill panel to the response of the infilled frame can be modeled by "replacing the panel" with a system of two diagonal masonry compression struts. The method takes into account the elastoplastic behavior of infilled frames, considering the limited ductility of infill materials. Various governing factors, such as the infill aspect ratio, the shear stresses at the infill-frame interface, and relative beam and column strengths are accounted for in this development. This model for masonry-infill panels was implemented in IDARC 2D (IDARC 2D Version 4.0), a computer-based analytical tool for the inelastic analysis.

El-Dakhakhni (2000, 2002) and El-Dakhakhni et al. (2001) replace the infill wall by one diagonal and two off-diagonal struts, making use of the orthotropic behavior of the masonry wall, and experimental observations and analytical simplifications in order to simplify the nonlinear modeling of these structures.

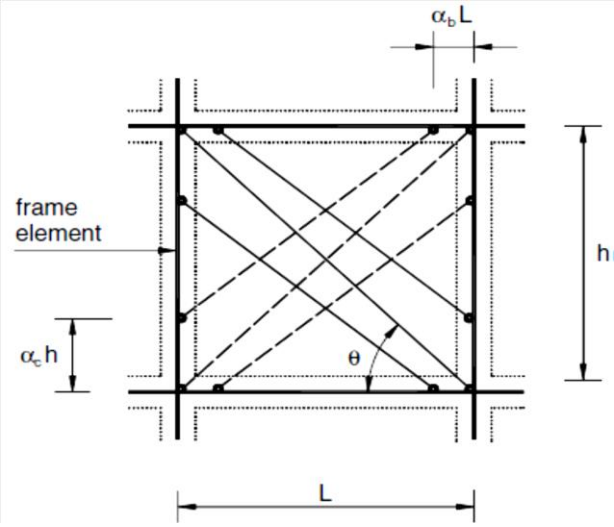

Fig-3.57,Six-strut model for masonry-infill panel

Crisafulli (1997) investigated numerical results, obtained from the single-, two-, and three-strut models, were compared with those corresponding to a refined finite element. For the multistrut models, the stiffness may change significantly depending on the separation between struts. The single-strut model underestimates the bending moment because the lateral forces are primarily resisted by a truss mechanism. On the other hand, the two-strut model leads to larger values than those corresponding to the finite element model. A better approximation is obtained from the three strut model although some differences arise at the ends of both columns.

Crisafulli and Carr (2007) proposed model which is implemented as a four-node panel element that is connected to the frame at the beam-column joints. Internally, the panel element accounts separately for the compressive and shear behavior of the masonry panel using two parallel struts and a shear spring in each direction, as shown in Fig. 6. This configuration allows an adequate consideration of the lateral stiffness of the panel and of the strength of masonry panel, particularly when a shear failure along mortar joints or diagonal tension failure is expected. Furthermore, the model is easy to apply in the analysis of large infilled frame structures. The primary limitation of the model results

from its simplicity. The panel is connected to the beam-column joints of the frame, so the model is not able to properly predict the bending moment and shear forces in the surrounding frame.

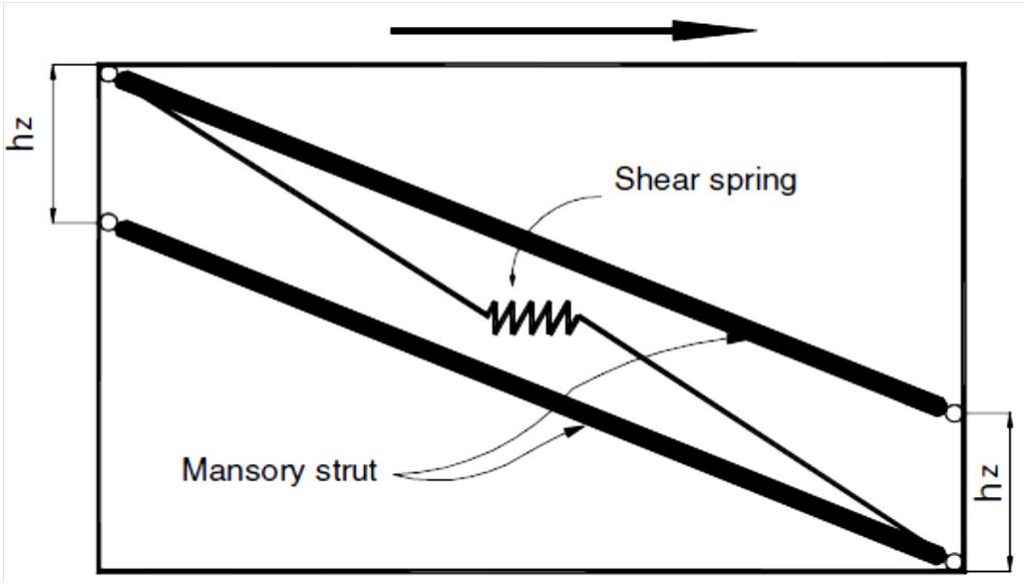

Fig-3.58, Multistrut model for masonry-infill panel (only the struts and the shear spring active in one direction are represented)

Comparison of Response of Different Strut Models- One of the difficulties that practicing engineers face is the reliable modeling of infilled frames with openings. Although the single-strut model can be used to represent with sufficient accuracy the behavior of solid infill walls, its applicability to infill walls with openings requires its calibration using finite-element analysis (FEMA 2000).

To illustrate the inadequacy a case study was carried out, where the infill walls were modeled with each of the two approaches of simple single-strut model or the double-strut (multistrut) model was chosen. The single-strut model used is a rather "gross" model that can be employed in commercial packages. But in multistrut it consists of a pair of diagonal elastic struts that are active at all times, each of which has a stiffness of 50% of the calculated infill-wall stiffness. The relative accuracy of the models is assessed through comparison with experimental results obtained from pseudo-dynamic tests .The frame was infilled with brick walls that included openings of different dimensions (Fig-3.59).

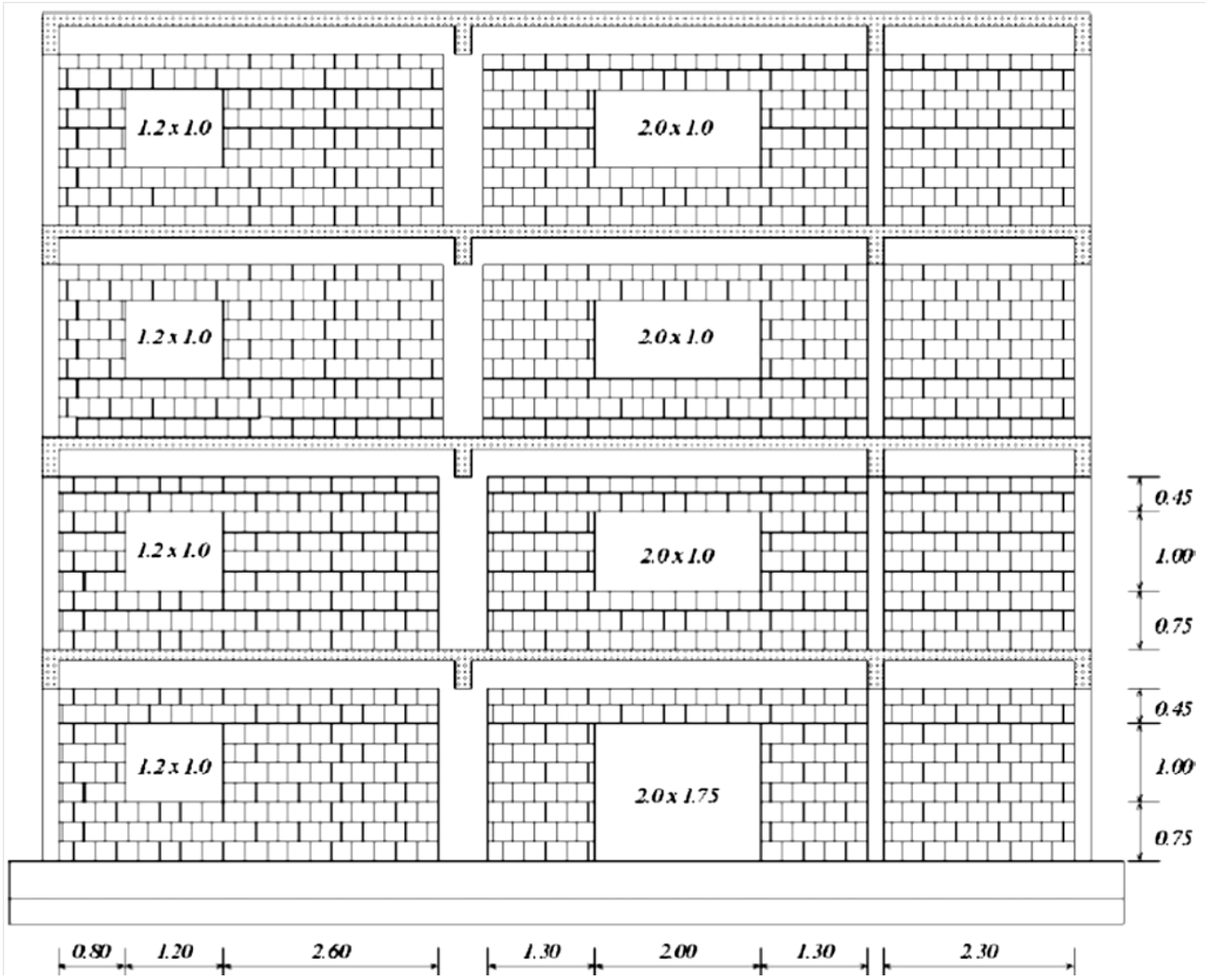

Fig-3.59,Elevation view of the infilled frame with location and dimensions (in m) of openings

The experimental seismic response was obtained with pseudo-dynamic testing, the frame that was subjected to three different, numerically specified seismic records. The acceleration time histories were artificially generated, and increasing return periods of 475 &975 years were used for the experiment. The nonlinear structural analysis program was employed for the analyses.

Representative numerical results obtained from the single and multistrut models are depicted in Fig. 8. It can be concluded that the multistrut model provides a very good fit to the experimental results, and better approximation with the use of finite elements is hardly justified. Conversely, the single-strut model lacks a similar ability to adequately represent the experimental behavior, providing significantly less accurate results.

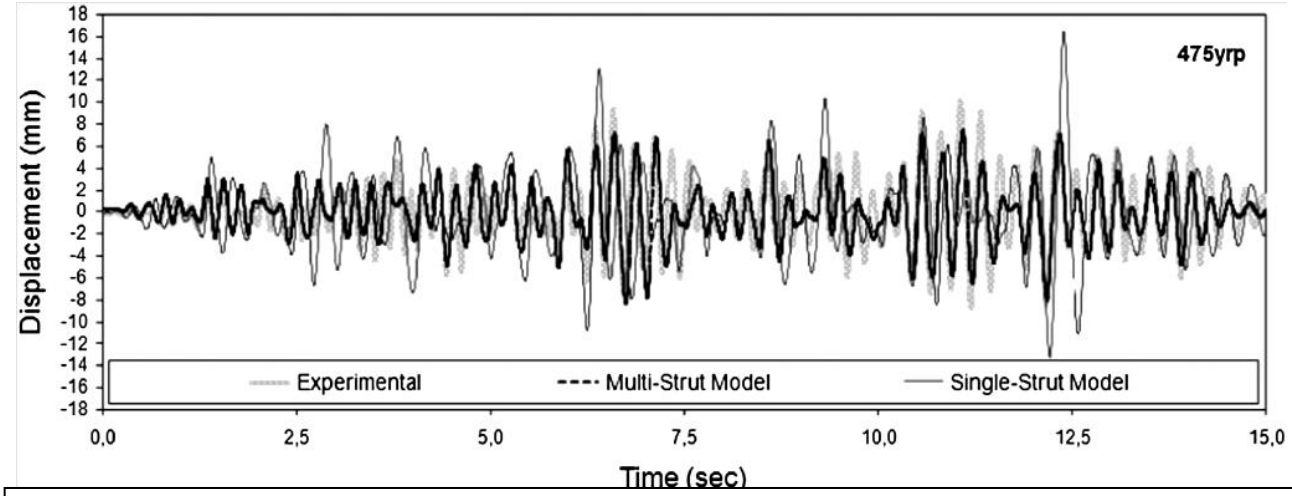

Fig-3.60,Comparison of the top displacement of the infilled frame and the two strut model (475 year return period record), Asteris, P.G et al.(2011)

Conclusion- Regarding the five possible failure modes of infills, there is a consensus that only the corner-crushing and sliding-shear modes are of practical importance, provided there are no openings in the infill. Regarding the other two, namely, diagonal compression and diagonal cracking, the first occurs very rarely because it requires a high slenderness ratio of the infill, and the second should not be considered a failure mode because the infill can carry additional load after it cracks.

The simpler one macromodels that can be used in everyday engineering are the equivalent-strut models, which represent infills with a diagonal strut element. The basic parameter of these struts is their equivalent width, which affects their stiffness and strength. In all the cases, there are considerable differences among the values obtained. The equation that has been adopted by most technical guidelines is the one proposed by Mainstone (1971). Compared to other proposed formulas, this formula represents a lower bound of the calculated equivalent strut width.

The three-strut models can more accurately predict the infill-frame interaction than the single-strut ones (are inadequate to represents the force distribution in the members of the bounding frame) but with a considerable increase in modeling complexity; whereas the two-strut models, although they cannot achieve the accuracy of the three-strut models, improve the prediction compared to the single struts, with less model complexity.

The available macro-models for infill walls do not possess the necessary simplicity and the required accuracy to be used in everyday engineering practice. The single-strut model, although very simple to implement in general-purpose finite-element commercial software, fails to capture the interaction between the bounding frame and the infill wall, and unless there is a hysteretic model defined, it cannot be used for response history analysis. On the other hand, multiple-strut models, although they can provide better modeling of both the infill and its interaction with the bounding frame, cannot be used in general-purpose finite-element software because of the complexities involved in their implementation.

CHAPTER-4

FINITE ELEMENTMODELLING OF INFILLED FRAME

4.1 GENERAL

This chapter is intended to give a description of the infilled frame (tested by Mehrabi et al.) that is to be FE modeled and analyzed to obtain the Lateral Load Vs Lateral displacement Curve analytically. The primary investigation is to verify the results already obtained by experimentally by pervious researchers.

In first part of the chapter the Infilled RC frame (experimentally analyzed at University of Colorado by Mehrabi et al.) is described in detail. This chapter also discusses the theory related to ATENA and information about finite elements currently implemented in ATENA in its second part. All the necessary steps to create these models are explained in detail and the steps taken to generate the analytical load-deformation response of the model are discussed.

As more and more emphasis is being laid on nonlinear analysis of RC infilled framed structures subjected to monotonic or cyclic excitation, the research and development on both non-linear static analysis as well as nonlinear dynamic analysis is in the forefront. Due to the prohibitive computational time and efforts required to perform a complete nonlinear dynamic analysis, researchers and designers all over the world are showing keen interest in nonlinear static analysis. However, all these procedures require determination of nonlinear force-deformation curves that are generated from analysis. This simplifies the structural model, but it provides insight information about the likely non-linear behavior of the structure. Therefore, it can be said that a very vital step towards a good performance estimation of the structure against earthquakes is the determination of correct force-deformation curve popularly known as “Load-Displacement Curve”.

4.2 GENERAL DESCRIPTION OF INFILLED RC FRAME

One of the major objectives of this work is to test a real-life structure analytically under monotonic and cyclic loads. In order to keep the structure as close to reality as possible, no special design for the structure as such was performed and instead a portion of a real life existing building was selected. Thus the infilled RC frame tested in this work was a replica of a part of an already tested by Mehrabi et all (1994). The portion (frame) was deliberately selected so that it ertain all frames behaviours.

Description of a test Specimen.-A six-story, three-bay, reinforced concrete moment-resisting frame, which is shown in Fig. 4.1, has been selected as a prototype structure. It represents an interior frame of a typical office building. The height/length ratio for each bay is 1/1.5. The service live load was taken to be 34.47×10^5 kN/mm^2 , and the dead load was estimated to be 89.632×10^5 kN/mm^2. In either case, the load resistance contributed by infill panels was ignored, as in standard design practice.

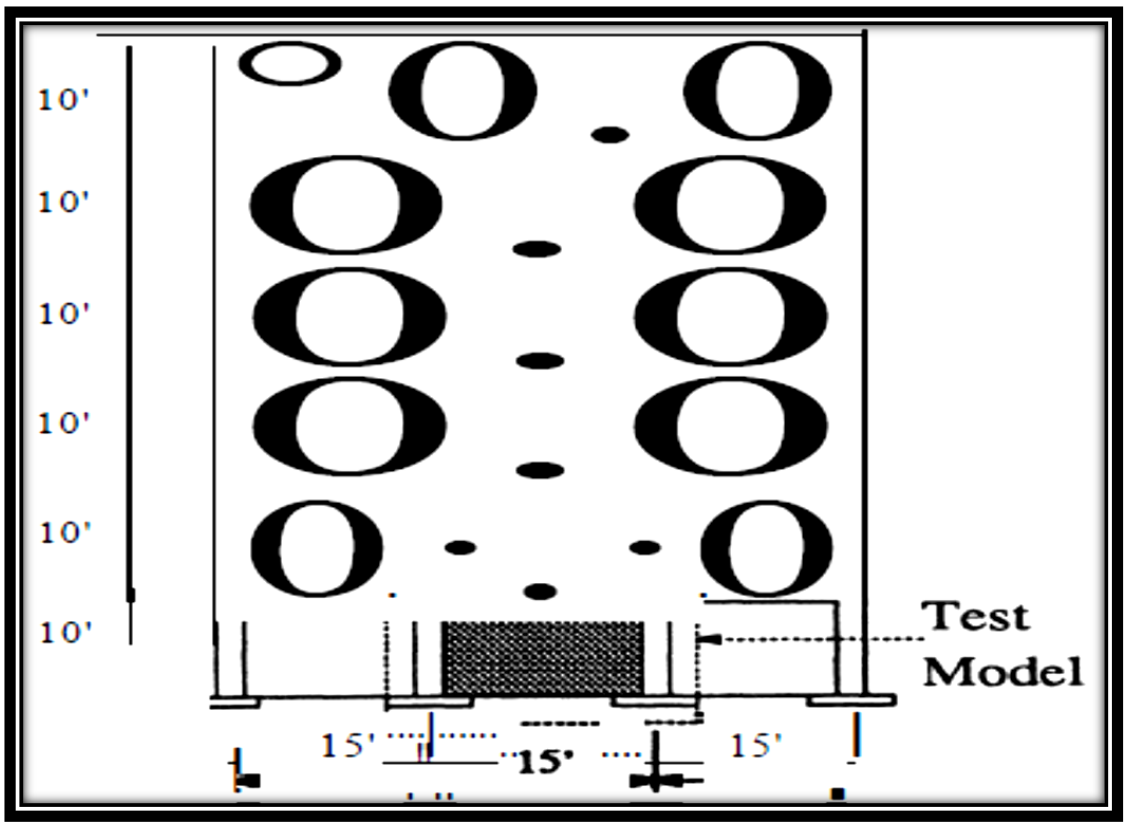

Fig-4.1, A Six Storey, three bay RCC moment resisting frame(Mehrabi et al.)

The single-bay test specimens were chosen to be 1/2-scale models representing the interior bay at the bottom story of the prototype frame as shown in fig-4.2 same as taken by Mehrabi et al.

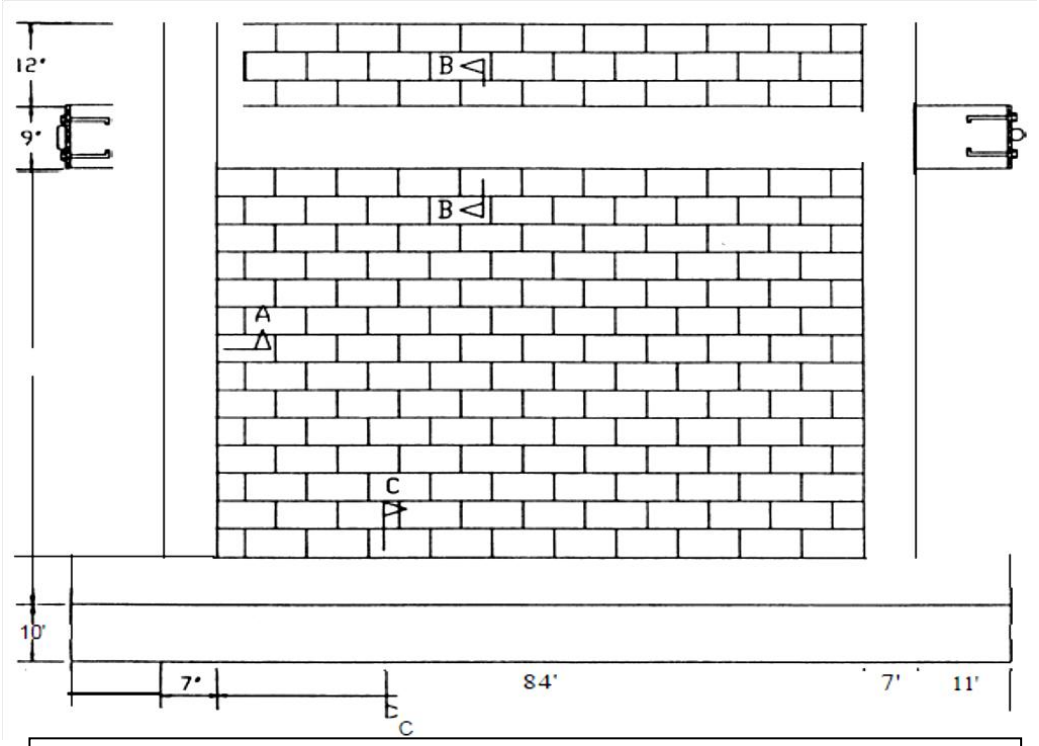

Fig-4.2, Specimen Consider for Experimental work by Mehrbi et al.1994

Analytical Work.

- Firstly verified analytically the RC infilled frame or bare frame, already tested by researcher.
- Secondly checked for Single strut for width of strut given by Holmes.
- Thirdly checked for Single strut for width given by Paulay and Prisly.
- Fourthly checked for Single strut for width given by Mainstone.
- Fifth checked above Single strut under cyclic loading.

4.2.1 Detail and Geometry of RC infilled Frame

4.2.1.1 Dimensions of beam and columns for Bare and infilled frame as shown in fig 4.3

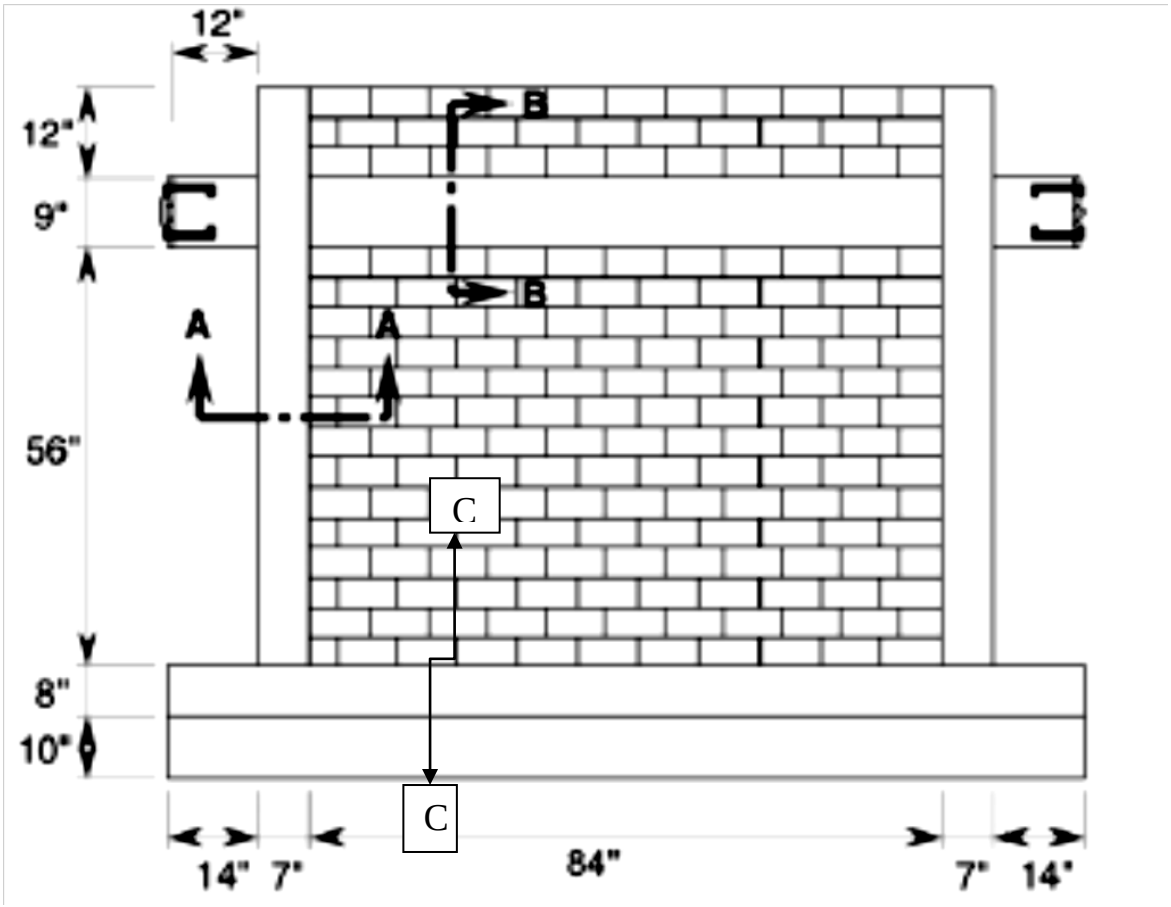

Fig-4.3 (a) Detail and Geometry of RC infilled Frame

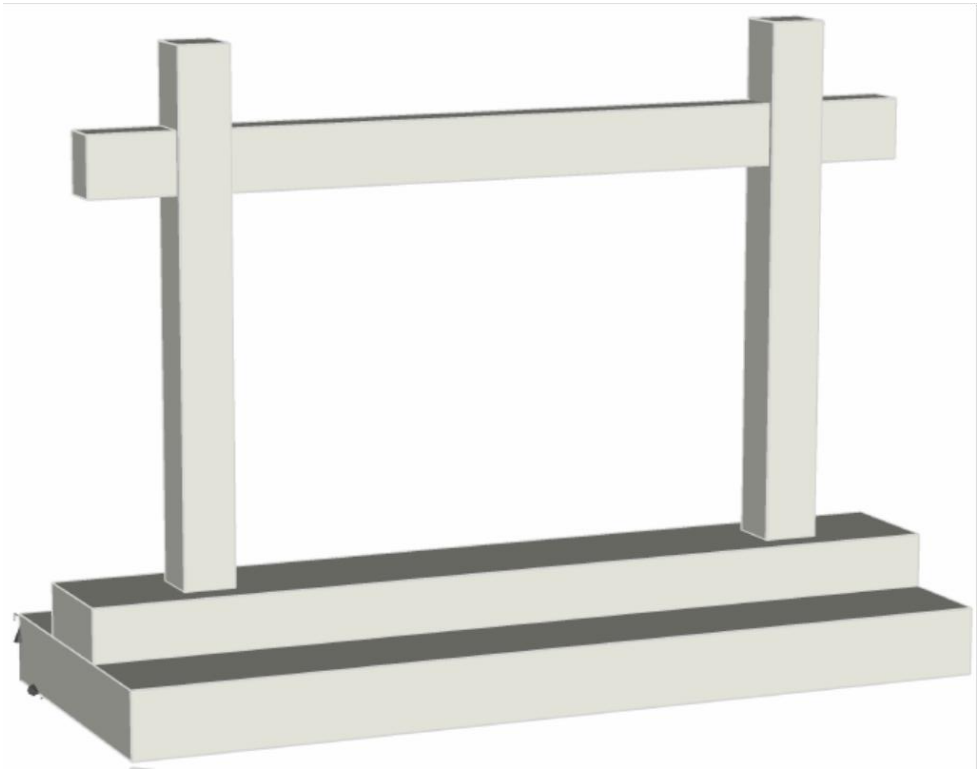

Fig-4.3(b) Geometry of bare frame

4.2.2 Material properties

5.2.2 (a) The material used for construction of Reinforced concrete bare frame and Infilled RC frame(Mehrabi et al.). The basic material properties used are as follows, all the material properties are as per ACI318-89:

Table -4.1 Material parameters for concrete in frame and masonry units

Description	Concrete in frame	Concrete in masonry solid units
Modulus of Elasticity	2.45 E-5 KN/mm^2	1.38 E-5 KN/mm^2
Poissions ratio	0.16	0.16
Tensile Strength	0.0027 KN/mm^2	0.00158 KN/mm^2
First mode fracture energy	6.205 E-7 KN/mm^2	6.205 E-7 KN/mm2
Shear retention factor	NA	NA
Compressive Strength	0.0206 kN/mm^2	0.00158 kN/mm^2
Fracture energy in compression	0.000151 kN/mm^2	0.000151 kN/mm^2
Shape of tensile stress/Strain curve	Exponential	Exponential
Shape of compressive stress/strain curve	Parabolic	Parabolic
Ultimate Strain in Bending ε_{cu}	0.0035	NA

4.2.1.2 Detail of frame with single strut having width given by Holmes, Mainstone & Paulay and Pristeley as shown in fig 4.4

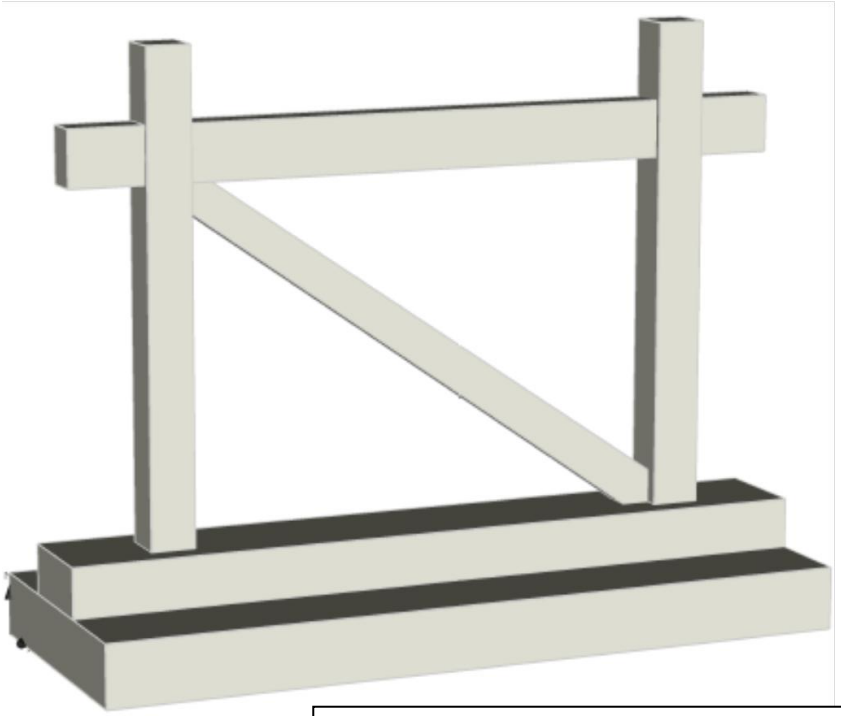

Fig 4.4 RC frame with single Strut

4.2.2 (b) **Material Properties** of concrete frame as already explained and material properties of single strut is same as that of Concrete masonry Solid Unit.

Table -5.2 Material parameters for concrete in frame and Single Strut.

Description	**Concrete in frame**	**Solid Single Strut**
Modulus of Elasticity	2.45 E-5 KN/mm^2	1.38 E-5 KN/mm^2
Poissions ratio	0.16	0.16
Tensile Strength	0.0027 KN/mm^2	0.00158 KN/mm^2
First mode fracture energy	6.205 E-7 KN/mm^2	6.205 E-7 KN/mm2
Shear retention factor	NA	NA
Compressive Strength	0.0206 kN/mm^2	0.00158 kN/mm^2
Fracture energy in compression	0.000151 kN/mm^2	0.000151 kN/mm^2
Shape of tensile stress/Strain curve	Exponential	Exponential
Shape of compressive stress/strain curve	Parabolic	Parabolic
Ultimate Strain in Bending ε_{cu}	0.0035	NA

4.2.2 (c) **Material Properties** of concrete frame as already explained and material properties of single strut is same as that of Concrete masonry Solid Unit.

Table -4.3 Material parameters for concrete in frame and Single Strut.

Description	**Concrete in frame**	**Solid Three Strut**
Modulus of Elasticity	2.45 E-5 KN/mm^2	1.38 E-5 KN/mm^2
Poissions ratio	0.16	0.16
Tensile Strength	0.0027 KN/mm^2	0.00158 KN/mm^2
First mode fracture energy	6.205 E-7 KN/mm^2	6.205 E-7 KN/mm2
Shear retention factor	NA	NA
Compressive Strength	0.0206 kN/mm^2	0.00158 kN/mm^2
Fracture energy in compression	0.000151 kN/mm^2	0.000151 kN/mm^2
Shape of tensile stress/Strain curve	Exponential	Exponential
Shape of compressive stress/strain curve	Parabolic	Parabolic
Ultimate Strain in Bending ε_{cu}	0.0035	NA

4.2.3 SECTION DIMENSIONS

The frame is made of various sections whose dimensions are enlisted in table 3.1 below. In the identification column, ‘B’ stands for beam, ‘C’ stands for column , ‘F’ stands for foundation and ‘S’ stands for Strut Single Strut or Three Strut as shown in fig 5.7(Mehrabi et al.).

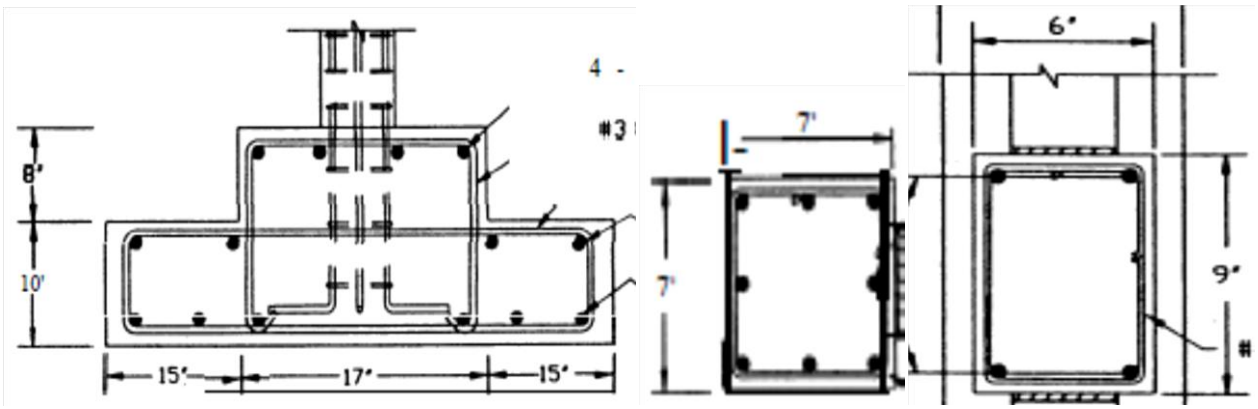

(a) Foundation Detail & Geometry

(b)Column Detail & Geometry

(c) Beam Detail & Geometry.

Fig-4.7 Sectional detail of various Components RC frame.

4.2.4 Properties & Details of Reinforcement

Detail reinforcement provided is as given in Table 4.4 is provided as per ACI codes.

Identification	Top Cover	Bottom Cover	Dia of Stirrups(as per American standard)	Converted as per Indian Standards in mm
Column Longitudinal bar	20mm	20mm	8no's- #4	8no.s-12.8mm dia
Column Stirrups	20mm	20mm	@3" - #2	@64mm-6.35mm
Beam Main Steel	20mm	20mm	2x2 no's- #5	4no's – 15.875mm
Beam Stirrups	20mm	20mm	@ 3"- #2	@75mm – 6.35mm
Bottom Foundation Main (bottom)	50mm	50mm	6no's - #5	6no's – 15.875mm
Bottom Foundation Main (top)	50mm	50mm	4no's - #4	4no's – 12.7mm
Bottom Foundation Stirrups	50mm	50mm	@4"- #3	@100mm – 9.525mm
Top Foundation Main	50mm	50mm	4no's - #6	4no's – 19.05 mm
Top Foundation Stirrups	50mm	50mm	@4"- #3	@100mm – 9.525mm

Properties of Reinforcement- Average Tensile Strengths of Reinforcing Steel.

Detail reinforcement provided is as given in Table 4.5 is provided as per ACI codes.

Bar Size	Type of Bar	Nominal Diameter	Yield Stress	Ultimate Stress
#2	Plain	6.35 mm	237.185 kN	290.14 kN
#3	Deformed	9.525 mm	271.45 kN	428 kN
#4	Deformed	12.7 mm	267 kN	428 kN
#5	Deformed	15.875 mm	271.45 kN	428 kN
#6	Deformed	19.05 mm	271.45 kN	428 kN

4.3 Analytical Work

The sub-assemblage a specimen is subjected to displacements controlled loading and another type is dead load in form of Point load.

4.3.1 MONOTONIC LOADING PATTERN

First type of loading consists of uniformly increasing monotonic displacement. In this displacements on structure are increased with each load step with the uniform increment of 1mm up to the failure of structure.

Table -4.6 Shows the Monotonic Loading Pattern for frame.

Step No.	1	2	3	4	5	6	7	8	9	10	11	12	13	14	15	16
Displacement(mm)	5	10	15	20	25	30	35	40	45	50	55	60	65	70	75	80

4.4 INTRODUCTION TO FE MODELLING

For structural design and assessment of reinforced concrete members, the non-linear finite element (FE) analysis has become an important tool. Over the last one or two decade numerical simulation of reinforced concrete structures and structural elements has become a major research area. A successful numerical simulation demands choosing suitable elements, formulating proper material models and selecting proper solution method.

4.4.1 Finite Element Method

The finite element method (FEM) or finite element analysis is a numerical technique for finding approximate solutions of partial differential equations (PDE) as well as of integral equations. The solution approach is based either on eliminating the differential equation completely (steady state problems), or rendering the PDE into an approximating system of ordinary differential equations, which are then numerically integrated using standard techniques.

In solving partial differential equations, the primary challenge is to create an equation that approximates the equation to be studied, but is numerically stable, meaning that errors in the input data and intermediate calculations do not accumulate and cause the resulting output to be meaningless. The Finite Element Method is a good choice for solving partial differential equations over complex domains.

4.5 FINITE ELEMENT MODELLING

The basic concept of FEM modelling is the subdivision of the mathematical model into disjoint (non-overlapping) components of simple geometry. The response of each element is expressed in terms of a finite number of degrees of freedom characterized as the value of an unknown function, or functions

or at a set of nodal points. The response of the mathematical model is then considered to be the discrete model obtained by connecting or assembling the collection of all elements.

Within the framework of the finite element method reinforced concrete frame can be represented either by superimposition of the material models for the constituent parts (i.e., for concrete, and reinforcing steel), or by a constitutive law for the composite concrete, embedded steel considered as a continuum.

The finite element method is well suited for superimposition of the material models for the constituent parts of a composite material. Several constitutive models covering these effects are implemented in the computer code ATENA, which is a finite element package designed for computer simulation of concrete structures. The graphical user interface in ATENA provides an efficient and powerful environment for solving many anchoring problems. ATENA enables virtual testing of structures using computers, which is the present trend in the research and development world. Material models of this type can be employed for virtually all kinds of reinforced concrete structural members. Depending on the type of material modelling to be solved in ATENA, concrete can be represented by solid brick elements; the reinforcement is modelled by bar elements (discrete representation).

Geometry and shape of any mathematical element help in proper placement of the nodal points and materials properties helps in using proper modelling.

4.6 MATERIAL MODELS

The program system ATENA offers a variety of material models for different materials and purposes. The most important material models in ATENA for RCC structure are concrete and reinforcement. These advanced models take into account all the important aspects of real material behaviour in tension and compression.

4.6.1 MODELLING OF CONCRETE

1) Geometry of the Concrete

Element geometric modelling of concrete has been done using 3D solid brick element with 8 up to 20 nodes in ATENA, shown in **Figure 4.8**

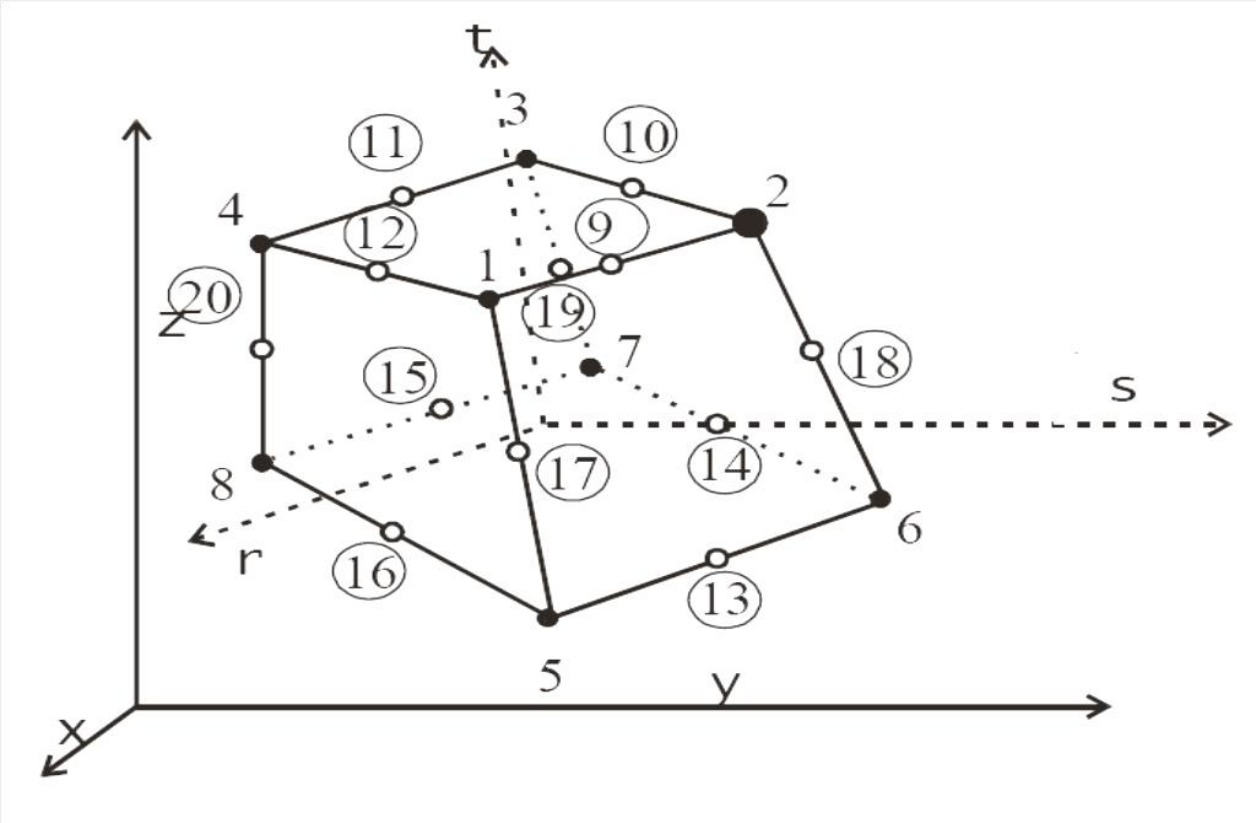

Fig-4.8 Geometry of Brick Elements.

2) Element Properties

3D solid brick element having three degree of freedom at each node: translations in the nodal x, y and z directions. This is an isoparametric elements integrated by Gauss integration at integration points. This element is capable of plastic deformation, cracking in three orthogonal directions, and crushing. The most important aspect of this element is the treatment of non-linear material properties.

3) Element Interpolation function

3D solid brick element interpolation functions for all variants of the elements are given below:

N1= (1/8) (1+r) (1+s) (1+t)
N2= (1/8) (1-r) (1+s) (1+t)
N3= (1/8) (1-r) (1-s) (1+t)
N4= (1/8) (1+r) (1-s) (1+t)
N5= (1/8) (1+r) (1+s) (1-t)
N6= (1/8) (1-r) (1+s) (1-t)
N7= (1/8) (1-r) (1-s) (1-t)
N8= (1/8) (1+r) (1-s) (1-t)

4.6.2 MODELLING OF REINFORCEMENT

1) Geometry of the reinforcement

Reinforcement modelling could be discrete or smeared. In our work, a discrete modelling of reinforcement has been done. The reinforcement has been modelled using bar elements in ATENA.

2) Element Properties

Reinforcement steel is a 3D bar element, which has three degrees of freedom at each node; translations in the nodal x, y and z direction. Bar element is a uniaxial tension-compression element. The stress is assumed to be uniform over the entire element. Also plasticity, creep, swelling, large deflection and stress-stiffening capabilities are included in the element.

3) Element Shape Functions:

The shape functions in natural co-ordinate system for the three dimensional bar element without rotational degrees of freedom.

N1= (1/2) (1+s) N2= (1/2) (1-s)

4.7 STRESS-STRAIN RELATIONS FOR CONCRETE

Concrete exhibits a large number of micro-cracks, especially, at the interface between coarser aggregates and mortar, even before subjected to any load. The presence of these micro-cracks has a great effect on the mechanical behaviour of concrete, since their propagation during loading contributes to the nonlinear behaviour at low stress levels and causes volume expansion near failure. Many of these micro-cracks are caused by segregation, shrinkage or thermal expansion of the mortar. Some micro-cracks may develop during loading because of the difference in stiffness between aggregates and mortar. Since the aggregate-mortar interface has a significantly lower tensile strength than mortar, it constitutes the weakest link in the composite system. This is the primary reason for the low tensile strength of concrete.

The response of a structure under load depends to a large extent on the stress-strain relation of the constituent materials and the magnitude of stress. Since concrete is used mostly in compression, the **stress-strain relation** in compression is of primary interest.

4.7.1 EQUIVALENT UNIAXIAL LAW

The nonlinear behaviour of concrete in the biaxial stress state is described by means of the so called effective stress σ_c^{ef}, and the equivalent uni-axial strain ε^{eq}. The effective stress is in most cases a principal stress.

The equivalent uni-axial strain is introduced in order to eliminate the Poisson‟s effect in the plane stress state. $\boldsymbol{\varepsilon^{eq} = \sigma_{ci} / E_{ci}}$

The equivalent uni-axial strain can be considered as the strain, that would be produced by the stress σci in a uni-axial test with modulus associated Eci with the direction *i*. Within this assumption, the nonlinearity representing damage is caused only by the governing stress σci. The complete equivalent uni-axial stress-strain diagram for concrete is shown in **Figure4.9.**

The numbers of the diagram parts in **Figure 4.9**(material state numbers) are used in the results of the analysis to indicate the state of damage of concrete.

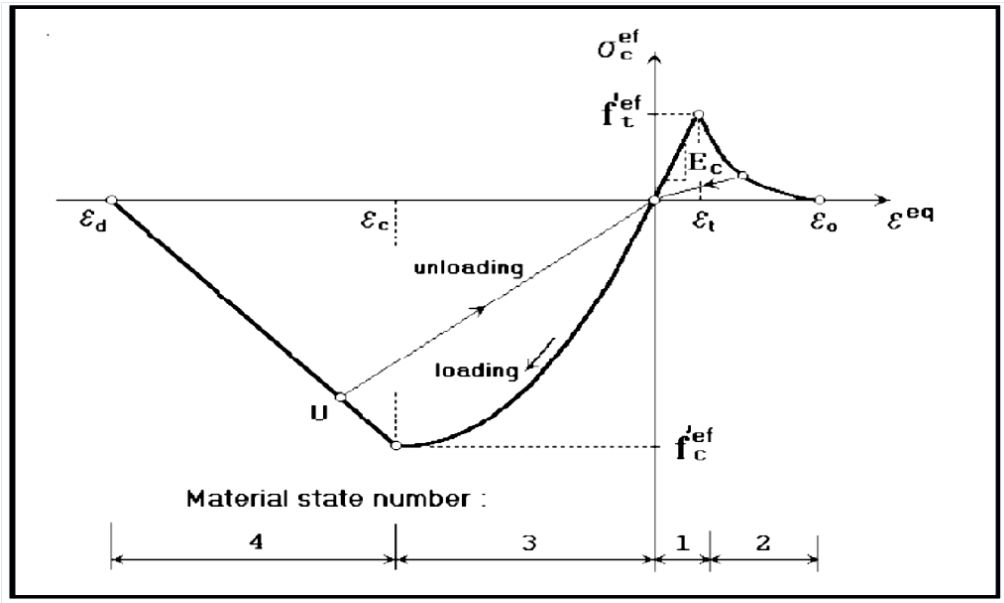

Fig-4.9,Uniaxial stress-strain law for concrete

Unloading is a linear function to the origin. An example of the unloading point *U* is shown in Figure 4.9. Thus, the relation between stress σ_c^{ef} and strain ε^{eq} is not unique and depends on a load history. A change from loading to unloading occurs, when the increment of the effective strain changes the sign. If subsequent reloading occurs the linear unloading path is followed until the last loading point *U* is reached again. Then, the loading function is resumed.

The peak values of stress in compression f_c^{ef} and in tension f_t^{ef} are calculated according to the biaxial stress state. Thus, the equivalent uni-axial stress-strain law reflects the biaxial stress state.

4.7.2 BIAXIAL STRESS FAILURE CRITERION OF CONCRETE

1) Compressive Failure

A biaxial stress failure criterion according to KUPFER et al. (1969) is used as shown in Figure4.10. In the compression-compression stress state the failure function is

$$\mathbf{f_c^{ef} = [(1+3.65a)/(1+a)^2]f'_c;} \qquad \mathbf{a = (\sigma_{c1}/\sigma_{c2})} \qquad (5.1)$$

Where σ_{c1}, σ_{c2} are the principal stresses in concrete and f_c is the uni-axial cylinder strength. In the biaxial stress state, the strength of concrete is predicted under the assumption of a proportional stress path.

In the tension-compression state, the failure function continues linearly from the point $\sigma_{c1} = 0$, $\sigma_{c2} = f_c$, into the tension-compression region with the linearly decreasing strength:

$$\mathbf{f_c^{ef} = f_c\, I_{ec}, \qquad r_{ec} = [1 + 5.3278(\sigma_{c1}/ f_c)]} \tag{5.2}$$

Where r_{ec} is the reduction factor of the compressive strength in the principal direction 2 due to the tensile stress in the principal direction

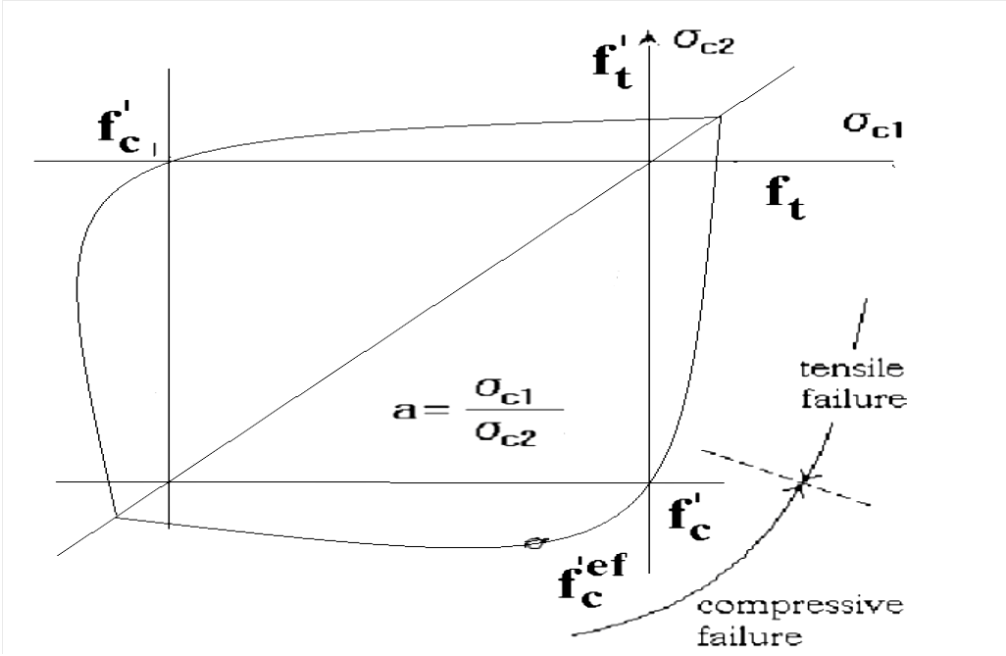

Fig-4.9,Biaxial failure functions for concrete

2) Tensile failures

In the tension-tension state, the tensile strength is constant and equal to the uniaxial tensile strength f_t. In the tension-compression state, the tensile strength is reduced by the relation:

$$\mathbf{f_t^{ef} = f_t\, r_{et}} \tag{5.3}$$

Where ret is the reduction factor of the tensile strength in the direction 1 due to the compressive stress in the direction 2. The reduction function has one of the following forms.

$$\mathbf{r_{et} = 1 - 0.8\,(\sigma_{c2}/ f_c)} \tag{5.4}$$

$$\mathbf{r_{et} = [A + (A - 1)\,B]/ AB; \qquad B = Kx + A; \qquad x = \sigma_{c2}/ f_c} \tag{5.5}$$

The relation in Eq. (5.4) is the linear decrease of the tensile strength and (5.5) is the hyperbolic decrease.

Two predefined shapes of the hyperbola are given by the position of an intermediate point *r, x*. Constants *K* and *A* defines the shape of the hyperbola. The values of the constants for the two positions of the intermediate point are given in the following table.

Type	Point		Parameters	
	r	X	A	K
A	0.5	0.4	0.75	1.125
B	0.5	0.2	1.0625	6.0208

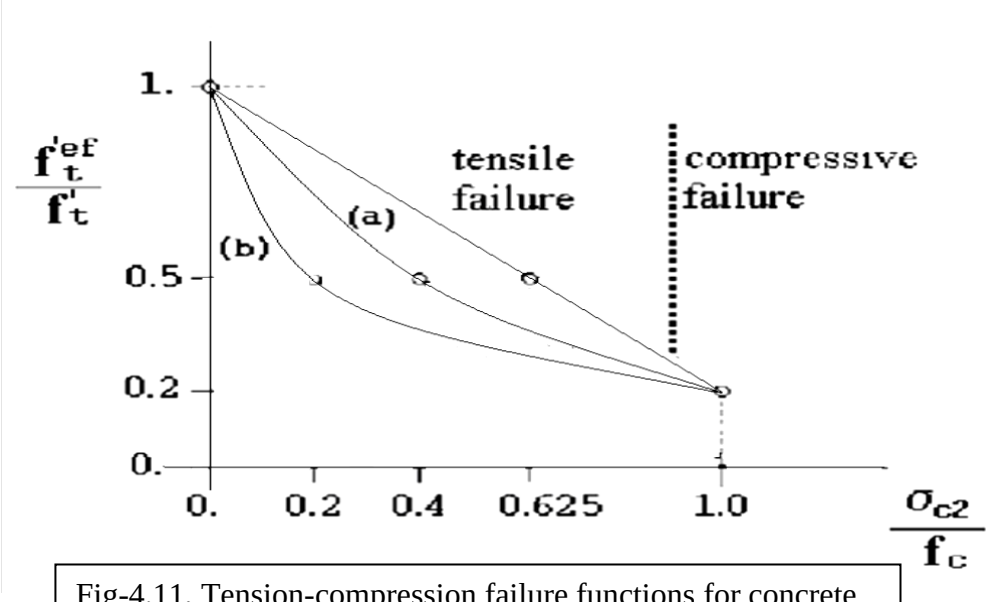

Fig-4.11, Tension-compression failure functions for concrete

4.7.3 TENSION BEFORE CRACKING

The behaviour of concrete in tension without cracks is assumed linear elastic. E_c *is* the initial elastic modulus of concrete, f_t^{ef} is the effective tensile strength derived from the biaxial failure function already describe above.

$$\sigma_c^{ef} = E_c \varepsilon^{eq}, 0 < \sigma_c < f_t^{ef}$$

4.7.4 TENSION AFTER CRACKING

A fictitious crack model is based on a crack-opening law and fracture energy. This formulation is suitable for modelling of crack propagation in concrete. It is used in combination with the crack band. It is a region (band) of material, which represents a discrete failure plane in the finite element analysis. In tension it is a crack, in compression it is a plane of crushing. In reality these failure

regions have some dimension. However, since according to the experiments, the dimensions of the failure regions are independent on the structural size, they are assumed as fictitious planes. In case of tensile cracks, this approach is known as rack the "crack band theory**", (*BAZANT OH 1983*).** Here is the same concept used also for the compression failure. The purpose of the failure band is to eliminate two deficiencies, which occur in connection with the application of the finite element model: element size effect and element orientation effect.

1) Element size effect.

The direction of the failure planes is assumed to be normal to the principal stresses in tension and compression, respectively. The failure bands (for tension L_t and for compression L_c) are defined as projections of the finite element dimensions on the failure planes.

2) Element Orientation Effect.

The element orientation effect is reduced, by further increasing of the failure band for skew meshes, by the following formula (proposed by (***CERVENKA et al. 1995*).**

$$\mathbf{L_t = \gamma L_t, \qquad L_c = \gamma L_c}$$

$$\mathbf{\gamma = 1 + (\gamma^{max} - 1)\,(\theta / 45), \qquad \theta\ \varepsilon\ (0; 45)} \qquad (5.6)$$

An angle θ is the minimal angle (min (θ_1, θ_2)) between the direction of the normal to the failure plane and element sides. In case of a general quadrilateral element the element sides" directions are calculated as average side directions for the two opposite edges. The above formula is a linear interpolation between the factor γ=1.0 for the direction parallel with element sides, and $\gamma=\gamma^{max}$ for the direction inclined at 45^o. The recommended (and default) value of γ max =1.5.

4.8 BEHAVIOUR OF CRACKED CONCRETE

4.8.1 DESCRIPTION OF A CRACKED SECTION

The nonlinear response of concrete is often dominated by progressive cracking which results in localized failure. The structural member has cracked at discrete locations where the concrete tensile strength is exceeded.

At the cracked section all tension is carried by the steel reinforcement. Tensile stresses are, however, present in the concrete between the cracks, since some tension is transferred from steel to concrete

through bond. The magnitude and distribution of bond stresses between the cracks determines the distribution of tensile stresses in the concrete and the reinforcing steel between the cracks.

Additional cracks can form between the initial cracks, if the tensile stress exceeds the concrete tensile strength between previously formed cracks. The final cracking state is reached when a tensile force of sufficient magnitude to form an additional crack between two existing cracks can no longer be transferred by bond from steel to concrete.

As the concrete reaches its tensile strength, primary cracks form. The number and the extent of cracks are controlled by the size and placement of the reinforcing steel. At the primary cracks the concrete stress drops to zero and the steel carries the entire tensile force. The concrete between the cracks, however, still carries some tensile stress, which decreases with increasing load magnitude. This drop in concrete tensile stress with increasing load is associated with the breakdown of bond between reinforcing steel and concrete. At this stage a secondary system of internal cracks, called bond cracks, develops around the reinforcing steel, which begins to slip relative to the surrounding concrete.

Since cracking is the major source of material nonlinearity in the serviceability range of reinforced concrete structures, realistic cracking models need to be developed in order to accurately predict the load-deformation behaviour of reinforced concrete members. The selection of a cracking model depends on the purpose of the finite element analysis. If overall load-deflection behaviour is of primary interest, without much concern for crack patterns and estimation of local stresses, the "smeared" crack model is probably the best choice. If detailed local behaviour is of interest, the adoption of a "discrete" crack model might be necessary. Unless special connecting elements and double nodes are introduced in the finite element discretization of the structure, the well established smeared crack model results in perfect bond between steel and concrete, because of the inherent continuity of the displacement field.

4.8.2 MODELLING OF CRACKS IN CONCRETE

The process of crack formation can be divided into three stages, Figure 5.12. The un-cracked stage is before a tensile strength is reached. The crack formation takes place in the process zone of a potential crack with decreasing tensile stress on a crack face due to a bridging effect. Finally, after a complete release of the stress, the crack opening continues without the stress.

The tension failure of concrete is characterized by a gradual growth of cracks, which join together and eventually disconnect larger parts of the structure. It is usually assumed that cracking formation

is a brittle process and that the strength in tension loading direction abruptly goes to zero after such cracks have formed.

Therefore, the formation of cracks is undoubtedly one of the most important non-linear phenomenon, which governs the behaviour of the concrete structures. In the finite element analysis of concrete structures, two principally different approaches have been employed for crack modelling. These are (a) discrete crack modelling (b) smeared crack modelling

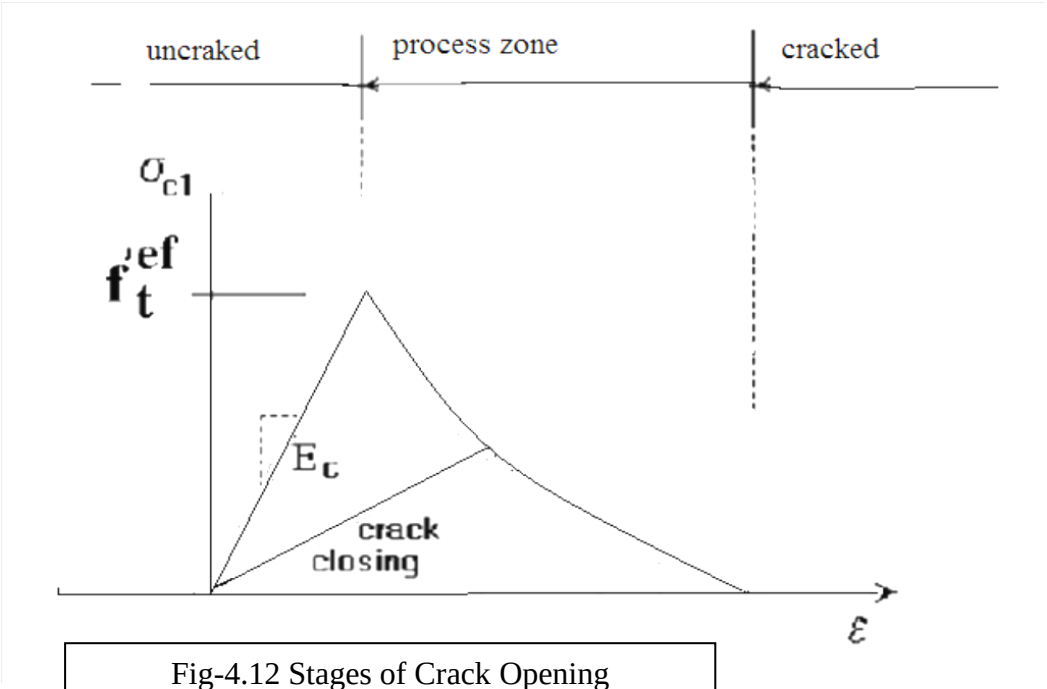

Fig-4.12 Stages of Crack Opening

The discrete approach is physically attractive but this approach suffers from few drawbacks, such as**,** it employs a continuous change in nodal connectivity, which does not fit in the nature of finite element displacement method; the crack is considered to follow a predefined path along the element edges and excessive computational efforts are required. The second approach is the smeared crack approach. In this approach the cracks are assumed to be smeared out in a continuous fashion.

Within the smeared concept two options are available for crack models: the fixed crack model and the rotated crack model. In both models the crack is formed when the principal stress exceeds the tensile strength. It is assumed that the cracks are uniformly distributed within the material volume. This is reflected in the constitutive model by an introduction of orthotropy.

1) Fixed Crack Model

In the fixed crack model (***CERVENKA 1985, DARWIN 1974***) the crack direction is given by the principal stress direction at the moment of the crack initiation. During further loading this direction is fixed and represents the material axis of the orthotropy.

The principal stress and strain directions coincide in the un-cracked concrete, because of the assumption of isotropy in the concrete component. After cracking the orthotropy is introduced. The weak material axis m1 is normal to the crack direction; the strong axis *m2* is parallel with the cracks. In a general case the principal strain axes ε1 and ε2 rotate and need not to coincide with the axes of the orthotropy *m1* and *m2*. This produces a shear stress on the crack face as shown in Figure. 5.12. The stress components σc1 and σc2 denote, respectively, the stresses normal and parallel to the crack plane and, due to shear stress, they are not the principal stresses.

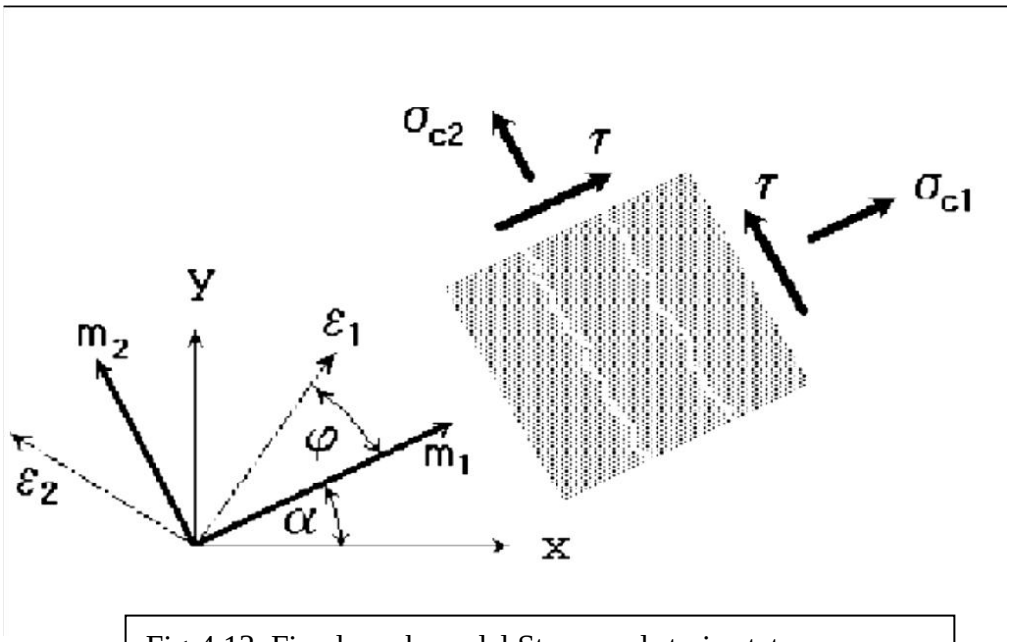

Fig-4.13, Fixed crack model Stress and strain state

2) Rotated Crack Model

In the rotated crack model, the direction of the principal stress coincides with the direction of the principal strain. Thus, no shear strain occurs on the crack plane and only two normal stress components must be defined, as shown in Figure 4.14.

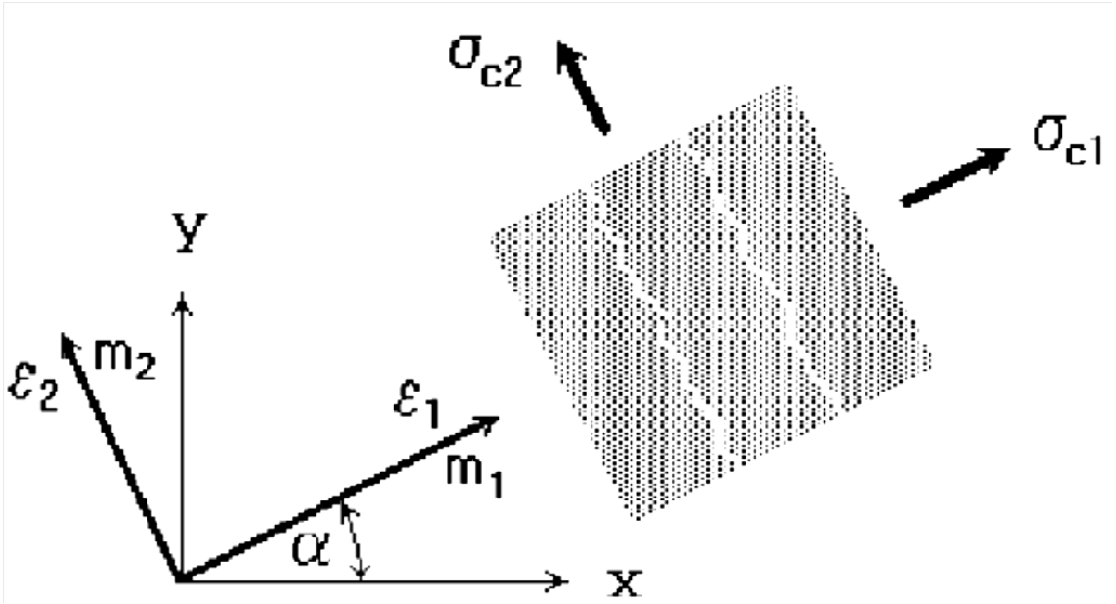

Fig-4.14 Rotated crack model. Stress and strain state

If the principal strain axes rotate during the loading the direction of the cracks rotates, too. In order to ensure the co-axiality of the principal strain axes with the material axes the tangent shear modulus *Gt* is calculated according to CRISFIELD 1989 as

$$G_t = (\sigma_{c1} - \sigma_{c2})/ 2\ (\varepsilon_1 - \varepsilon_2)$$

4.9 STRESS-STRAIN LAWS FOR REINFORCEMENT

4.9.1 INTRODUCTION

Reinforcement can be modelled in two distinct forms: discrete and smeared. Discrete reinforcement is in form of reinforcing bars and is modelled by truss elements. The smeared reinforcement is a component of composite material and can be considered either as a single (only one-constituent) material in the element under consideration or as one of the more such constituents. The former case can be a special mesh element (layer), while the later can be an element with concrete containing one or more reinforcements. In both cases the state of uniaxial stress is assumed and the same formulation of stress-strain law is used in all types of reinforcement.

4.9.2 BILINEAR LAW

The bilinear law, elastic-perfectly plastic, is assumed as shown in Figure 4.15. The initial elastic part has the elastic modulus of steel E_s. The second line represents the plasticity of the steel with hardening and its slope is the hardening modulus E_{sh}. In case of perfect plasticity E_{sh} =0. Limit strain ε_L represents limited ductility of steel.

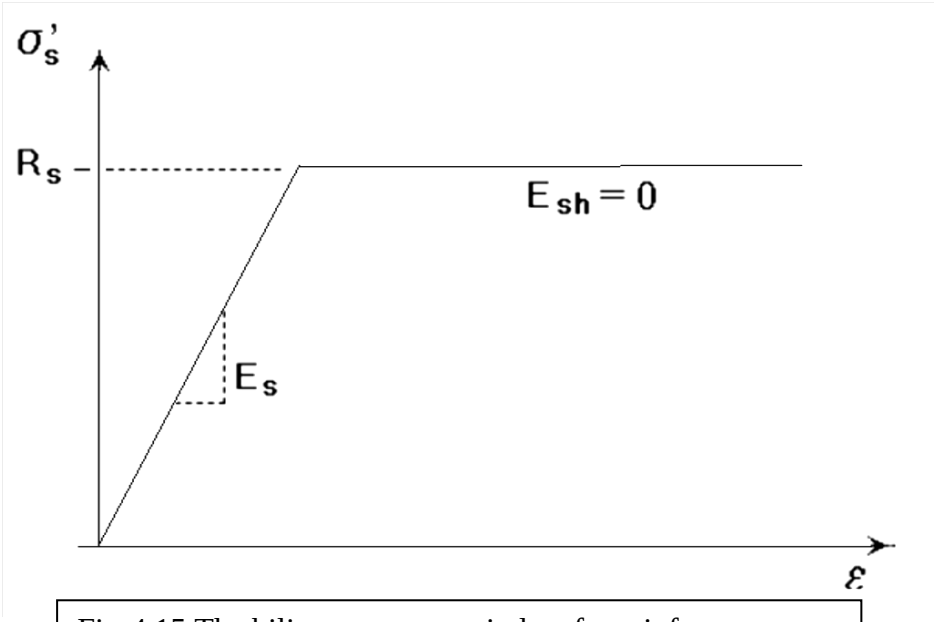

Fig-4.15 The bilinear stress-strain law for reinforcement

4.9.3 MULTI-LINEAR LAW

The multi-linear law consists of four lines as shown in Figure 4.16**.** This law allows modelling of all four stages of steel behaviour: elastic state, yield plateau, hardening and fracture. The multi-line is defined by four points, which can be specified by input.

The above described stress-strain laws can be used for the discrete as well as the smeared reinforcement. The smeared reinforcement requires two additional parameters: the reinforcing ratio *p* and the direction angle β as shown in Figure. 4.17.

Where ρ = (Area of steel/ Area of concrete)

The spacing *s* of the smeared reinforcement is assumed infinitely small. The stress in the smeared reinforcement is evaluated in the cracks; therefore it should include also a part of stress due to tension stiffening. $\sigma_{scr} = \sigma_s + \sigma_{ts}$

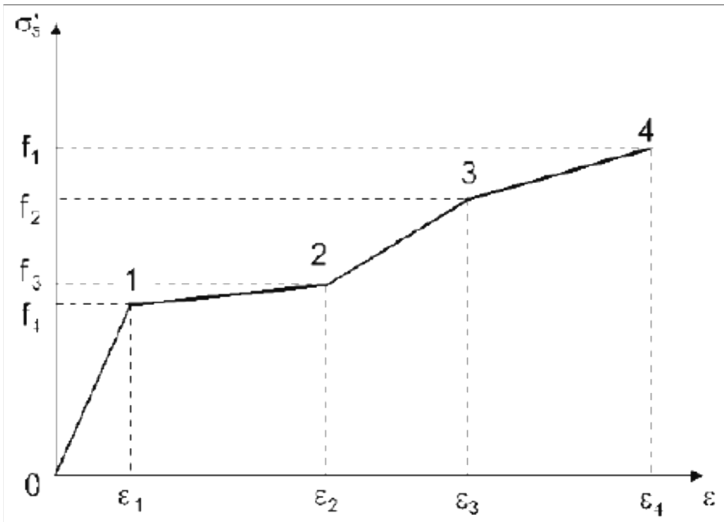

Fig-4.16 The multi-linear stress-strain law for reinforcement

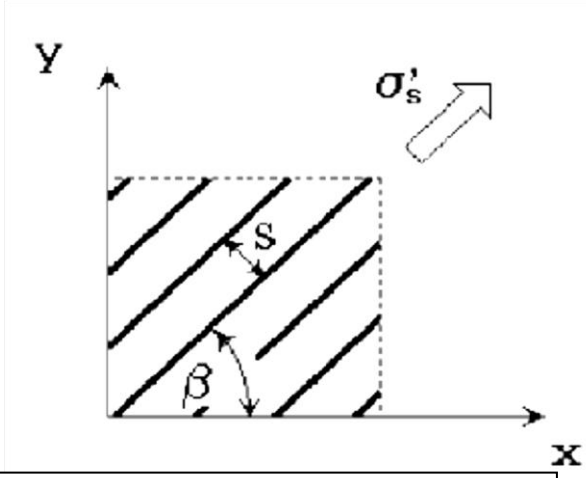

Fig-4.17 Smeared reinforcement

where σ_s is the steel stress between the cracks (the steel stress in smeared reinforcement),

σ_{scr} is the steel stress in a crack. If no tension stiffening is specified $\sigma_{ts} = 0$ and $\sigma_{scr} = \sigma_s$. In case of the discrete reinforcement the steel stress is always σ_s.

Once we understand the finite element modelling, the next step is the analytical programming. The main objective of this analytical program is to get the result of under reinforced concrete frame and compare with the experimental results. In the analytical programming, first we select the materials and its properties and create geometry of the frame.

The frame is tested up to its failure point and the ultimate load deflection values are plotted as graphs. For modelling the control members in ATENA, concrete, reinforcement bars of different diameters, steel plates, and concrete masonry prism is used as materials.

4.10 F.E. analysis using ATENA

Once we understand the finite element modeling, the next step is the analytical programming. The main objective of this analytical program is to get the result of RC Bare, Infilled and frame with single or three struts and compare with the results experimental. In the analytical programming, first we select the materials and its properties and create geometry of the structure. The frame is tested by subjecting it to the loading pattern as described earlier & load deflection values are plotted as graphs.

4.10.1 MATERIAL PROPERTIES

Concrete, reinforcement steel, steel plates, & contact element have been used to model the RCC bare, infilled, single strut or three strut frame. The specification and the properties of these materials are as under:

1) Concrete

In ATENA, concrete material is modelled as a 3D nonlinear cementitious2. The physical properties of 3D nonlinear cementitious2 material are given in **Table 4.7**. The values are taken as per ACI318-89.

2) Reinforcement Bars

Steel of grade different diameter are used as main steel while #2 and #3 diameter bars are used as shear reinforcement. The properties of these bars are shown in **Table 4.8.**

Table 5.8 Material Properties of Concrete

Description	**Concrete in frame**	**Solid Struts or Brick**
Modulus of Elasticity	2.45 E-5 KN/mm^2	1.38 E-5 KN/mm^2
Poissions ratio	0.16	0.16
Tensile Strength	0.0027 KN/mm^2	0.00158 KN/mm^2
First mode fracture energy	6.205 E-7 KN/mm^2	6.205 E-7 KN/mm2
Shear retention factor	NA	NA
Compressive Strength	0.0206 kN/mm^2	0.00158 kN/mm^2
Fracture energy in compression	0.000151 kN/mm^2	0.000151 kN/mm^2
Shape of tensile stress/Strain curve	Exponential	Exponential
Shape of compressive stress/strain curve	Parabolic	Parabolic
Ultimate Strain in Bending ε_{cu}	0.0035	NA

Table 4.8 Material Properties of Reinforcement

Bar Size	Type of Bar	Nominal Diameter	Yield Stress	Ultimate Stress
#2	Plain	6.35 mm	237.185 kN	290.14 kN
#3	Deformed	9.525 mm	271.45 kN	428 kN
#4	Deformed	12.7 mm	267 kN	428 kN
#5	Deformed	15.875 mm	271.45 kN	428 kN
#6	Deformed	19.05 mm	271.45 kN	428 kN

3) Steel Plate

The function of the steel plate in the ATENA is for support and for loading. Here, the property of steel plate is same as the reinforcement bar except its yield strength. The HYSD steel of grade Fe-415 was used for steel plate.

4.11 FE MODELLING OF RCC FRAME IN ATENA

Modeling in ATENA is divided into three parts.

Preprocessing :-This window allows the definition of various material properties, shape, dimensions, supporting conditions, monitoring points & loads on structure.

Analysis :- After defining the various material properties, geometry, supports & loading conditions of structure the F.E. analysis are preformed in analysis window.

Post processing :-After the F.E. analysis of structure is completed, results are shown in post processing window

Procedure: In pre-processing window following steps are performed:-

Step1: Geometry of FE model is created .It has been presented in **Figure 4.18**.

Step2: Material properties are assigned to the various elements of the frame.

Step3: Supports and various supports, loadings and monitoring points are defined. **(Figure 4.19 & 4.20)**

Step4: Finite element meshing parameters are given and meshing of the model is generated accordingly. **(Figure 4.21)**

Step5: Various analysis steps are defined. The FE non-linear analysis is done in Run window. The FE non-linear static analysis calculates the effects of steady loading conditions on a structure, while ignoring inertia and damping effects, such as those caused by time-varying loads. A static analysis can, however, include steady inertia loads (such as gravity and rotational velocity), and time-varying loads that can be approximated as static equivalent loads (such as the static equivalent wind and seismic loads commonly defined in many building codes).

Static analysis is used to determine the displacements, stresses, strains, and forces in structures or components by loads that do not induce significant inertia and damping effects.

Step6: When the FE non linear static analysis is completed the, the results are shown in third part of the ATENA i.e. Post processing. The stress- strain values at every step, crack pattern and cracks propagation at every step shown help in to analyze the behaviour of the elements at every step of load deflection.

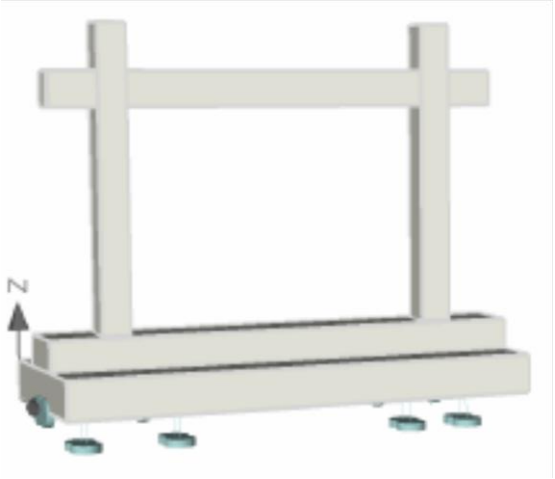

Fig-4.18- F.E model of Bare frame Geometry (With Surface)

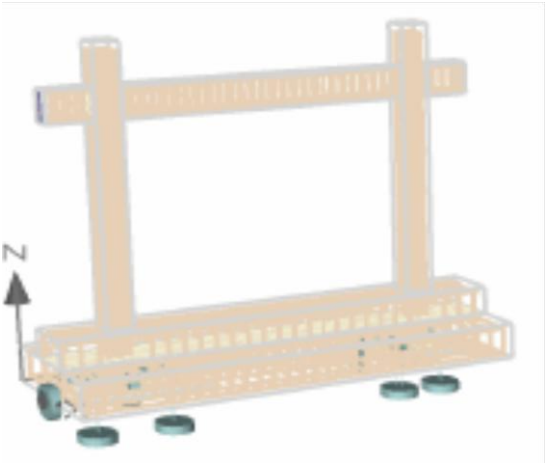

Fig-4.19-F.E Model of bare frame with supports (Without Surface)

Shaded area in **Fig. 4.19** represents contact between surfaces. At the interface of beam & column, contact surface has been edited to no connection as per the configuration of joint. Bottom of foundation beam is attached with steel plates which have been restrained in all 3 directions i.e. in X, Y & Z direction. Deformation has been applied at the centre of beam end in Y direction. 10mm thick steel plate has been added at the left hand side of beam surface in order to avoid local failure of beam.

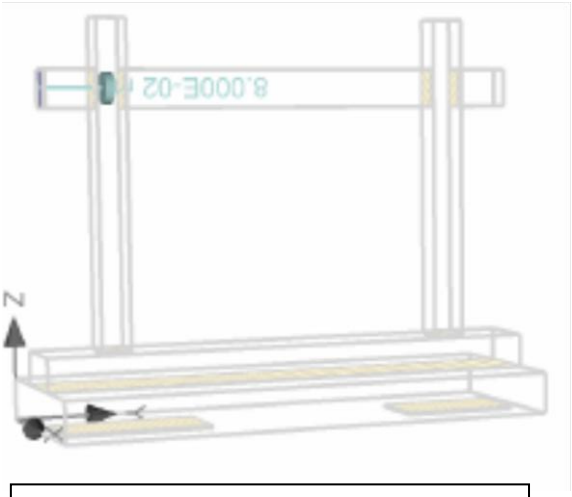

Fig-4.20- F.E model with loading.

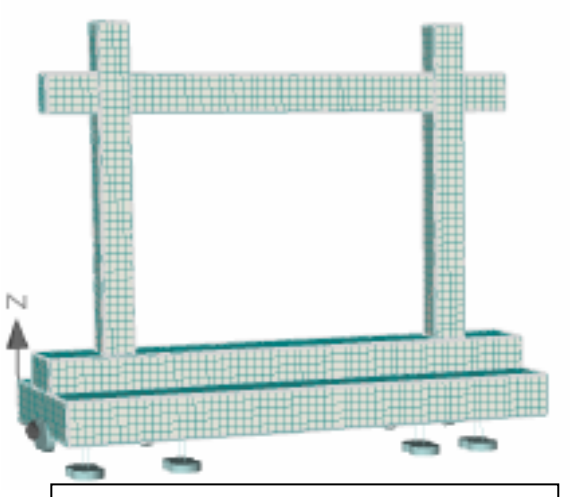

Fig-4.21-F.E mesh model

4.12 METHODS FOR NON-LINEAR SOLUTION

The best part of the ATENA is the simpler way of solving the non-linear structural behaviour through finite element method and its incremental loading criteria. Different methods are available in ATENA for solving non-linear equations such as, linear method, Newton-Raphson Method, Modified Newton-Raphson method, Arc Length methods are used in ATENA.

Among these the Newton-Raphson Method and Modified Newton-Raphson Method are more commonly used methods. In our present study, Newton-Raphson method is used for solving the simultaneous equations. It is an iterative process of solving the non-linear equations.

One approach to non-linear solutions is to break the load into a series of load increments. The load increments can be applied either over several load steps or over several sub steps within a load step. At the completion of each incremental solution, the program adjusts the stiffness matrix to reflect the nonlinear changes in structural stiffness before proceeding to the next load increment. .

The ATENA program overcomes this difficulty by using Full Newton-Raphson method, or Modified Newton-Raphson method, which drive the solution to equilibrium convergence (within some tolerance limit) at the end of each load increment. In Full Newton-Raphson method, it obtains the following set of non-linear equations:

$$K(p)\,\Delta p = q - f(p)$$

where: q is the vector of total applied joint loads,
f(p)is the vector of internal joint forces,
Δp is the deformation increment due to loading increment,
p are the deformations of structure prior to load increment,
K(p) is the stiffness matrix, relating loading increments to deformation increments.

Figure 4.19 illustrates the use of Newton-Raphson equilibrium iterations in nonlinear analysis. Before each solution, the Newton-Raphson method evaluates the out-of -balance load vector, which is the difference between the restoring, forces (the loads corresponding to the element stresses) and the applied loads. The program then performs a linear solution, using the out-of -balance loads, and checks for convergence. If convergence criteria are not satisfied, the out-of-balance load vector is re-evaluated, the stiffness matrix is updated, and a new solution is obtained. This iterative procedure continues until the problem converges.

But sometimes, the most time consuming part of the Full Newton-Raphson method solution is the re-calculation of the stiffness matrix K (pi−1) at each iteration. In many cases this is not necessary and we can use matrix K (p0) from the first iteration of the step. This is the basic idea of the so-called Modified Newton-Raphson method. It produces very significant time saving, but on the other hand, it also exhibits worse convergence of the solution procedure. The simplification adopted in the Modified Newton-Raphson method can be mathematically expressed by:

$$K(p_i - 1) = K(p_0)$$

The modified Newton-Raphson method is shown in Figure 4.22. Comparing Figure4.22 and Figure4.23, it is apparent that the Modified Newton-Raphson method converges more slowly than the original Full Newton-Raphson method. On the other hand a single iteration costs less computing time, because it is necessary to assemble and eliminate the stiffness matrix only once. In practice a careful balance of the two methods is usually adopted in order to produce the best performance for a particular case. Usually, it is recommended to start a solution with the original Newton-Raphson method and later, i.e. near extreme points, switch to the modified procedure to avoid divergence.

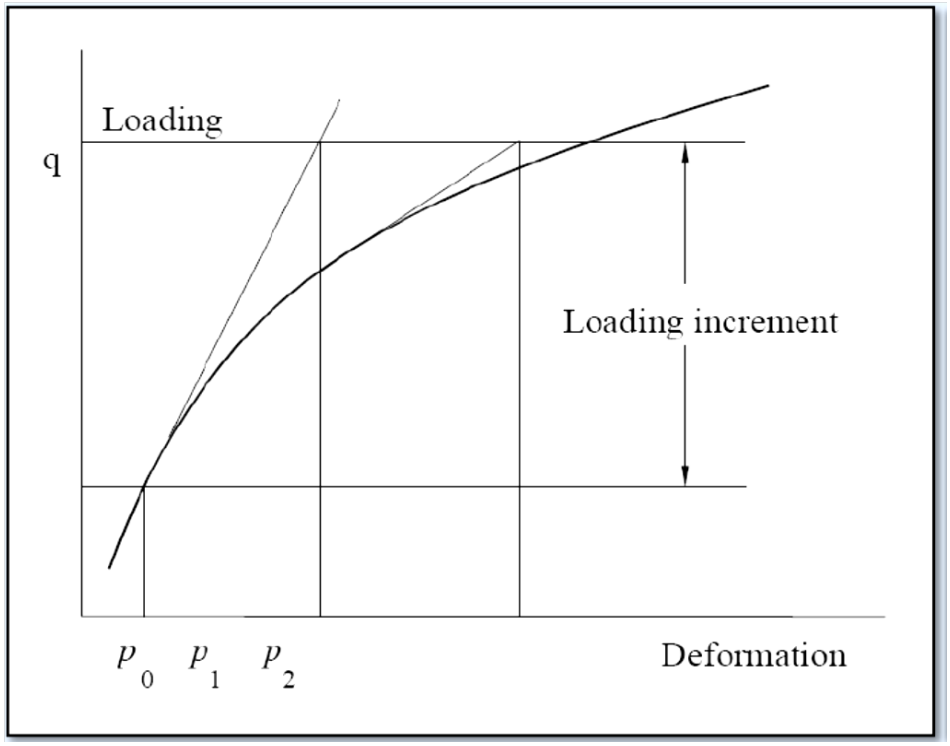

Fig-4.22, Full Newton-Raphson Method.

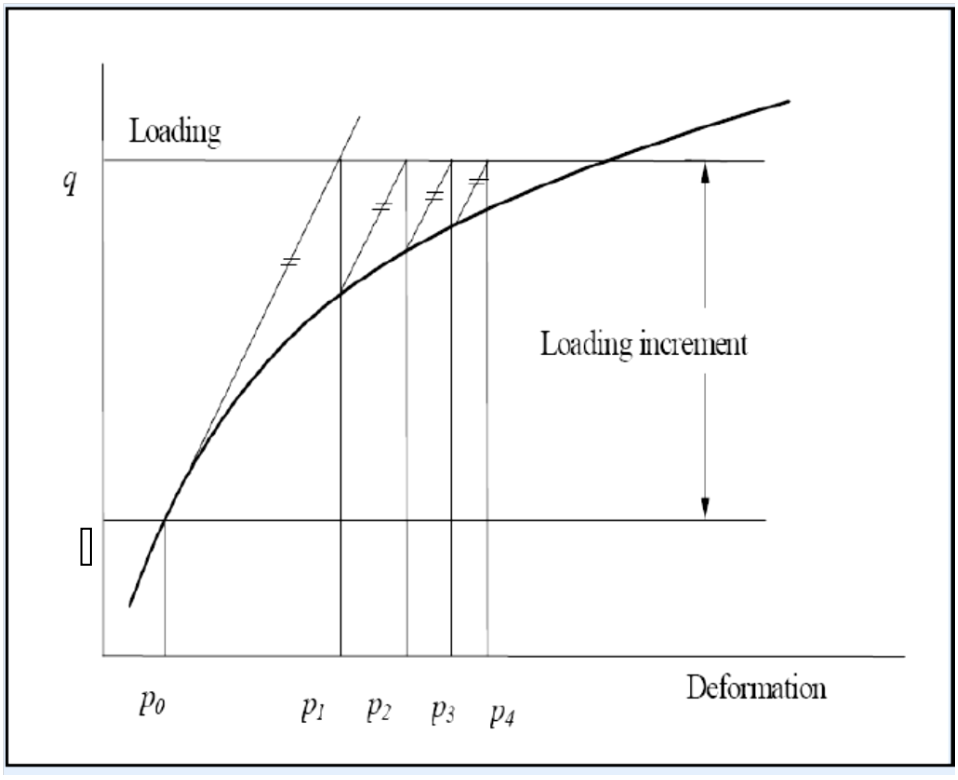

Fig-4.23 Modified Newton-Raphson Method.

This chapter presents the results of Finite element analysis of masonry infill RCC frame and bare frame under the static incremental and cyclic loading has been performed using ATENA software. Subsequently results of bare frame and infilled frame are compared with experimental load deflection curve as taken from (Mehrabi et al 1994). This is followed by load displacement curve and hysteretic loop and the cracking behaviour obtained from the analytical analysis. Firstly a bare frame as taken by Mehrabi (1994) et al. is modelled in ATENA. Then the behaviour of same frame is analysed by infilling it with masonry to study the effect of infill on bare frame, In the next phase of study the various models for modelling infills which are proposed by various researchers for modelling infill are verified the results of Finite Element analysis of RC bare frame, infilled frame, Single strut, and then the same models are studied for cyclic loading to obtain hysteretic graph under deformation controlled loading pattern previously discussed using ATENA software.

5.1 FE MODEL RESULTS OF CONTROL FRAME UNDER MONOTONIC LOADING

In the present study, non-linear response of RCC control frame modelled as per details already discussed in pervious chapter, using FE modelling under incremental loading and cyclic loading has been carried out.

Results of RC bare Frame under monotonic loading.

5.1.1 Experimental results RC bare frame.

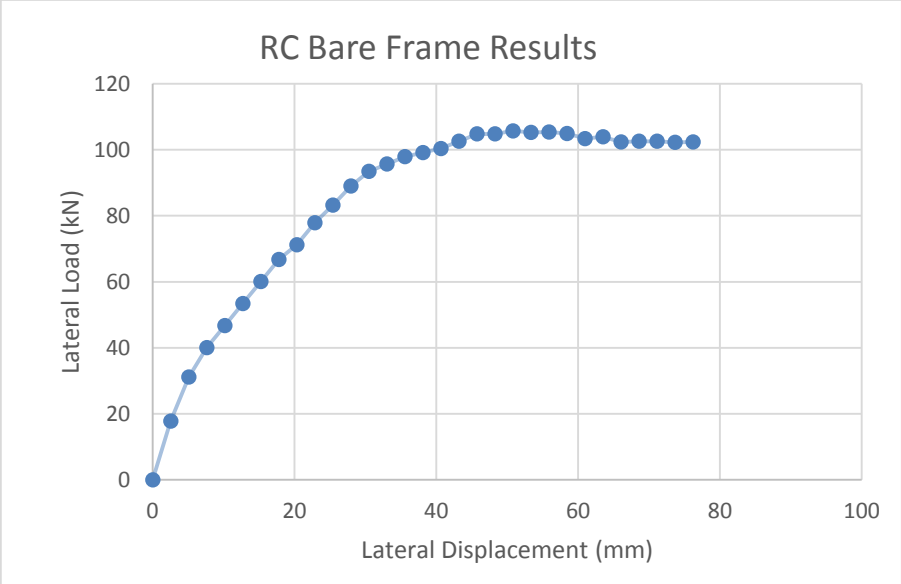

Figure- 5.1-Load displacement curve by Mehrabi et al.(1994)

Experimental results of bare frame tested by Mehrabi et al.(1994) from a six storey, three bay reinforced moment resisting frame has been selected as a prototype model.The lateral load was applied by means of two servo controlled hydraulic actuators. To avoid any tensile force on the RC beam, four stiff steel rods were used to transmit the pulling force to the specimen. The vertical loads were exerted by manually controlled hydraulic jacks, whose forces were directly monitored by strain gages attached to the vertical loading rods. The reaction frame and the specimen were anchored onto a two-foot-thick strong floor. Strain gages and displacement transducers (LVDT's) were installed in each test to monitor the strains in the reinforcing bars and the deformations of the specimen at different locations. The data from strain gages were used to derive the moments, curvatures, and axial forces developed at critical beam and column sections.

5.1.2 Analytical results of RC bare Frame.

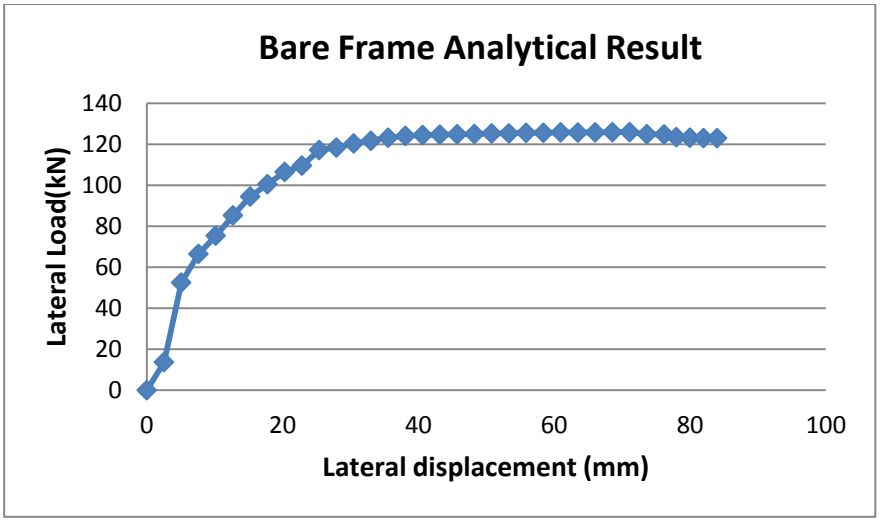

Figure-5.2-Load displacement curve for RC Bare frame under monotonic loading.

5.1.2.1 Comparison of Analytical and experimental results of RC bare Frame.

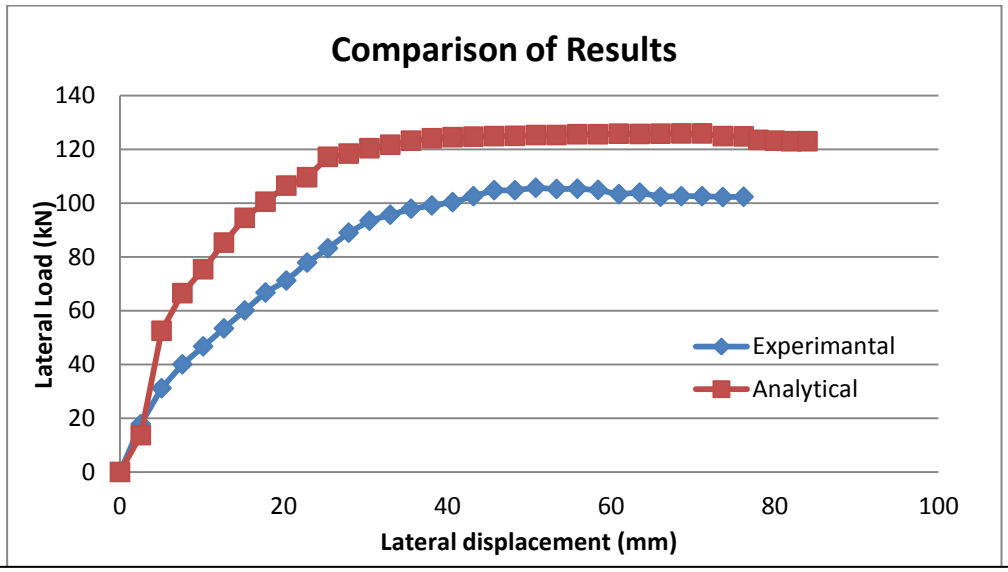

Fig-5.2a-Comparison of Load displacement curve for RC Bare frame under monotonic loading.

5.1.3 Stress Contour for RC Bare Frame

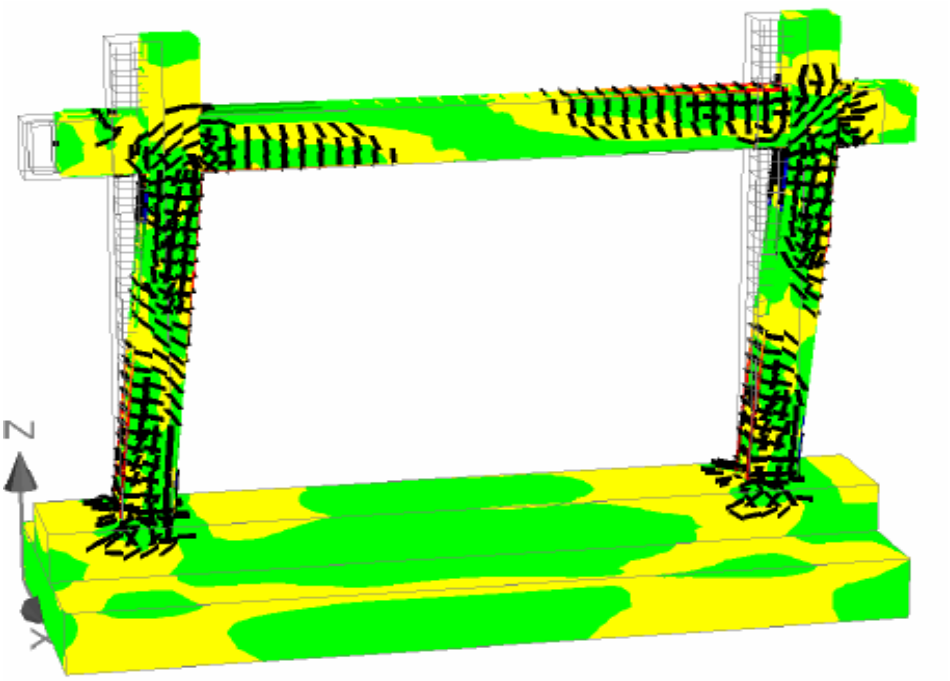

Figure-5.3- Stress Contour or Failure Pattern for RC Bare frame under monotonic loading.

Results and Discussions of RC bare frame.

The failure pattern of bare frame is shown in figure-5.3.From the figure-5.3, we conclude that the bare frame, which exhibited a fairly ductile behavior with initially bottom cracks developed in the columns in analytically as well as in experimentally. The load displacement curve of Bare Frame which has been drawn from analytical analysis is shown in Fig. 5.2.From the above figures, we conclude that the flexural cracks initiated at the bottom sections of both columns in analytical and experimental is at a lateral load of about 60kN and 48.95kN respectively. Major shear cracks (4mm) developed in the beam-to-column joints in analytically as well as in experimentally at lateral load of 81.27kN and 71.2kN respectively. The longitudinal reinforcement at the bottom sections of the columns yielded at a lateral load of 63kN and a lateral displacement of 14.5mm in analytical, but in experimentally at a lateral load of 62.3 and a displacement of 13.7mm. While the flexural reinforcement at the end sections of the beam yielded in analytical and experimental at about 82kN, and 75.65kN with lateral displacement of 20mm and 18.75mm respectively. Concrete crushing was observed at the upper end of the loaded column and the lower end of the adjacent column at the maximum load of 124kN and a lateral displacement of about 32mm, after which the lateral resistance remained more or less constant. Ductility Ratio (yield displacement /ultimate displacement) 0.12.

5.2 Results of RC infilled Frame under monotonic loading.

5.2.1 Experimental results RC infilled frame.

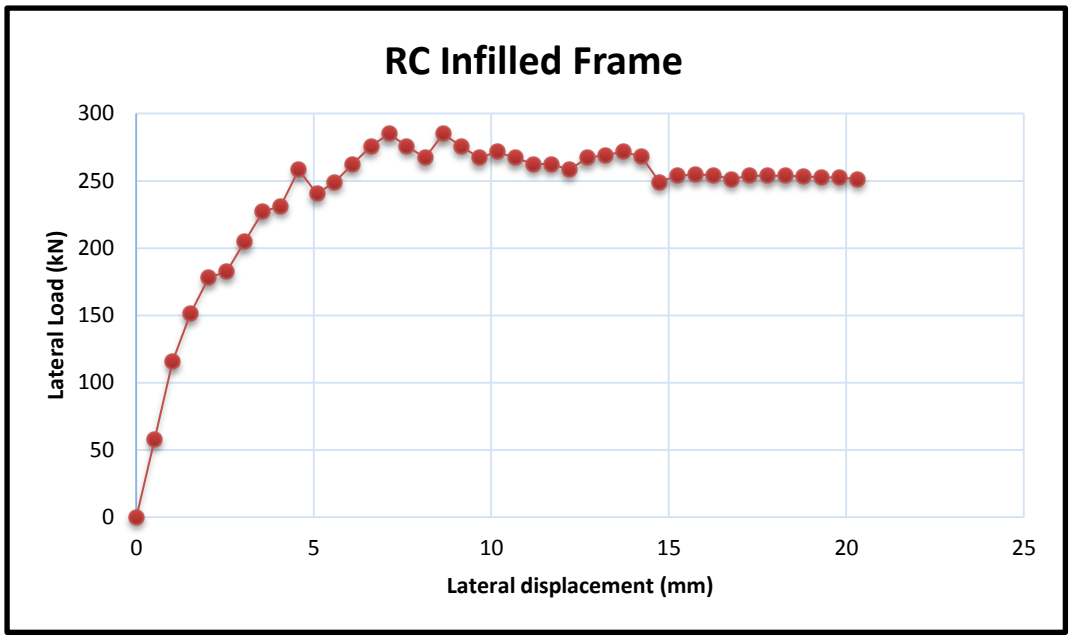

Figure-5.4- Load displacement curve for RC infilled frame under monotonic loading by Mehrabi et al (1994).

5.2.2 Stress Contour or Failure Pattern for RC Infilled Frame

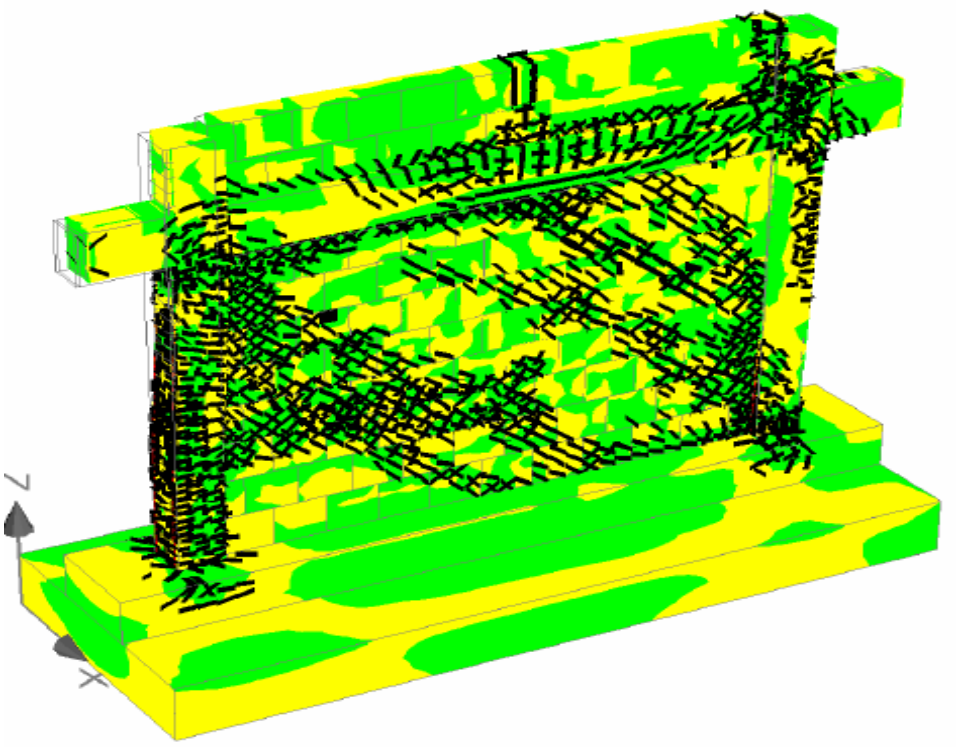

Figure-5.5- Stress Contour or failure Pattern for RC infilled frame under monotonic loading.

5.2.3 Load Displacement Curve for RC Infilled Frame

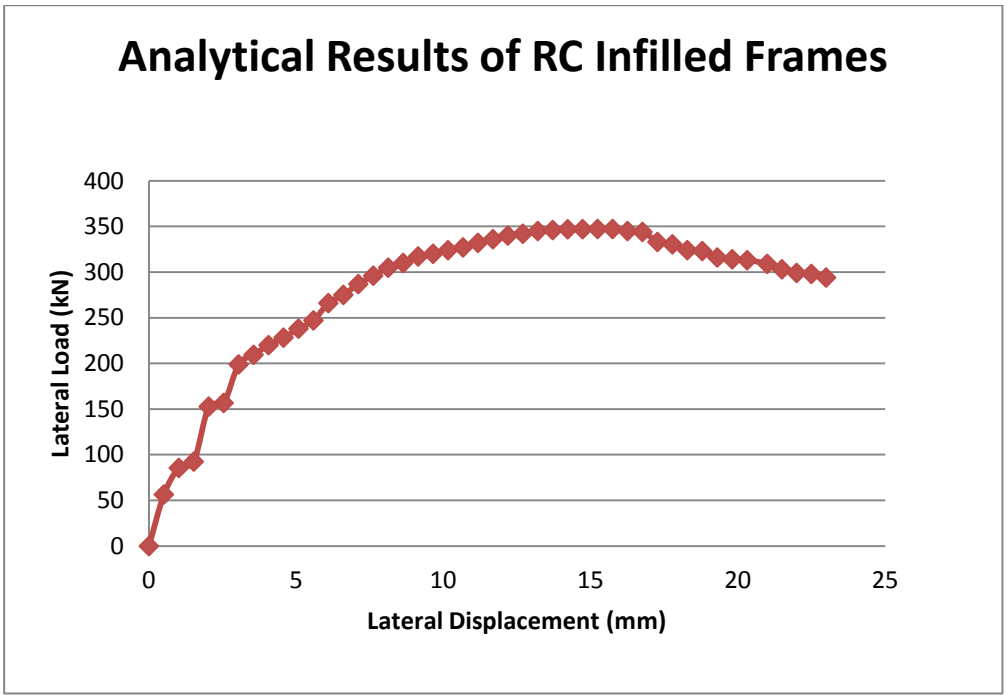

Figure-5.6- Load displacement curve for RC infilled frame under monotonic loading.

5.2.3.1 Comparison of Analytical and Experimental Results of RC Infilled Frame

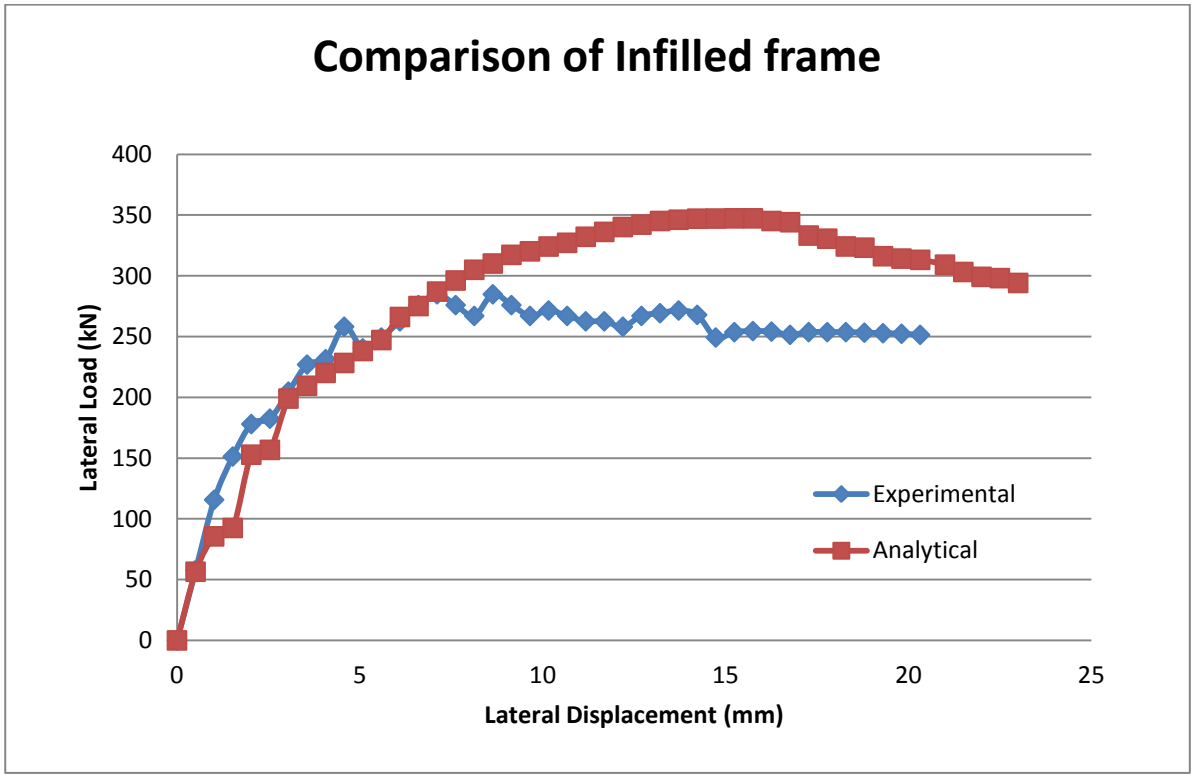

Fig-5.6a-Comparison of Load displacement curve for RC infilled frame under monotonic loading.

Results and Discussions of RC Infilled frame.

The failure pattern of infilled frame is shown in figure-5.5.From the figure-5.5 and from load displacement curve of RC infilled frame, we conclude that in infilled frame first diagonal/sliding crack occurred in the infill in analytical as well as in experimental analysis at the maximum lateral load of 347kN and 277.7kN and lateral displacement of 13.8mm and 10.2mm respectively, after which the lateral load dropped to 335kN and 277.68 in analytically and experimental and shear cracks appeared at the top of the left column. The lateral load drops to 300kN again at a lateral displacement of 20.8mm. The shear crack at the top of the left column widened at a lateral displacement of about 22mm. Major shear cracks (4mm) developed in the left column at about 325kN at lateral displacement of 20mm.The experiment was terminated when concrete crushing was observed at the bottom section of the right column and crushing of bricks are observed. The lateral load-lateral displacement curve levels cuts at 290kN when the lateral displacement is close to 30mm. Ductility Ratio (yield displacement /ultimate displacement) 0.109.

5.3 Results of RC Single Strut Frame (Holmes) under monotonic loading.

5.3.1 Stress Contour or Failure Pattern results of RC Single Strut (Holmes) frame.

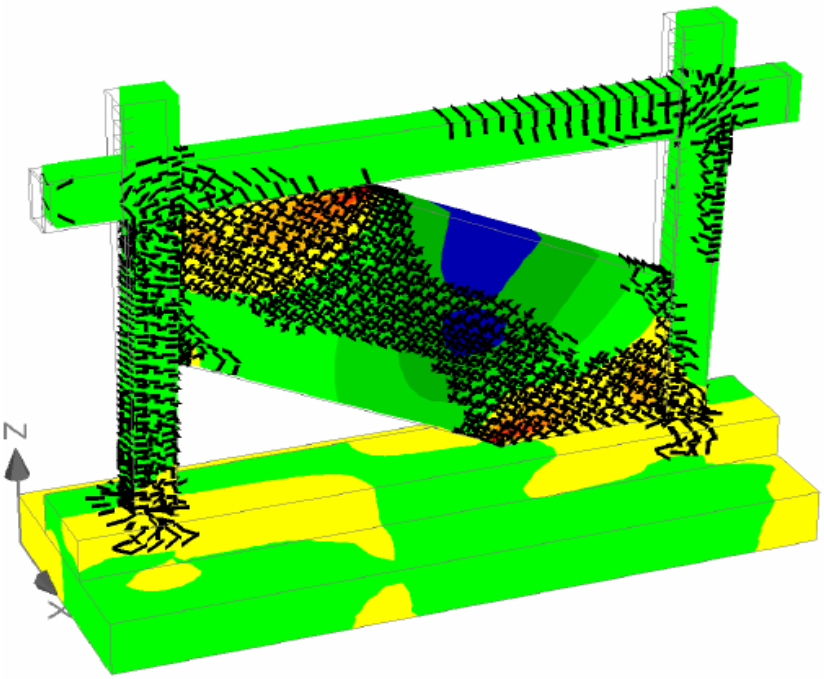

Figure-5.7, Stress Contour or Failure Pattern for RC Single Strut (Holmes) frame under monotonic Loading.

5.3.2 Analytical results RC Single Strut frame (Holmes) Model.

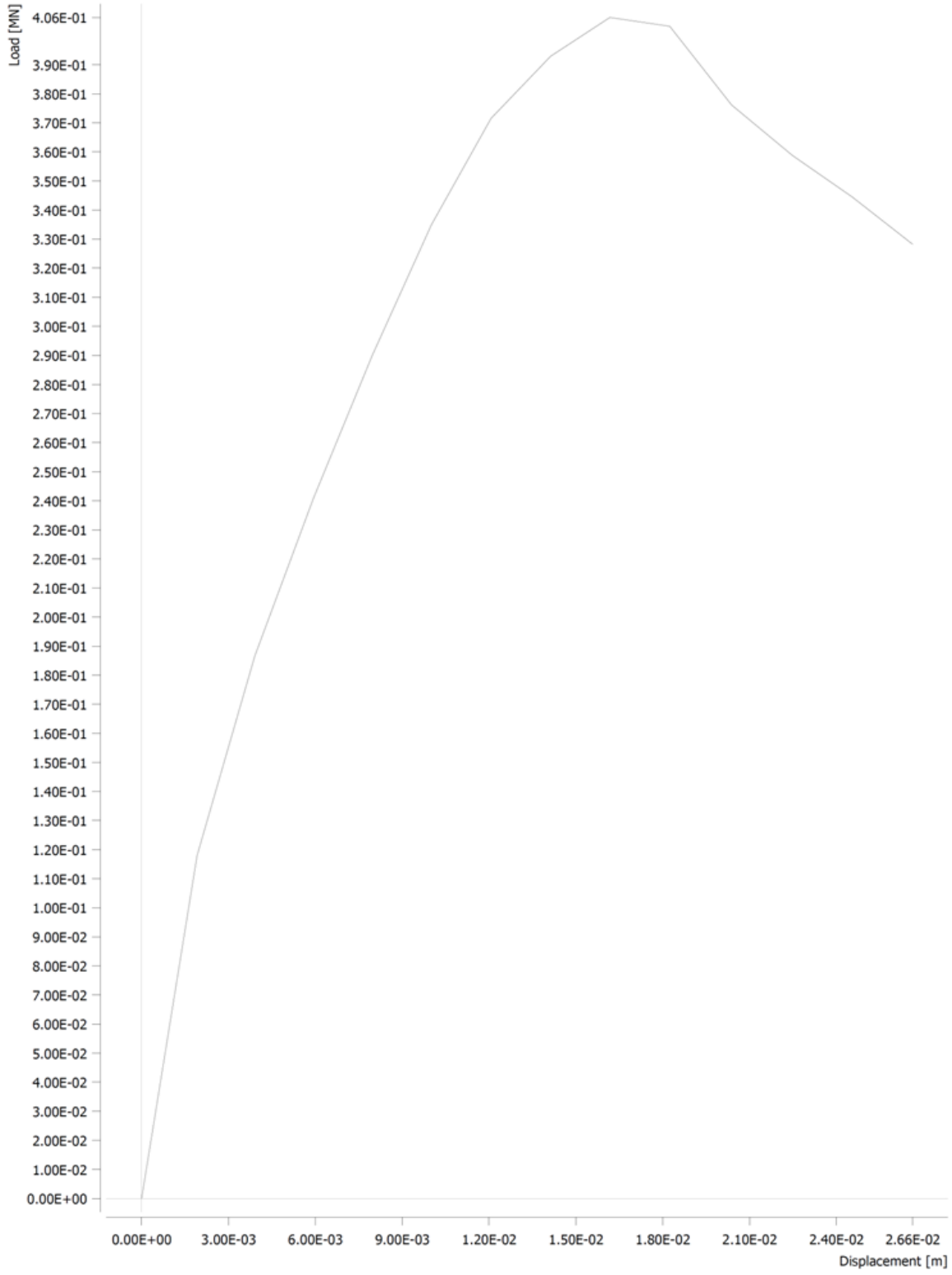

Figure-5.8, Load displacement curve for RC Single Strut (Holmes) frame under monotonic Loading.

Results and Discussions of RC Single Strut (Holmes) frame.

The failure pattern of Single Strut (Holmes) frame is shown in figure-5.7.From the figure-5.7 and from load displacement curve of RC Single Strut (Holmes) frame as shown in (fig-5.8), we conclude that in the Single Strut frame starts yielding at load of 370kN at lateral displacement of 12.6mm also major diagonal/sliding crack (4mm) occurred in the Single Strut at the maximum lateral load of 406kN and a lateral displacement of 16.7mm, after which the lateral load dropped to 397.69kN at lateral displacement of 18mm and shear cracks appeared in the left column and bottom of the right column. Then lateral load drops to 370kN again at a lateral displacement of 26.6mm. The shear crack in the left column and in Single Strut gets widened at a lateral displacement of about 22mm. Major shear cracks (4mm) developed in the Single Strut of load about 400kN at lateral displacement of 16.2mm in the middle of Single Strut. The experiment was terminated when high stress zone was observed in the Single Strut at the middle. The lateral load-lateral displacement curve levels cuts at 320kN when the lateral displacement is almost close to 28mm. Ductility Ratio (yield displacement /ultimate displacement) 0.7.

5.4 Results RC Single Strut frame (Mainstone) under monotonic loading.

5.4.1 Stress Contour or Failure Pattern for Single strut RC frames (Mainstone) Model.

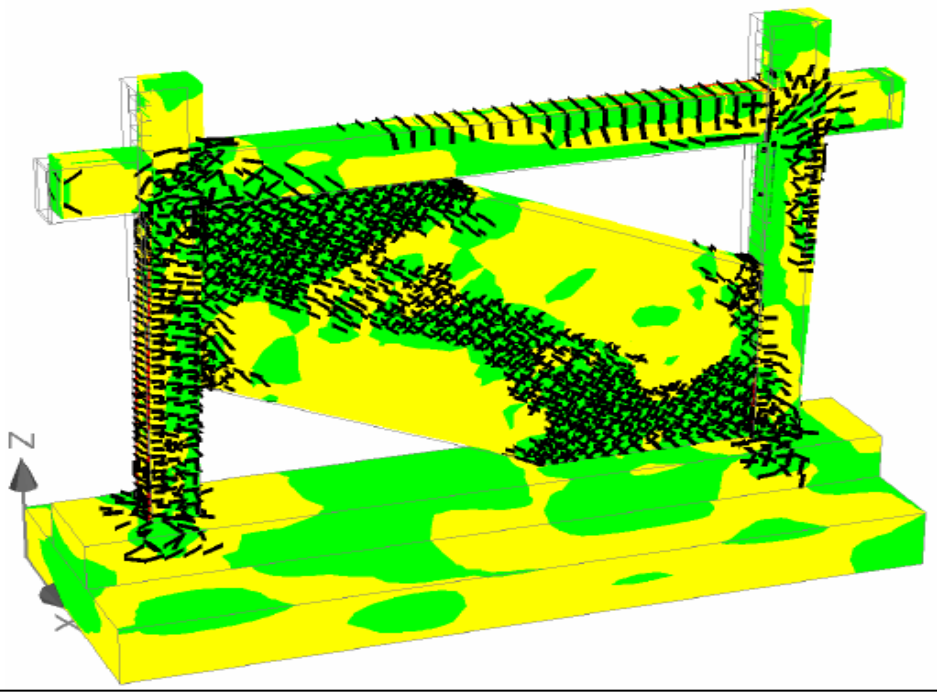

Fig-5.9, Stress Contour or Failure Pattern for RC Single Strut (Mainstone) frame under monotonic Loading.

5.4.2 Analytical results RC Single Strut frame (Mainstone) Model.

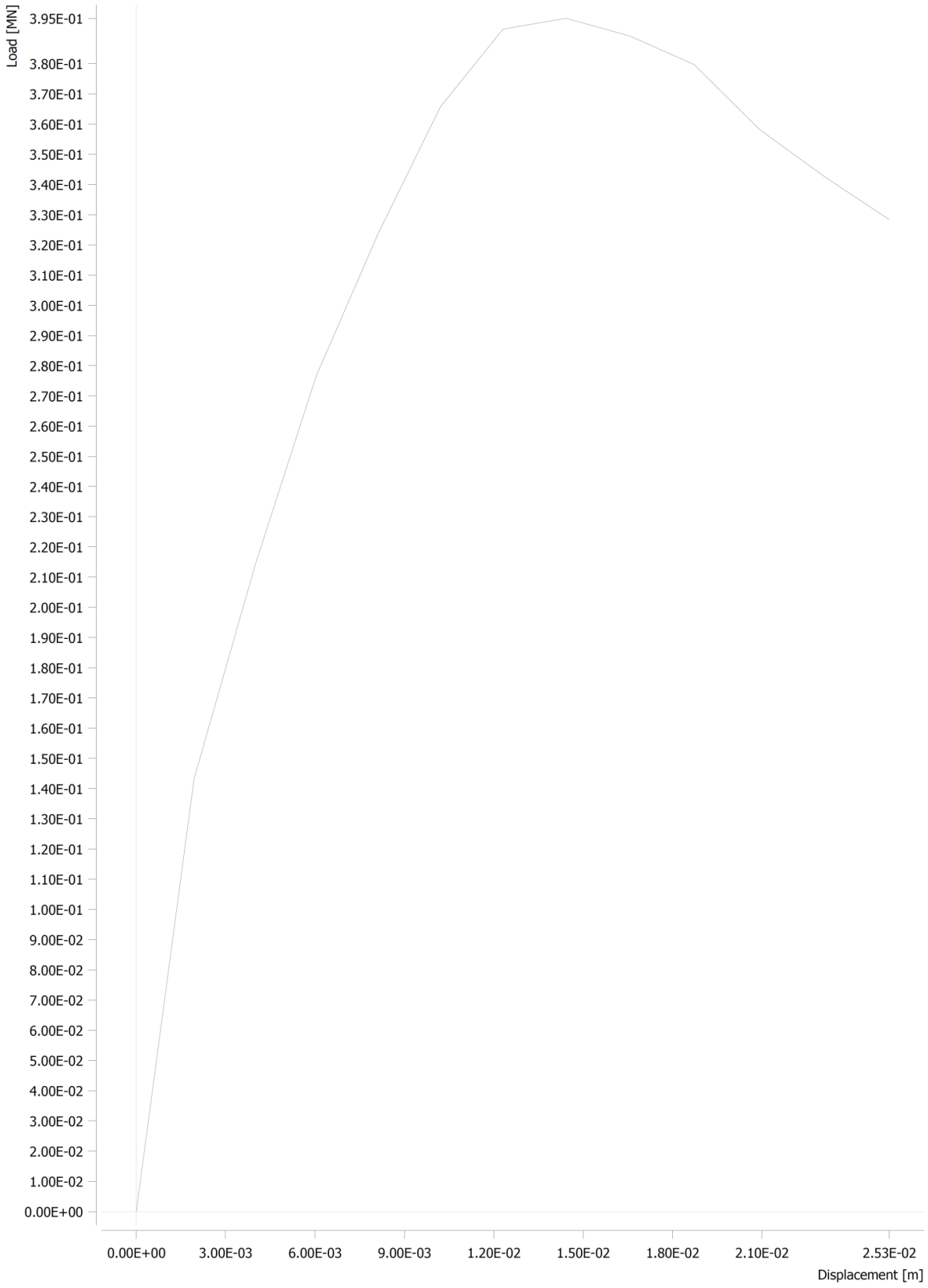

Fig-5.10, Load displacement curve for RC Single Strut (Mainstone) frame under monotonic Loading.

Results and Discussions of RC Single Strut (Mainstone) frame.

The failure pattern of Single Strut (Mainstone) frame is shown in figure-5.9.From the figure-5.9 and from load displacement curve of RC Single Strut (Mainstone) frame as shown in (fig-5.10), we conclude that in the Single Strut frame starts yielding at load of 367kN at lateral displacement of 10.2mm also major diagonal/sliding (4mm) crack occurred in the Single Strut at the maximum lateral load of 394kN and a lateral displacement of 14.7mm, after which the lateral load dropped to 379kN at lateral displacement of 17.2mm and shear cracks appeared in the left column, bottom of the right column and also in Single Strut. Then lateral load drops to 370kN again at a lateral displacement of 19.6mm. The shear crack in the left column and in Single Strut gets widened at a lateral load of about 359kN at lateral displacement of about 21mm. Major shear cracks (4mm) developed in the Single Strut of load about 395kN at lateral displacement of 15.2mm in the middle of Single Strut. The experiment was terminated when high stress zone was observed in the Single Strut starts and at ends. The lateral load-lateral displacement curve levels cuts at 325kN when the lateral displacement is close to 25mm. Ductility Ratio (yield displacement /ultimate displacement) 0.56

5.5 Results RC Single Strut frame (Paulay & Prisley) under monotonic loading.

5.5.1 Stress Contour or Failure Pattern for Single strut RC frame

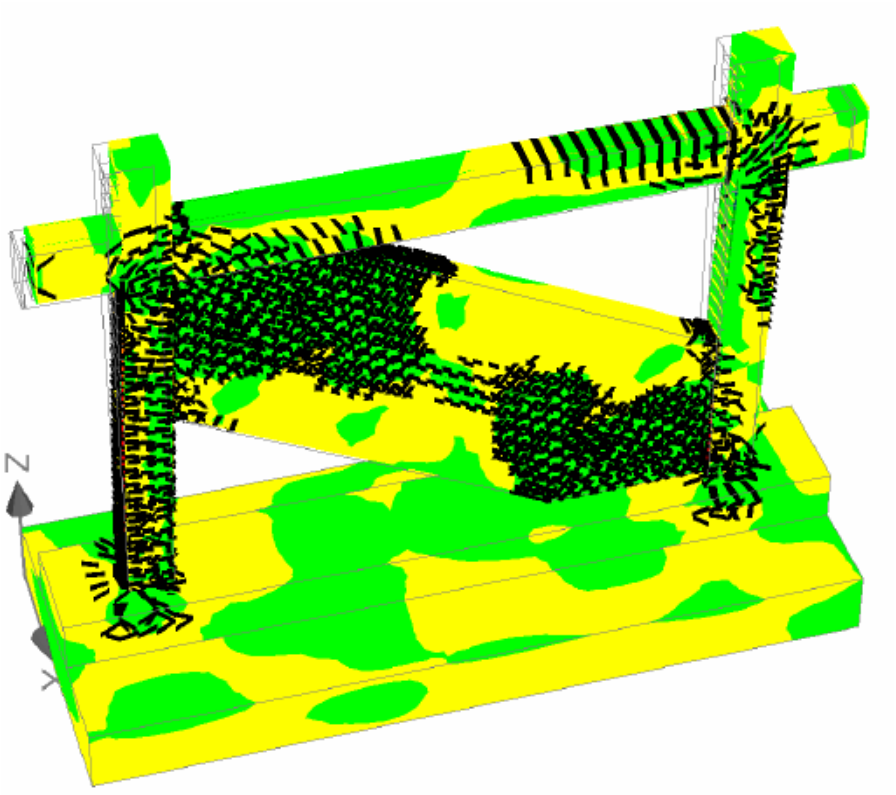

Fig-5.11, Stress Contour or Failure Pattern for RC Single Strut (Pauley & Prisley) frame under monotonic Loading.

5.5.2 Analytical results RC Single Strut frame (Pauley & Prisley) Model.

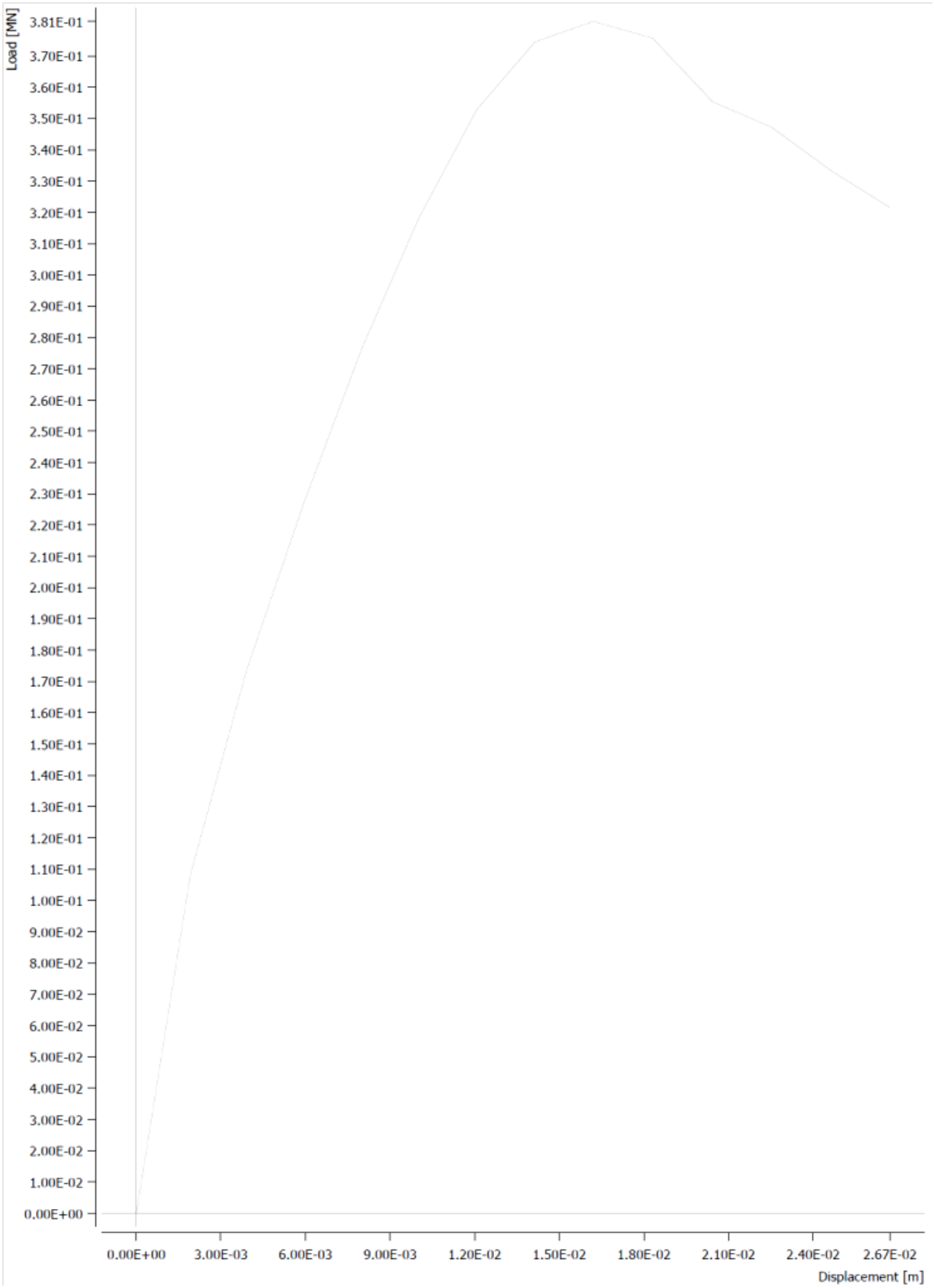

Figure-5.12, Load displacement curve for RC Single Strut frame (Pauley & Prisley) under Monotonic Loading.

Results and Discussions of RC Single Strut (Pauley & Prisley) frame.

The failure pattern of Single Strut (Pauley & Prisley) frame is shown in figure-5.11.From the figure-5.11 and from load displacement curve of RC Single Strut (Pauley & Prisley) frame as shown in (fig-5.12), we conclude that in the Single Strut frame starts yielding at load of 352kN at lateral displacement of 12.2mm also major diagonal/sliding crack (4mm) occurred in the Single Strut at the maximum lateral load of 381kN and a lateral displacement of 16mm, after which the lateral load dropped to 375kN at lateral displacement of 19.2mm and shear cracks appeared in the left column, beam column joint of the right column and also in Single Strut. Then lateral load drops to 356kN again at a lateral displacement of 20.6mm. The shear crack in the left column and in Single Strut gets widened at a lateral load of about 348kN at lateral displacement of about 22.5mm. Major shear cracks (4mm) developed in the Single Strut of load about 381kN at lateral displacement of 16.2mm in the top and bottom of Single Strut. The experiment was terminated when high stress zone was observed in the Single Strut starts and at ends. The lateral load-lateral displacement curve levels cuts at 321kN when the lateral displacement is almost close to 27mm. Ductility Ratio (yield displacement /ultimate displacement) 0.58

5.6 FE MODEL RESULTS OF CONTROL FRAME UNDER CYCLIC LOADING

Cyclic loading has been carried out to obtain the hytereysis loop for Specific energy in various models at different loadings.

5.6.1 Results of RC Infilled Frame under Cyclic Loading.

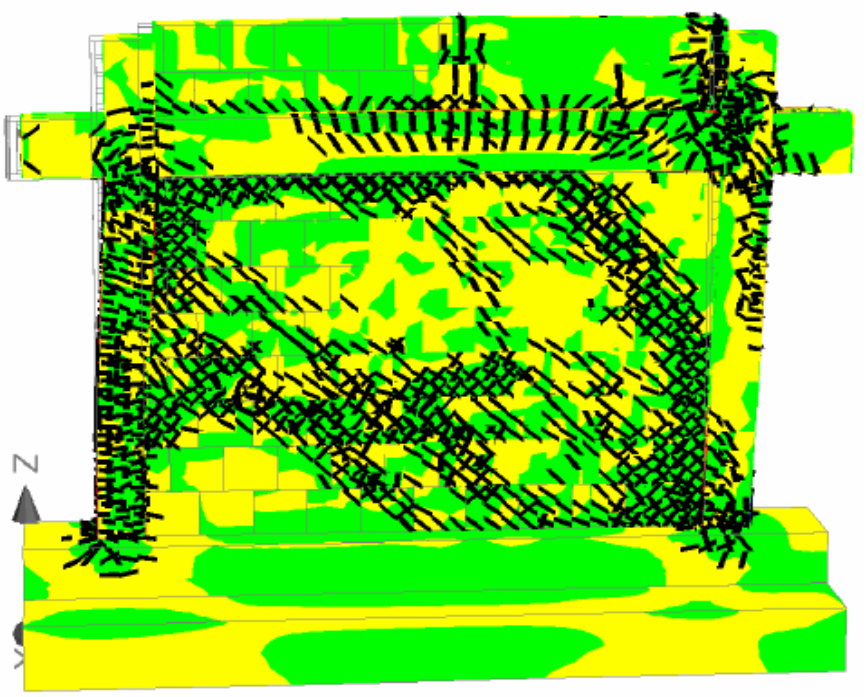

Fig-5.13, Failure Pattern and Stress Contour for RC Infilled Frame under Cyclic Loading

5.6.2 Analytical results RC Infilled frame Model under Cyclic Loading.

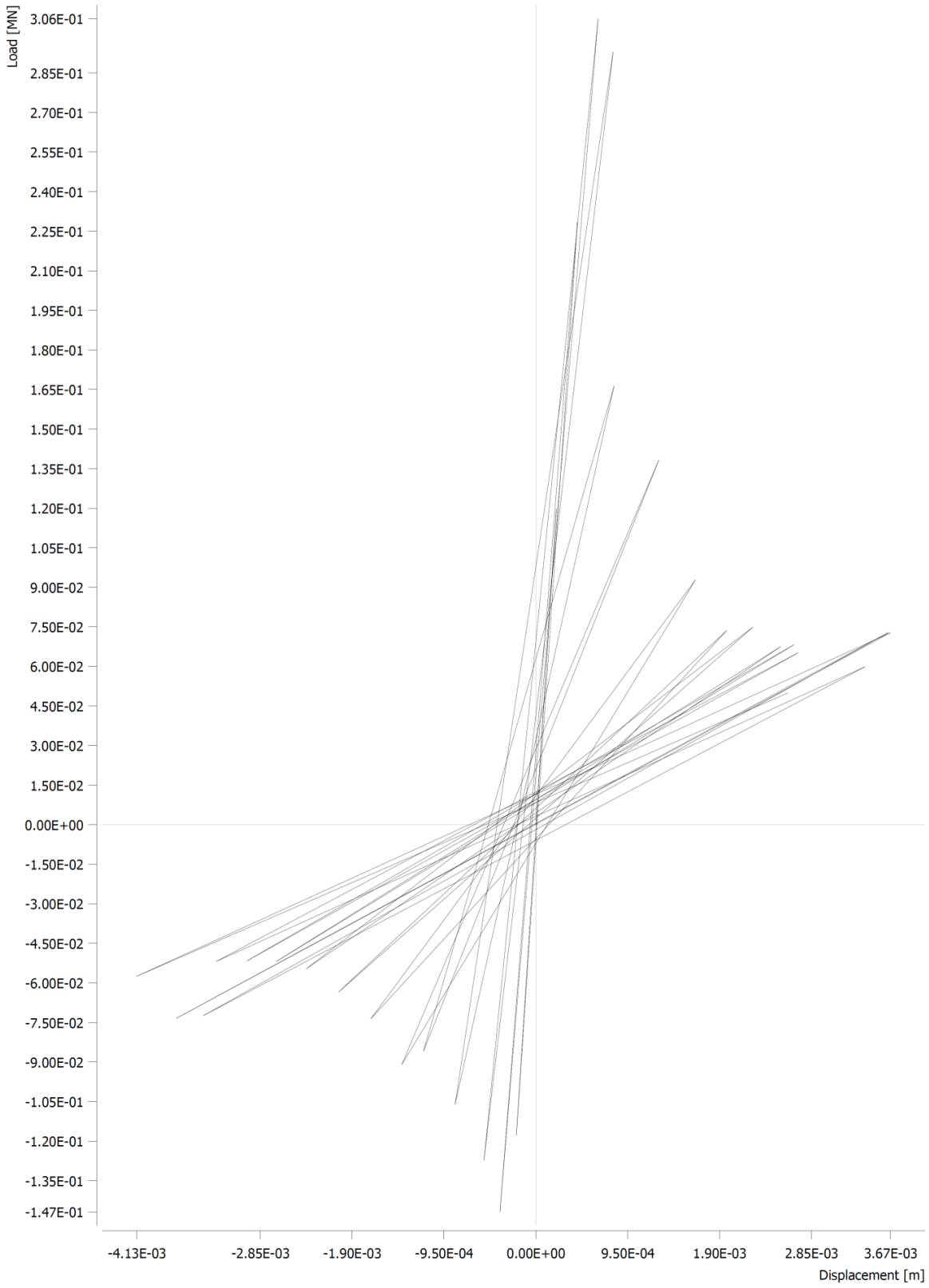

Fig-5.14, Load –Displacement Hysteresis Curve for Infilled Frame

Results and Discussions of RC Infilled frame.

The failure pattern of RC Infilled frame under cyclic loading as shown in Fig-5.13. The hysteresis curves in Fig. 5.14. From the Fig-5.13 & 5.14 we conclude that the first diagonal/sliding cracks in the infill were observed at a lateral load of 255kN in the positive direction and 120kN in the negative direction. The corresponding lateral displacements were 7mm and 1.5mm, respectively. This led to a drop of the lateral resistance. At this point, shear cracks appeared at the top of the left column in each direction. The shear cracks widened significantly (3mm) at the maximum lateral resistance of 306kN in the positive direction and 147kN in the other. Slips along the horizontal cracks and the openings of the diagonal cracks were observed in the infill at about 2.3mm displacement. Crushing of infill started at about a lateral displacement of 23.6mm in both directions. The longitudinal reinforcement at the bottom sections of the columns starts yielded at a lateral displacement of 28mm, but no yielding was detected for the longitudinal reinforcement in the beam. From the hysteresis loops we conclude that the in first few cycles they get maximum load and consume maximum specific energy but as the crack starts and propagation load carrying capacity goes on decreasing as well as specific energy goes on decreasing. Due to the spalling of crushed masonry inside the infill near left and right column, the lateral resistance dropped considerably at about 3.7mm displacement. Concrete crushing started at the bottom section of the left column and beam column joint in right column at about 3.7mm in one and 4.13mm in other direction displacement in each direction.

5.7 Result of Single Strut (Holmes) Frame under Cyclic loading.

5.7.1 Stress Contour or Failure Pattern of Single strut

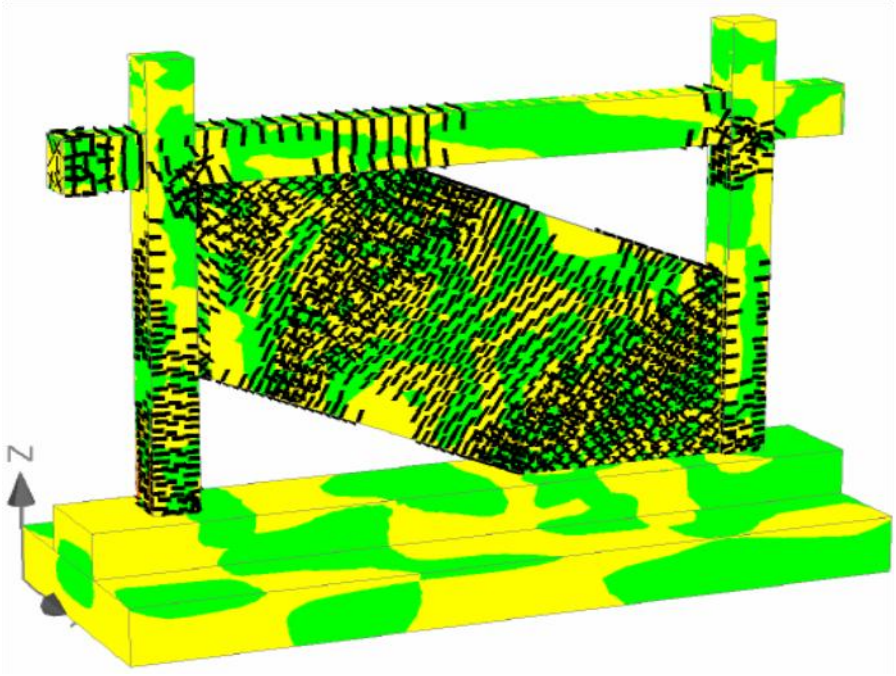

Fig-5.15, Failure Pattern and Stress Contour for RC Single Strut (Holmes) Frame under Cyclic Loading

5.7.2 Analytical Results of RC Single Strut (Holmes) Frame under Cyclic Loading.

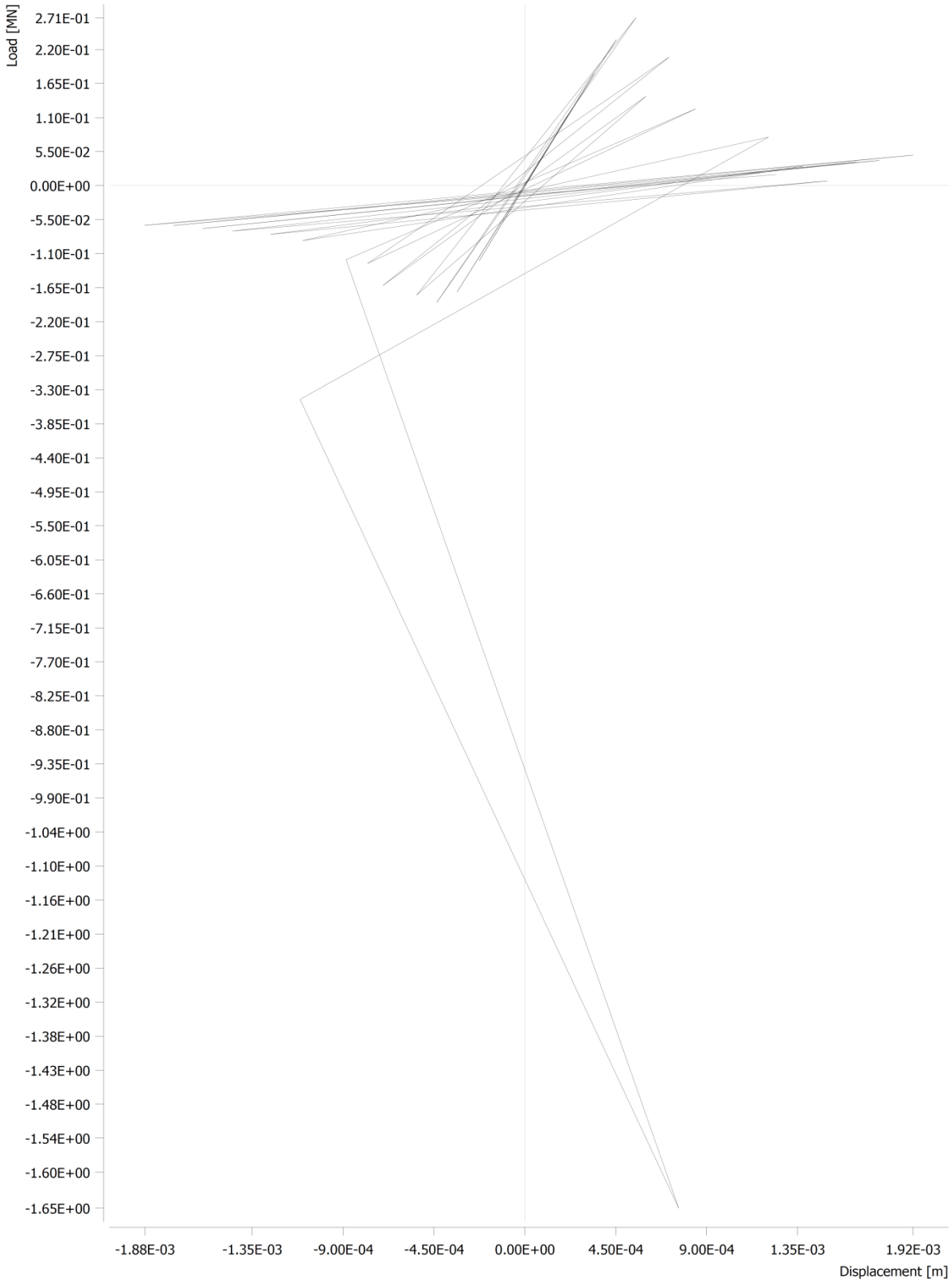

Fig-5.16, Load –Displacement Hysteresis Curve for Single Strut (Holmes) Frame

Results and Discussions of RC Single Strut (Holmes) frame.

The failure pattern of RC Single Strut (Holmes) frame under cyclic loading as shown in Fig-5.15. The hysteresis curves in Fig. 5.16. From the Fig-5.15 & 5.16 we conclude that the first diagonal/sliding cracks in the infill were observed at a lateral load of 235kN in the positive direction and 145kN in the negative direction. The corresponding lateral displacements were 0.45mm and 0.1mm, respectively. This led to a drop of the lateral resistance. At this point, shear cracks appeared at the bottom of the left column. The shear cracks widened significantly (3mm) at the maximum lateral resistance of 271kN in the positive direction and 175kN in the other. Slips along the horizontal cracks and the openings of the diagonal cracks were observed in the infill at about 1mm displacement. Crushing of Single Strut started at about a lateral displacement of 1.80mm in both directions. The longitudinal reinforcement at the bottom sections of the columns yielded at a lateral displacement of 0.8mm, but no yielding was detected for the longitudinal reinforcement in the beam. From the hysteresis loops we can say that the in first few cycles they get maximum load and consume maximum specific energy but as the crack starts and propagation load carrying capacity goes on decreasing as well as specific energy goes on decreasing. Due to the spalling of crushed masonry inside the infill near left and right column, the lateral resistance dropped considerably at about 1.2mm displacement. Concrete crushing started in the Single Strut at 1.7mm displacement in each direction.

5.8 Result of Single Strut (Mainstone) Frame under Cyclic loading.

5.8.1 Stress Contour or Failure Pattern of Single strut

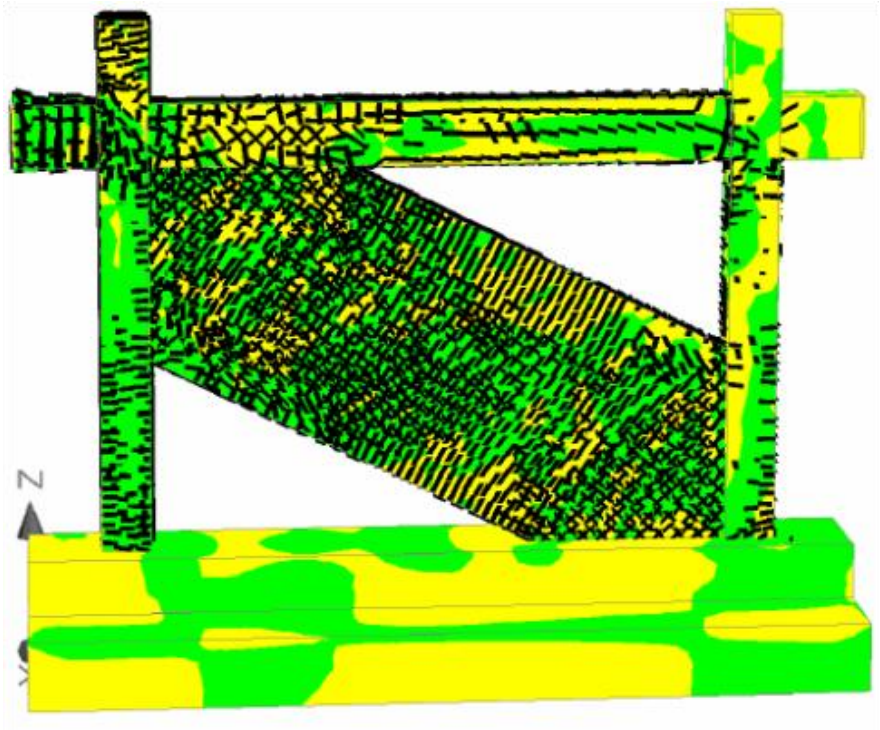

Fig-5.17, Failure Pattern and Stress Contour for RC Single Strut (Mainstone) Frame under Cyclic Loading

5.8.2 Analytical Results of RC Single Strut (Mainstone) Frame under Cyclic Loading.

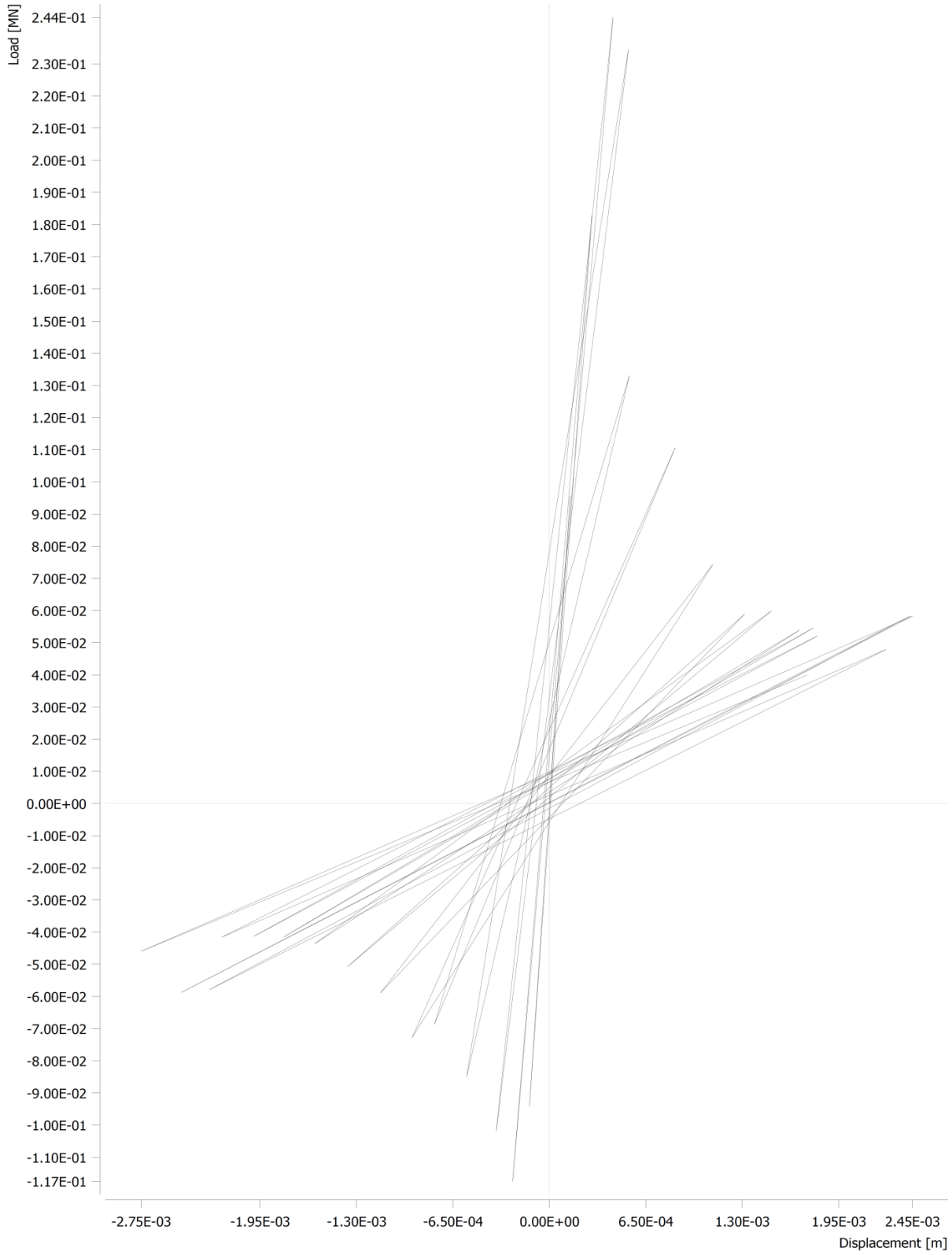

Fig-5.18, Load –Displacement Hysteresis Curve for Single Strut (Mainstone) Frame

Results and Discussions of RC Single Strut (Mainstone) frame.

The failure pattern of RC Single Strut (Mainstone) frame under cyclic loading as shown in Fig-5.17. The hysteresis curves in Fig. 5.18. From the Fig-5.17 & 5.18 we conclude that the first diagonal/sliding cracks in the infill were observed at a lateral load of 230kN in the positive direction and 105kN in the negative direction. The corresponding lateral displacements were 0.5mm and 0.3mm, respectively. This led to a drop of the lateral resistance. At this point, shear cracks appeared at the top of the left column. The shear cracks widened significantly (3mm) at the maximum lateral resistance of 245kN in the positive direction and 117kN in the other. Slips along the horizontal cracks and the openings of the diagonal cracks were observed in the infill at about 1mm displacement in each direction. Crushing of Single Strut started at about a lateral displacement of 1.70mm in both directions. The longitudinal reinforcement at the bottom sections of the columns yielded at a lateral displacement of 1.7mm, but no yielding was detected for the longitudinal reinforcement in the beam. From the hysteresis loops we conclude that the in first few cycles they get maximum load and consume maximum specific energy but as the crack starts and propagation load carrying capacity goes on decreasing as well as specific energy goes on decreasing. Due to the spalling of crushed concrete at top of left column, the lateral resistance dropped considerably at about 0.7mm displacement. Concrete crushing started in the Single Strut at 2.3mm displacement in each direction.

5.9 Result of Single Strut (Pauley & Prisley) Frame under Cyclic loading.

5.9.1 Stress Contour and Failure Pattern of Single strut.

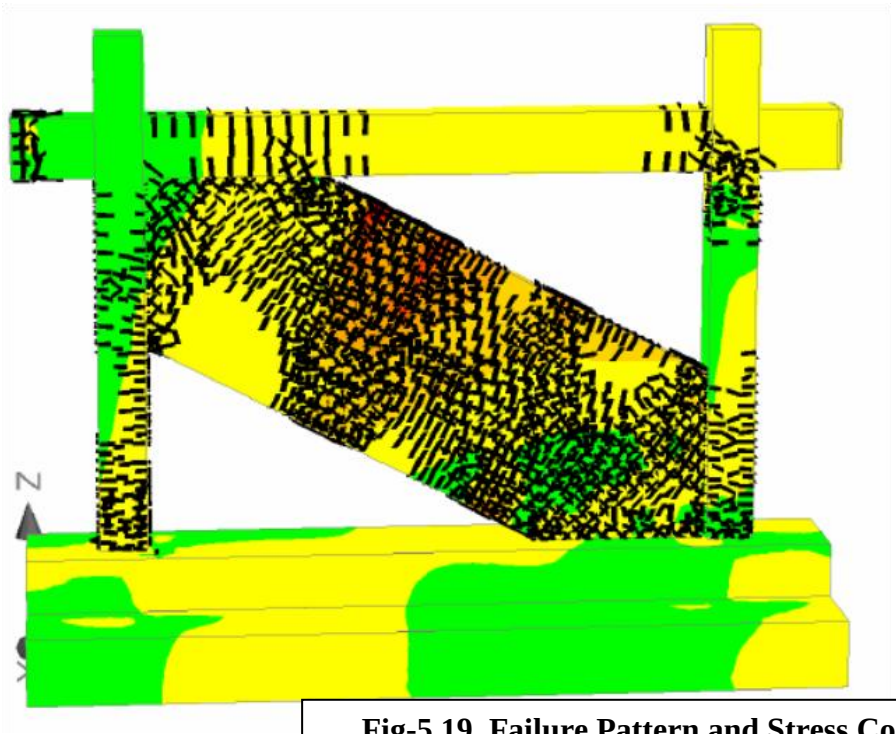

Fig-5.19, Failure Pattern and Stress Contour for RC Single Strut (Pauley & Prisley) Frame under Cyclic Loading

5.9.2 Analytical Results of RC Single Strut (Pauley & Prisley) Frame under Cyclic Loading.

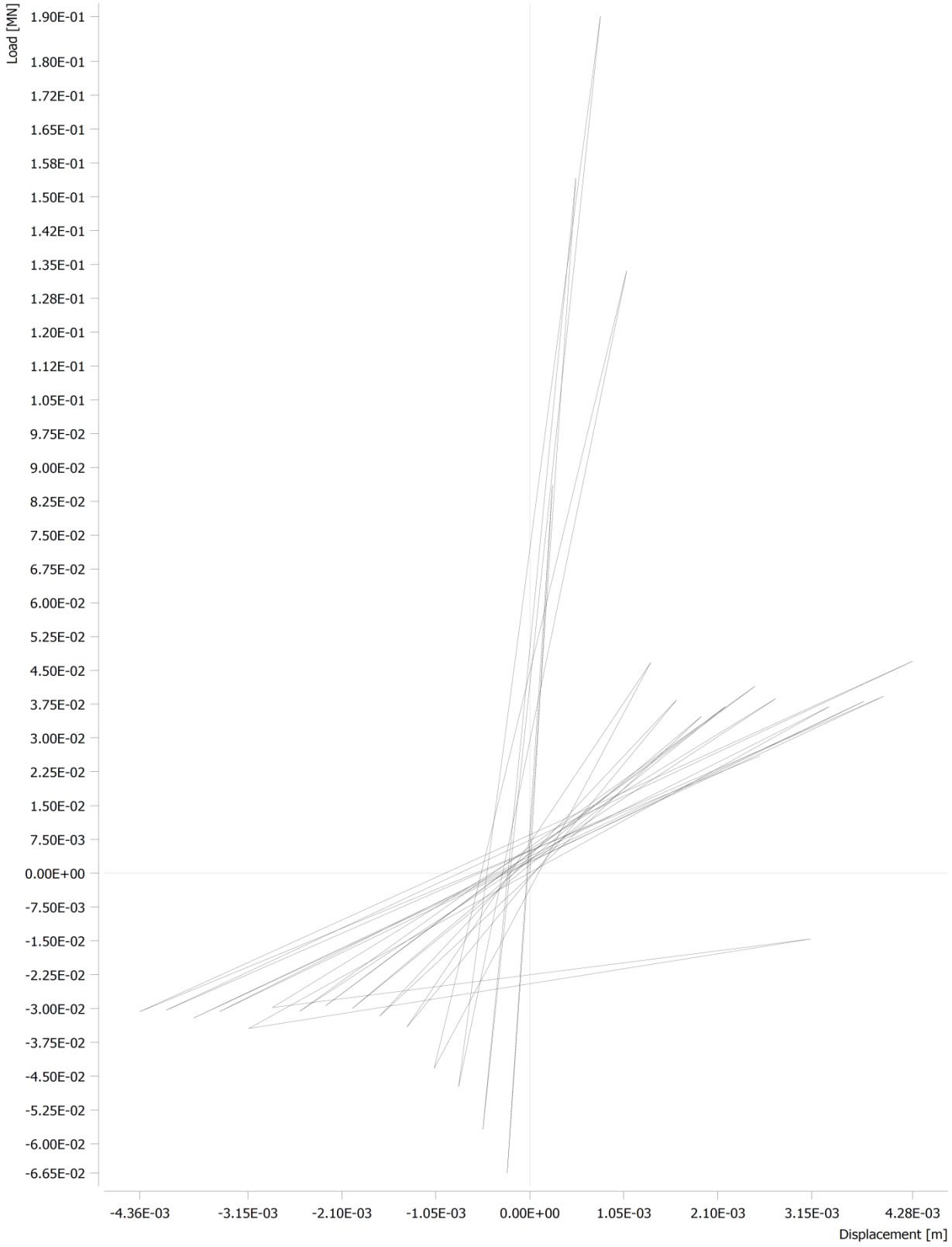

Fig-5.20, Load –Displacement Hysteresis Curve for Single Strut (Pauley & Prisley) Frame.

Results and Discussions of RC Single Strut (Pauley & Prisley) frame.

The failure pattern of RC Single Strut (Pauley & Prisley) frame under cyclic loading as shown in Fig-5.19. The hysteresis curves in Fig. 5.20. From the Fig-5.19 & 5.20 we conclude that the first diagonal/sliding cracks in the infill were observed at a lateral load of 158kN in the positive direction and 60kN in the negative direction. The corresponding lateral displacements were 0.7mm and 0.5mm, respectively. This led to a drop of the lateral resistance. At this point, shear cracks appeared at the bottom of the left and right column. The shear cracks widened significantly (3mm) at the maximum lateral resistance of 135kN in the positive direction and 45kN in the other. Slips along the horizontal cracks and the openings of the diagonal cracks were observed in the infill at near 3.5mm displacement in each direction. Crushing of Single Strut started at about a lateral displacement of 3.9mm in both directions. The longitudinal reinforcement at the bottom sections of the columns yielded at about a lateral displacement of 3.1mm, but no yielding was detected for the longitudinal reinforcement in the beam. From the hysteresis loops we conclude that the in first few cycles they get maximum load and consume maximum specific energy but as the crack starts and propagation load carrying capacity goes on decreasing as well as specific energy goes on decreasing. Due to the spalling of crushed concrete at bottom of both columns, the lateral resistance dropped considerably at about 0.7mm displacement. Concrete crushing started in the Single Strut at 2.3mm displacement in each direction.

CONCLUSION CHAPTER-6

From Comparative analytical study, we conclude Firstly, the five possible failure modes of infills, there is a consensus that only the corner-crushing and sliding-shear modes are of practical importance, provided there are no openings in the infill. The mode of frame failure may be also considered, as it has been observed to occur many times in the field. Regarding the other two, namely, diagonal compression and diagonal cracking, the first occurs very rarely because it requires a high slenderness ratio of the infill, and the second should not be considered a failure mode because the infill can carry additional load after it cracks. The out-of-plane failure is an additional mode that should be considered, especially for double leaf walls.

With these complexities in mind, a number of researchers have attempted to model infill frames over the last 60 years. The macromodels that can be used in everyday engineering are of practical importance. The simpler ones are the equivalent-strut models, which represent infills with a diagonal strut element. The basic parameter of these struts is their equivalent width, which affects their stiffness and strength. Several formulas have been proposed by researchers to calculate this equivalent width. In all the cases, there are considerable differences among the values obtained. The equation that has been adopted by most technical guidelines is the one proposed by Mainstone (1974). Compared to other proposed formulas, this formula represents a lower bound of the calculated equivalent strut width.

From Analytical Study, we try to find that, the infills in a single-storey, single bay RC frame, the 1-strut model was found to be predicting the global behaviour (initial stiffness and ultimate failure load) of the system with reasonable accuracy. On the other hand, 3-strut model was found to be estimating the force resultants in the frame members more accurately as compared to that of a 1-strut model. Moreover, the 3-strut model was found to model local failures in the frame members in addition to the compressive failure of struts.

Under lateral forces when strut action develops with certain finite area of infill is physically connected to the beams and columns of the frame. This finite area, which can be effectively modeled using a 3-strut model, is responsible for distribution of large stiffness of infill walls to a larger area on beams and columns; this prevents abrupt failure of masonry infills under increasing lateral forces. The finite area is also responsible for local shear failure in beams and columns, and in a 3-strut model, this failure mode can be represented in a more appropriate manner. Moreover, design force

resultants in RC beams and columns can be obtained more accurately when 3-strut models are used. Therefore, the 3-strut model appears to be physically more appropriate than the 1-strut model for masonry-infilled RC frames.

Noting that single-strut models are inadequate for accurately representing the interaction between the infill and the bounding frame and thus cannot accurately predict the force distribution in the members of the bounding frame, researchers have made attempts to represent infill walls with multiple struts. Models with two, three, and more than three struts have been proposed. The merits and shortcomings of each of these models have been discussed in this paper, showing that the three-strut models can more accurately predict the infill-frame interaction than the single-strut ones, but with a considerable increase in modeling complexity; whereas the two-strut models, although they cannot achieve the accuracy of the three-strut models, improve the prediction compared to the single struts, with less model complexity. The multiple-strut models also have the advantage of being able to take into account the presence of openings in infills, either through their load-displacement and hysteretic models for the two- and three strut models, or through the positioning of the struts for models with more than three struts.

REFFERENCES

1) Al-Chaar, G.K.(1998);Nonductile Behaviour of Reinforced Concrete Frames with masonry infill panels subjected to in-plane loading. United States-IIIinios, University of IIIinios at Chicgo.

2) Asteris, P. G. (1996). "A method for the modelling of infilled frames (Method of Contact Points." Proc., 11th World Conf. on Earthquake Engrg., Paper No. 953, Acapulco, Mexico.

3) Asteris, P.G, Antoniou,S.T, Sophianopoulos, D.S, Chrysostomou, C.Z (2011),"Mathematical Macromodelling of Infilled frames; State of the Art.

4) Asteris, P.G (2008).Finite Element Micro Modeling of Infilled Frames.

5) ATENA theory manual, part 1 from Vladimir Cervenka, Libor Jendele and Jan Cervenka.

6) ATC-40(1996), Seismic Evaluation and Retrofit of Concrete Buildings, California.

7) CEB, RC Frames Earthquake Loading-State of the Art Report, Thomas Telford, 1996.

8) Crisafulli,F" Analysis of infilled Frame Structures" presentation for Seminar on Masonry and Earthen Structures at Universidade do Minho.

9) Chrysostomou, C.Z. (1991). Effects of degrading infill walls on the nonlinear seismic response of two-dimensional steel frames, PhD thesis, Cornell University.

10) Dhanasekar, M. and Page, A.W. (1986). "Influence of brick masonry infill properties on the behavior of infilled frames", *Proc., Instn. Civ. Engrs.*, London, Part 2, 81, 593-605.

11) Dorji,J(2009). "Seismic Performance of Brick Infilled RC Frame Structures in Low and Medium Rise Buildings in Bhutan, Phd Thesis,Queensland Uni.

12) Drydale, R.G, Hamid,A.A and Baker, L.R., Masonry structures- Behaviour and Design, Practice Hall, Ennglewood Cliffs, New Jersey, 1994.

13) El-Dakhakhni, W. W., Elgaaly, M., and Hamid, A. A. (2003). Three-Strut Model for Concrete Masonry-Infilled Steel Frames. Journal of Structural Engineering **129:2**, 177–185.

14) FEMA (2000). Prestandard and Commentary for the Seismic Rehabilitation of Buildings (FEMA 356). Prepared by ASCE for Federal Emergency Management Agency, Washington, D.C., USA.

15) Ghosh, A. K. and Amde, A. M. (2002). "Finite Element Analysis of Infilled Frames", J. Struct. Eng., 128 (7), 881-889.

16) Ghassan,Al-chaar, Mehrabi,A.B and Manzouri, T(2009).”Finite Element interface Modelling and Experimental Verification of Masonry-Infilled R/C Frames.

17) Ghassan,Al-chaar, Mehrabi,A.B(2008).”Constitutive Models for Nonlinear Finite Element Analysis of Masonry Prisms and Infill walls(US Army Corps of Engineers).

18) Holmes, M. (1961). Steel Frames with Brickwork and Concrete Infilling. Proceedings of Institute of Civil Engineers **19:2**, 473-478.

19) IS 1893, Criteria for Earthquake Resistant Design of Structures-Part 1, General Provision and Buildings (fifth revision); Bureau of Indian Standards, New Delhi, 2002.

20) Jain, S.K. Mondal,G.(2008) “Lateral Stiffness of Masonry Infilled Reinforced Concrete Frames with Central Opening’’.Earthquake Spectra,(24)701-723.

21) Kaushik, H.B., Rai, D.C., and Jain, S.K. (2006). A Rational Approach to Analytical Modeling of Masonry Infills in Reinforced Concrete frame Buildings; The 14th World Conference on Earthquake Engineering October 12-17, 2008, Beijing, China.

22) Kaushik, H.B., Rai, D.C., and Jain, S.K. (2006). Code Approaches to Seismic Design of Masonry Infilled Reinforced Concrete Frames: A State-of-the-Art Review. Earthquake Spectra **22:4**, 961-983.

23) Liauw, T.C. and Kwan, K.H. (1984). “Nonlinear behaviour of non-integral infilled frames”, *Comp. and Struct.*, 18, 551-560.

24) Madan,A. Hashmi, A.K (2008),Analytic Prediction of the Seismic performance of masonry infilled reinforce concrete frames subjected to near-field earthquakes’’ Journal of structural Engineering 134(9);1569-1581.

25) Mallick, D.V. and Garg, R.P. (1971). “Effect of openings on the lateral stiffness of infilled frames”, Proc., Instn. Civ.Engrs., 49, 193-209.

26) Mehrabi, A.B., Shing, P.B., Schuller, M. and Noland, J. (1996).“Experimental evaluation of masonry-infilled RC frames”,J. Struct. Eng., 122(3), 228-237.

27) Mehrabi, A.B., Shing, P.B., Schuller, M. and Noland, J. (1994).“Performance of Masonry Infilled R/C Frames under In-Plane Lateral Loads ”,J. Struct. Eng.

28) Mehrabi,A.B. Shing,P.B (2002). “Behaviour and analysis of masonry-infilled frames”,Prog.Struct.Engrg Matter;320-331.

29) Polyakov, S.V. (1960). “On the interaction between masonry filler walls and enclosing frame when loading in the plane of the wall”, Translation in earthquake engineering, Earthquake Engineering Research Insitute, San Francisco, 36-42.

30) Puglisi, M. Uzcategui, M. Florez-Lopez, J. Modeling of masonry of infilled frames, Part I:The Plastic Concentrator, Eng Struct 2009;31(1):113_118.

31) Rodrigues, H. Varum, H. Costa,A. (2010)Simplified Macro-Model for Infill Masonry Panels; Journal of Earthquake Engineering; 14;390-416.

32) Smith, B.S. (1966). “Behavior of square infilled frames”, J.Struct. Div., ASCE, ST1, 381-403.

33) Stafford-Smith, B., and Carter, C. (1969). A Method of Analysis of Infilled Frames. Proceedings of the Institution of Civil Engineers **44**, 31-48.